

NAVAL POSTGRADUATE SCHOOL

Monterey, California



THESIS

UNDERSTANDING MESOSCALE ERROR GROWTH AND PREDICTABILITY

by

Michael A. Kuypers

June 2000

Thesis Advisor:
Second Reader:

Wendell A. Nuss
Douglas K. Miller

Approved for public release; distribution is unlimited.

20000721 042

DTIC QUALITY INSPECTED 4

REPORT DOCUMENTATION PAGE

Form Approved
OMB No. 0704-0188

Public reporting burden for this collection of information is estimated to average 1 hour per response, including the time for reviewing instruction, searching existing data sources, gathering and maintaining the data needed, and completing and reviewing the collection of information. Send comments regarding this burden estimate or any other aspect of this collection of information, including suggestions for reducing this burden, to Washington headquarters Services, Directorate for Information Operations and Reports, 1215 Jefferson Davis Highway, Suite 1204, Arlington, VA 22202-4302, and to the Office of Management and Budget, Paperwork Reduction Project (0704-0188) Washington DC 20503.

1. AGENCY USE ONLY (Leave blank)

2. REPORT DATE
June 2000

3. REPORT TYPE AND DATES COVERED
Master's Thesis

4. TITLE AND SUBTITLE Understanding Mesoscale Error Growth and Predictability

5. FUNDING NUMBERS

6. AUTHOR(S)

Kuypers, Michael A.

7. PERFORMING ORGANIZATION NAME(S) AND ADDRESS(ES)

Naval Postgraduate School
Monterey, CA 93943-5000

8. PERFORMING ORGANIZATION
REPORT NUMBER

9. SPONSORING / MONITORING AGENCY NAME(S) AND ADDRESS(ES)

10. SPONSORING / MONITORING
AGENCY REPORT NUMBER

11. SUPPLEMENTARY NOTES

The views expressed in this thesis are those of the author and do not reflect the official policy or position of the Department of Defense or the U.S. Government.

12a. DISTRIBUTION / AVAILABILITY STATEMENT

Approved for public release; distribution is unlimited.

12b. DISTRIBUTION CODE

13. ABSTRACT

Technological advances have made atmospheric mesoscale modeling at very fine resolutions readily available to a great number of organizations. Though initial operational results show some skill with respect to synoptic scale forecasts, many of the problems associated with mesoscale error growth and predictability have been ignored. Understanding mesoscale error is critical to accurately interpreting mesoscale model results and output from tactical decision aids (TDA's).

This study examines mesoscale error growth and predictability through controlled numerical model experiments. A known "true" atmosphere is created through the use of the US Navy's Coupled Oceanographic/Atmospheric Mesoscale Prediction System (COAMPS). Virtual observations are randomly sampled from this atmosphere to provide data for ingest into forecasts using the NCAR/Penn State MM5 mesoscale model. Forecast results for ten cases are compared against the "true" atmospheric solution and error statistics are calculated for wind speed and geopotential height fields. Results show how error growth and predictability are affected by different variables such as boundary conditions, weather regime, sample size and sample distribution. A scale separation of error is also performed in order to assess the impact of synoptic scale error on mesoscale error.

14. SUBJECT TERMS

Mesoscale Modeling, Coupled Ocean-Atmosphere Mesoscale Prediction System (COAMPS), Error growth, Predictability

15. NUMBER OF
PAGES

114

16. PRICE CODE

17. SECURITY
CLASSIFICATION OF
REPORT

Unclassified

18. SECURITY CLASSIFICATION OF
THIS PAGE

Unclassified

19. SECURITY CLASSIFI- CATION
OF ABSTRACT

Unclassified

20. LIMITATION OF
ABSTRACT

UL

NSN 7540-01-280-5500

Standard Form 298 (Rev. 2-89)
Prescribed by ANSI Std. Z39-18

Approved for public release; distribution is unlimited

UNDERSTANDING MESOSCALE ERROR GROWTH AND PREDICTABILITY

Michael A. Kuypers
Lieutenant, United States Navy
B.S., United States Naval Academy, 1991

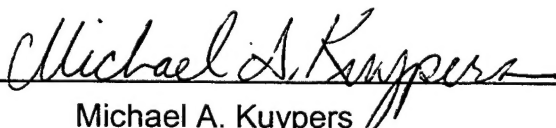
Submitted in partial fulfillment of the
requirements for the degree of

**MASTER OF SCIENCE IN METEOROLOGY AND PHYSICAL
OCEANOGRAPHY**

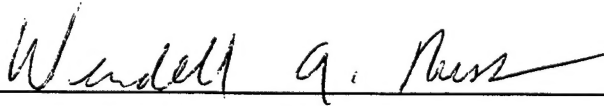
from the

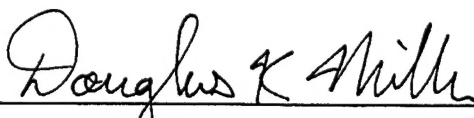
**NAVAL POSTGRADUATE SCHOOL
June 2000**

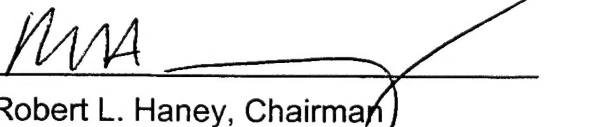
Author:


Michael A. Kuypers

Approved by:


Wendell A. Nuss, Thesis Advisor


Douglas K. Miller, Second Reader


Robert L. Haney, Chairman
Department of Meteorology

ABSTRACT

Technological advances have made atmospheric mesoscale modeling at very fine resolutions readily available to a great number of organizations. Though initial operational results show some skill with respect to synoptic scale forecasts, many of the problems associated with mesoscale error growth and predictability have been ignored. Understanding mesoscale error is critical to accurately interpreting mesoscale model results and output from tactical decision aids (TDA's).

This study examines mesoscale error growth and predictability through controlled numerical model experiments. A known "true" atmosphere is created through the use of the US Navy's Coupled Oceanographic/Atmospheric Mesoscale Prediction System (COAMPS). Virtual observations are randomly sampled from this atmosphere to provide data for ingest into forecasts using the NCAR/Penn State MM5 mesoscale model. Forecast results for ten cases are compared against the "true" atmospheric solution and error statistics are calculated for wind speed and geopotential height fields. Results show how error growth and predictability are affected by different variables such as boundary conditions, weather regime, sample size and sample distribution. A scale separation of error is also performed in order to assess the impact of synoptic scale error on mesoscale error.

Results indicate that error growth and predictability are dependent on all the above mentioned variables. Domain size and location define the wavelengths of error that are allowed to grow while boundary conditions limit which error grows within the domain. Contrary to previous studies, errors did grow on the mesoscale within a 24 hour forecast cycle. Scale separation results show that mesoscale error is dominated by synoptic scale error.

TABLE OF CONTENTS

I.	INTRODUCTION	1
A.	THE OPERATIONAL SIGNIFICANCE OF PREDICTABILITY	1
B.	WHAT IS PREDICTABILITY THEORY?	3
C.	HYPOTHESES	6
D.	EXPECTED RESULTS	8
II.	APPROACH	11
A.	"IDEAL" ATMOSPHERE SPECIFICATION	13
B.	RANDOM "OBSERVATIONS"	15
C.	THREE DIMENSIONAL MULTIQUADRIC INTERPOLATION	16
D.	WEATHER REGIMES	17
1.	The Winter Regime	18
2.	The Summer Regime	20
E.	NUMERICAL MODELING FORECAST ERROR (NMFE)	21
F.	SCALE SEPARATION OF ERROR	22
G.	TERMINOLOGY	24
III.	FINDINGS.....	27
A.	THE EFFECT OF SAMPLE DISTRIBUTION ON ERROR GROWTH	27
1.	Correlation between Analyses and Forecast Error	28
2.	Asymptoting Error Values	30
B.	THE EFFECT OF SAMPLE SIZE ON ERROR GROWTH	31
1.	Increasing Sample Size	31
a.	Impact by weather regime	32
b.	Impact by boundary condition	33
c.	Impact by domain size	33
2.	NOGAPS Firstguess Forecast	34
C.	THE EFFECT OF LATERAL BOUNDARY CONDITIONS ON ERROR GROWTH	35
D.	THE EFFECT OF MODEL SPIN UP ON ERROR GROWTH	37
E.	WEATHER REGIME DEPENDENCIES	38
1.	Kinetic Energy	38
2.	Unique Mesoscale Structure	39
F.	DOMAIN SIZE DEPENDENCIES	40
G.	SYNOPTIC SCALE INFLUENCE ON THE MESOSCALE	41
1.	Synoptic and Mesoscale Correlation	41
2.	Scale Separation of Error	42
IV.	DISCUSSION	45
A.	CHARACTERISTIC WAVELENGTHS	45
B.	LATERAL BOUNDARY CONDITIONS	46
C.	SYNOPTIC SCALE INFLUENCES	48

D.	OBSERVATIONAL SAMPLE SIZE AND DISTRIBUTION	50
E.	WEATHER REGIME DEPENDENCIES	50
V.	CONCLUSIONS	53
A.	MESOSCALE CERTAINTIES AND UNCERTAINTIES	54
B.	FURTHER RESEARCH	56
1.	Vary Weather Regimes and Geographic Locations	56
2.	Calculate Error Growth Using other Model Parameters.....	57
3.	Better Experimental Design.....	57
4.	Error Growth Compared to Synoptic Forecast Over Time	58
5.	Use of Spectral Analysis to Perform Scale Separation	58
6.	Topography	58
	APPENDIX A. FIGURES.....	61
	LIST OF REFERENCES	101
	INITIAL DISTRIBUTION LIST	103

ACKNOWLEDGEMENT

I would like to thank the many people who contributed in different ways to the accomplishment of this work. I thank Dr. Wendell Nuss for his unique insight into the world of mesoscale modeling and for his thought provoking questions that helped spur the direction of this study. His diligence in providing the necessary tools for analysis as well as his enthusiasm for teaching and research were invaluable. I look forward to the many contributions he will make to the mesoscale modeling field in the future. I also thank Dr. Doug Miller for his encouragement and partnership in this study. His timely and accurate comments helped to sharpen the focus of this study and made it a better product. I would like to thank the Meteorology department for its strong support during my time at NPS. In particular, I thank Bob Creasey and Bill Thompson for their technical assistance and making sure there was always enough disk space. I also thank my classmates, Eric, Sean, Denise, and Cindy for their friendship these past two years.

I especially want to thank my wonderful wife, Claire, for her dedication and devotion to me. Her love and support at home kept me going and truly made this thesis a team effort. I couldn't ask for a better partner! I also thank my two wonderful children, Rebecca and Nathan, for understanding when daddy had to work. Thank you also to my parents, for the love and support you have always given me. I love all you guys.

Finally and most importantly, I want to thank our Lord and Savior, Jesus Christ, for His ultimate sacrifice, which makes this one pale in comparison. May God continue to keep us guessing at His awesome creation and thereby employed!

I. INTRODUCTION

The vast number of technological breakthroughs in the last decade have allowed for enormous growth and opportunity in the field of mesoscale modeling. The increase in computer speed and power and the widespread availability of quality computing hardware has continued to fuel the vision that we can and should predict our environment at the finest resolutions imaginable. This growth has also engendered in some minds a belief that the finer the resolution, the better the forecast. While the recent growth in mesoscale modeling and increased resolutions has led to some useful insights into the key physical properties that govern mesoscale dynamics (Doyle 1997, Thompson et al. 1997), the general question of predictability and the influence that the synoptic scale has on the predictability limit of the mesoscale has been largely misunderstood or ignored.

A. THE OPERATIONAL SIGNIFICANCE OF PREDICTABILITY

The operational significance of the general predictability of mesoscale models and, in particular, specific mesoscale features cannot be overlooked. A good understanding of these concepts is crucial to effectively using today's mesoscale model generated fields. The US Navy and other services are increasingly relying on the accuracy of their mesoscale models not only to

produce a detailed mesoscale forecast but also provide accurate information into sophisticated tactical decision aids (TDA's). The output of these TDA's can give detailed guidance to the warfighter who is trying to assess the environment he/she will be working in, but very rarely gives him/her a good picture of the reliability of that guidance. The model information is passed to the TDA and assumed to be accurate and relatively error free, yet there is no indication given that a particular mesoscale feature may not even be "predictable" at the temporal or spatial scale of the operation. While a good forecaster can and should accurately assess the character of the error in a particular model forecast through experience and comparison with other sources, there is currently no means by which a TDA can identify error. Further uncertainty in the guidance is brought about by the fact that very little, if any, actual mesoscale observations are assimilated into the mesoscale model. Thus, we must rely on the accuracy of the synoptic scale initial conditions to pass their dynamically significant features down to the mesoscale. At what scale then must we routinely observe the atmosphere in order to accurately forecast mesoscale weather events? And how accurate must we be on the synoptic scale in order to achieve a desired degree of accuracy on the mesoscale? Finally, how does the variability in sample size and location, mesoscale structure pattern, and boundary conditions affect error growth and ultimately predictability? It is with these questions in mind that we approached this work, with the ultimate desired result being a better understanding of error growth and predictability on the mesoscale.

B. WHAT IS PREDICTABILITY THEORY?

The bulk of predictability work in the past two decades has been accomplished by Lorenz (1982, 1993) and Anthes (1984). Lorenz' work focused on the concept of the predictability time limit, which represents the span of time between the best estimate of the state of the atmosphere based on initial observations and an estimate of its state at a future time. The predictability time limit represents the point where the forecast becomes essentially unusable due to inherent numerical model forecast errors. Beyond the predictability time limit, the likelihood of verifying the forecast is no better than random guesswork. The best estimate for the state of the atmosphere at the initial time depends first on the quality of the observational sample and then on the method of data assimilation. Based on Lorenz' reasoning, the better this estimate, the longer the time before the predictability time limit is reached. Figure 1 shows a hypothetical change in numerical model forecast error (NMFE) over time and highlights the impact initial error has on predictability. At the initial time, the NMFE is small but grows rapidly due to the lack of dynamic consistency between the initial model state analyzed by observations and the dynamic allowances set forth in the model physics. As the model spins up, this initial state develops into a state that is more consistent with the models physical equations and thus a relative minimum occurs in the forecast error. Further development in the simulation shows that forecast error continues to grow due to the incompleteness of the model's physical equations, its discretization, and truncation error. At

some point, the NMFE reaches a critical level where the model essentially has no skill - the predictability time limit.

The critical level of NMFE can be defined in various ways. In global atmospheric models, the critical NMFE is defined as the error variance (mean square of the difference of some variable) associated with two randomly chosen atmospheric states, or twice the climatological error variance (Anthes 1986). From the perspective of the warfighter, however, the critical level of NMFE is dependent on the nature of the operation which requires the numerical guidance, and may in fact be much lower. A third possible measure of the predictability time limit is the use of the standard deviation about the mean of a particular model variable. Though more a measure of the forecast skill of a particular solution, this measure also gives us insight into the predictability of the solution. If the root mean square error of two numerical model solutions beginning with small differences at the initial time exceeds the standard deviation about the mean for a particular solution, then the other solution has in effect reached its predictability time limit with respect to the first solution. By calculating the mean of a certain variable such as wind speed in a control environment and then comparing the RMS error of a particular numerical solution to the standard deviation about the mean of the control, one can gain an accurate measure of the skill of that particular forecast solution. If the RMS value exceeds the standard deviation about the mean of the control, then in essence, the forecast has no skill, and simply taking the mean winds across the domain would provide

a better forecast. We have utilized this third means of measuring predictability for all the error growth comparisons in this study.

A similar predictability limit to the time limit can also be applied in space and is called the predictability spatial limit. It represents the spatial scale at which small scale variations become essentially randomly distributed and beyond which there is little useful information upon which to base a forecast. The distinction between the two predictability limits is that forecasts become less meaningful for *increasing* time scales, whereas they become less meaningful for *decreasing* spatial scales. Thus, as mesoscale modeling efforts seek to define increasingly smaller spatial scales over increasingly longer time scales, it becomes clear that understanding the predictability of certain features becomes even more important.

The question of a theoretical predictability limit becomes more complex in that it often differs for different mesoscale phenomena. Although previous research suggested that predictability decreases rapidly with scale to limit mesoscale predictability to less than a day, common experience with mesoscale models shows that this is not always the case and that practical predictability time limits are often much longer. Baumhefner (1984) showed that for the synoptic scale, predictability decreases with decreasing scale at a typical error doubling time of about two days. Tennekes (1978) suggested that the mesoscale would reach the predictability time limit faster than the synoptic scale due to the transfer of energy from the small to larger scales by three dimensional

turbulence. However, for the mesoscale phenomena that do not fit the average spectrum of atmospheric turbulence, the rate of this transfer of energy and thus forecast error, may differ considerably. Warner (1992) also suggested that some mesoscale phenomena, in particular those forced by fixed features such as a coastal mountain range, might be more predictable. Shukla (1984) found that since atmospheric variability is less in low latitudes than in middle latitudes, the limit to deterministic predictability is shorter in the tropics than in the mid-latitudes, provided the error growth rates for a particular feature are the same. These results were all primarily obtained by performing predictability experiments on global models. This thesis will seek to examine and confirm a few of the results from Anthes, Baumhefner and Shukla's experiments but also seeks to uncover some of the recent nuances of error growth on the mesoscale by utilizing current mesoscale model capabilities in a self-contained numerical modeling experiment.

C. HYPOTHESES

This thesis studies the dependence of mesoscale error growth and predictability on several different factors. Consequently, we suggest that the initial error growth as well as the predictability in a numerical forecast is strongly influenced by four factors:

- (1) The observational sample size, scale and distribution.
- (2) The method of data assimilation used to project information and error from observations onto the forecast model.
- (3) The choice of boundary conditions and frequency at which they are applied.
- (4) The characteristic structure of the mesoscale regime.

Regarding factor (1), we seek to discover at what scale we must routinely observe the state of the atmosphere in order to accurately forecast mesoscale weather events. Regarding factor (2), we seek to understand how sensitive mesoscale forecasts are to both synoptic and mesoscale uncertainty in the initial conditions for a particular data assimilation system. Regarding factor (3), we seek to understand how boundary conditions impact the character of the error growth at all domain sizes. Finally, regarding factor (4), we seek to understand how the predictability time limit changes for different mesoscale regimes. Our specific hypotheses are that:

- 1. Variation in the observational sampling pattern at the synoptic scale leads to variation in analyses that directly impact error growth and predictability in mesoscale forecasts.**

2. For a limited area model, the choice of boundary conditions and domain size directly impacts the character of the error growth by restricting the wavelength of allowable solutions.
3. Error growth on the mesoscale correlates with error growth on the synoptic scale although errors grow more rapidly at smaller scales.
4. Mesoscale predictability is weather regime dependent and error tends to be larger in scale and more variable in weather regimes with greater kinetic energy.

D. EXPECTED RESULTS

The expected results of this thesis are in essence a better understanding of error growth and predictability as it applies to the mesoscale. We will show that normal variations in observational sampling size and distribution, model horizontal grid spacing, as well as the system of data assimilation and boundary conditions all impact error growth and thus predictability. We will also estimate the shape of the NMFE growth curves as a function of these variables. By defining the critical NMFE amount as the standard deviation about the mean of our control atmosphere, we will evaluate the forecast skill and the predictability limit for different mesoscale regimes, hopefully showing that model forecasts initialized from better observational sampling regimes, and thus better analyses,

will extend the predictability time limit for most mesoscale features. We also expect that at horizontal resolutions where there are little or no observations, the predictability time limit will be much shorter and mesoscale forecasts more suspect.

Finally, we expect our results will produce more questions as we uncover the nature of the relationship of various factors to error growth on the mesoscale. Practically speaking, we will never be able to fully observe the atmosphere at the scales at which we desire to predict. The question that remains is then one of understanding and managing the error growth that we are certain will exist at those scales. By better understanding how synoptic scale variations impact the mesoscale domain, we may be able to develop techniques to limit these variations or at the very least, be able to identify when a mesoscale forecast is suspect and when it may be the right tool for the job.

THIS PAGE INTENTIONALLY LEFT BLANK

II. APPROACH

One of the difficulties of performing atmospheric predictability studies is the inability to completely sample the entire atmosphere and thereby have a well-defined reference grid with which to perform the studies. Since operational observational sampling does not often capture true mesoscale structure, doubt is cast upon the accuracy of the error calculations for specific points within the domain. This study's approach therefore, utilized the benefits of a controlled environment using numerical model experiments. Although described in more detail in the following sections, the basic approach of our study follows.

Instead of relying on operational sampling to describe a particular mesoscale regime, an idealized atmosphere was generated from a mesoscale model forecast. These model grids were then taken as the "true" atmospheric conditions for the course of the experiments providing the advantage of knowing the structure of the atmosphere at every point on the grid. Virtual observations were then developed by randomly sampling the ideal atmosphere in order to help assess the impact of observational sampling differences on both analyses and forecast. By combining the virtual observations with a synoptic scale first guess field, we performed several mesoscale model runs via a separate model in order to produce forecast fields for comparison. We could then determine the characteristic error in the model as well as the shape of the NMFE curves by comparing the analysis and forecast results to the "true" control initial

atmosphere. This procedure was performed for two separate weather patterns (winter and summer), and two distinct model predicted fields (geopotential height) and wind speed. Other sampling strategies included varying the number of observations in the analyses as well as running an experiment with no virtual observations, producing an analysis and forecast from initial guess points only.

To understand the effects of boundary conditions on error growth, we also performed identical forecast experiments using two separate boundary conditions. In one experiment we utilized the Navy Operational Global Atmospheric Prediction System (NOGAPS) as the boundary conditions since this simulated the conditions actually used in Navy operations today, while in the other we utilized the "ideal" atmospheric conditions at the boundary to give us a sense of the "best" case forecast error growth. Finally, in order to understand how error might be passed down from one scale to another, we performed a scale separation of error for a single random case run. Throughout the testing phase, the main criteria for assessing the impact of the various sampling approaches on the forecast error growth was the change in forecast skill and the predictability time limit as described by the numerical model forecast error curves. Table 1 below summarizes the various experiments performed with the created data sets.

Summary of Experiments	
<u>Goal</u>	<u>Design</u>
1. Determine how varying sample size affects error growth.	Compared analyses of experiments using 0, 100, 200, and 400 point samples to the "true" atmosphere and calculated RMS error. Noted trend in error with increasing point samples.
2. Determine how various random distributions of observations affect error growth.	"Sampled" random observations from the "true" initial atmosphere, producing analysis and forecast for ten separate cases. Calculated RMS errors for wind speed at 500mb and noted the error growth differences between the various numerical solutions.
3. Determine how error growth is affected by varying mesoscale regimes	Calculated error growth statistics for a definitive winter and summer pattern.
4. Determine how mesoscale error is affected by larger scale error.	Performed a scale separation of error by projecting larger scale fields onto 4km grid and then calculated the associated scale error.
5. Determine how choice of boundary conditions affects error growth.	Ran identical forecast simulations for both winter and summer regimes using two different sets of boundary conditions.

Table 1. Summary description of various experiments contained within the study.

A. "IDEAL" ATMOSPHERE SPECIFICATION

The idealized mesoscale atmosphere used as the basis for all the experiments and the random observations was created by running the US Navy's Coupled Ocean/Atmosphere Mesoscale Prediction System (COAMPS) at 40 vertical levels for a 36 hour "observing" period using four nested domains having horizontal grid spacings of 108, 36, 12, and 4 km centered over the San

Francisco and Monterey Bay region (Figure 2). A 12 hour data assimilation forecast was run for the 12 hours prior to the time period of initialization in order to spin up reasonable mesoscale horizontal and vertical structure along with dynamically consistent cloud and rain fields. The initial conditions for the data assimilation and the outermost domain's lateral boundary conditions originated from the 2.5 degree NOGAPS analyses for the corresponding time period.

The experimental forecast fields used for comparison to the "true" atmosphere's forecast were created using the NCAR/Penn State MM5 mesoscale model. The model contained 30 vertical levels and was run with full physics. MM5 was chosen as the forecast model in order to allow for unique model solutions and to prevent reintroduction of error specific to the COAMPS model. Initial analyses on 12 vertical levels were created with NOGAPS first guess fields, and the randomly selected observations from the COAMPS "truth" mentioned above. The 12 level analyses were then interpolated to the 30 vertical levels to initialize the MM5 forecasts.

It should be noted that in order to provide a control forecast using MM5, the original COAMPS "true" atmosphere at reduced vertical resolution but with identical horizontal grid points was used for initialization. Since the experimental forecasts were run with MM5 starting from a 12 vertical level analysis (as in NOGAPS) , the MM5 control forecast also had to contain 12 vertical levels to provide fair estimates of error that were independent of the differing vertical resolutions. Although the control forecast contained less vertical structure than

the original COAMPS "true" atmosphere, the horizontal resolutions remained the same. The control forecast thus represented the best prediction that MM5 could achieve based on the COAMPS "true" atmosphere at consistent vertical resolution and was therefore a good basis for comparison to the experimental forecast runs. Figure 3 is a schematic diagram which summarizes the experiment's design.

B. RANDOM "OBSERVATIONS"

In order to provide consistent amounts of observations for the initialization of the forecast runs, we utilized a random number generator to select random observations from the 108 km COAMPS "true" atmosphere. Ten cases, representing ten separate seed numbers into the random number generator, were run to provide some statistical significance to the study. 100 observations were selected randomly for each case run except for the sample size studies where we selected 200 and 400 observations respectively. The same seed numbers used in the winter case were also used for the summer case in order to provide consistency for comparison between the two weather regimes. The forecast runs were thus initialized with NOGAPS global fields and the randomly selected observations added. Figure 4 shows the random distribution of observations for a specific seed number with 100, 200 and 400 observations respectively.

C. THREE DIMENSIONAL MULTIQUADRIC INTERPOLATION

Three dimensional multiquadric(3DMQ) interpolation was used as the data assimilation method for these experiments due to its relative simplicity and the researcher's familiarity with the method. An added advantage of using the 3DMQ approach was that it had the ability to resolve features at the smallest scales that were represented by observations in a particular region of the analysis domain (Nuss and Titley 1994). This ensured that we could accurately calculate the error associated with the finest mesoscale features.

3DMQ uses radial basis functions which assume isotropic structure functions for the environment (Nuss and Titley 1994). This approach differs from the anisotropic error covariance structure functions of Optimal Interpolation (OI) and three dimensional variational analysis (3DVAR) schemes. These data assimilation schemes rely on prior knowledge of the true state of the atmosphere in order to give an optimal analysis based on an estimated error covariance function. However, error in the estimates of the observation and background error covariance functions strongly impact the accuracy of the optimal fit. 3DMQ interpolation is not affected by errors in covariance estimates since it does not rely on prior knowledge of the true state of the atmosphere. Theoretically then, there would be smaller potential error variations from one weather regime to another, allowing for consistent analysis between different weather regimes, which particularly suited the dual weather pattern approach of this experiment.

D. WEATHER REGIMES

The idealized mesoscale atmosphere was generated for two distinct weather regimes, 1) a deep extratropical cyclone with an associated front interacting with the coastline occurring on February 6th, 1998, and 2) a summer high pressure pattern which produced a typical sea breeze pattern in the Monterey Bay region, occurring on August 25th, 1997. Figures 5[a-e] and 6[a-e] show the progression of each weather pattern for the 24 hour forecast period for the "true" atmosphere. Of primary importance in the differing weather regimes is the mesoscale structure associated with each regime and the amount of kinetic energy that each system contains. For instance, we expect that on the 4km nest, error growth associated with the winter pattern would be primarily influenced by the passage of the cold front and the model's correct timing and orientation of this event. For the summer pattern, however, we expect the error growth on the 4km nest to be associated more with the background flow and with the correct representation of the marine planetary boundary layer. Due to the greater amounts of energy associated with the winter pattern, we also expect that the magnitude of the errors associated with this system will be greater than those in the summer pattern. Another factor to consider is the start time of the models for the two weather regimes. The winter pattern begins at 00Z and thus the first 12 hours of the forecast are in the "cold" part of the forecast cycle. The summer regime however, started at 12Z and thus in this case, the first 12 hours of the forecast are in the "hot" part of the forecast cycle.

1. The Winter Regime

Figure 5a shows the winter pattern beginning at 00Z on 6 February, 1998. A 987mb surface low pressure system is located in the Gulf of Alaska with an associated baroclinic frontal zone extending to the southeast. The low has begun occluding already at this point and a wave is forming along the frontal boundary at approximately 35N, 130W, which later develops into a new low pressure system. South of the wave, the frontal band extends to the southwest and is located approximately 450 nautical miles from the Monterey Bay, which encompasses the majority of the 4km domain. Surface winds in the vicinity of the Monterey Bay are southerly at 25kts. At 500mb, the 108km domain is dominated by a significant long wave trough whose axis lies between 135W and 140W, notably behind the surface front. At 00Z, a vorticity maximum is entering the base of the trough and has an associated 105kt jet maximum. The front left quadrant of the vorticity maximum corresponds with the developing wave at 35N, 130W.

By six hours into the forecast, the Gulf of Alaska low pressure system has occluded and moved off to the northwest. The surface front extending from the new low pressure center at 35N, 127W is now about 300 nautical miles (nm) away while surface winds near Monterey have begun to turn to the southwest and have increased to 30kts. At the 500mb level, the vorticity maximum has begun to progress through the base of the trough and has taken on a more

northwesterly orientation. The trough axis is located at approximately 130W, still behind the surface front. The jet maximum has reduced in speed to 90 kts.

Figure 5b shows the development of the pattern twelve hours into the forecast. The surface front has entered the 4km domain and has made landfall near the California/Oregon border, though it is still approximately 50 nm away from Monterey. Surface pressures in the vicinity of Monterey have decreased by 8-10mb over the 12 hour period and surface winds have continued turning to the west while maintaining speed at 30 kts. The low pressure center is now located at 37N, 125W, just off the northern California coast. The upper level pattern shows that the vorticity maximum has continued to translate through the base of the trough and both the trough axis and the vorticity maximum are nearly in the same location as the surface front. The jet maximum has remained relatively constant.

Sometime between 12 and 18 hours into the forecast, a significant event occurs which eventually is reflected in the error growth curves for the winter pattern. During this time frame, the surface front enters the western portion of the 4km domain and makes landfall in the vicinity of Monterey. By 18 hours however, the surface front has passed through Monterey and the other side of the 4km domain and surface winds have shifted completely to the west and northwest. The low pressure center has continued to move to the northeast and is now located over the California/Oregon border with a central pressure of

996mb. At the 500mb level, the vorticity maximum has completely passed through the base of the trough indicating the trough has stopped deepening.

Figure 5c shows the final progression of the winter pattern 24 hours into the forecast. The entire 4km domain and the majority of the other domains are under the influence of the subsidence behind the cold front and the atmosphere has become relatively stable again. At the 500mb level, the vorticity maximum has moved inland a considerable distance while the trough has filled. The jet maximum has also decreased to 70 kts and is now located well to the south of California.

2. The Summer Regime

Figures 6(a-c) show the 24 hour forecast for the summer pattern beginning at 12Z on 25 August, 1997. Unlike the winter regime, the summer pattern remains fairly dynamically consistent throughout the forecast cycle. The synoptic scale is dominated by an upper level trough to the north in the Gulf of Alaska that is also reflected at the surface as a filling low pressure system, and to the south by a weak high pressure ridge. There is a weak stationary front that separates the two systems that also does not move considerably during the 24 hour forecast.

The primary influence on the 4km domain is the presence of the weak high pressure ridge extending from just north of Pt. Conception to the southwest. The associated surface winds around the high set up a weak onshore flow and

favorable conditions for the development of thermally forced sea and land breezes in the Monterey Bay area. Although this case is a bit climatologically atypical for the summer considering the location and strength of the trough at the coast, it was chosen for its stark contrast to the spatially and temporally dynamic winter pattern.

E. NUMERICAL MODELING FORECAST ERROR (NMFE)

Thus far, we have only alluded to the general concept of Numerical Modeling Forecast Error, its existence, and its impact on forecast accuracy. How this error is defined specifically, however, depends on many factors. This study will in part show how NMFE varies as a function of weather regime, sample size and distribution, boundary conditions, and horizontal model grid spacing. Since generating root-mean-square (RMS) error statistics was the simplest method for calculating NMFE with time, we utilized this approach as the primary method for determining the NMFE. We also calculated the bias errors for selected model parameters. The drawback associated with the simple RMS approach to NMFE is that it gave little insight into the source of the error; whether it was related to location, timing or intensity. To compensate for this shortcoming, we attempted to categorize the errors by other means in order to better quantify the NMFE for the above-mentioned factors. Another factor to consider was the fact that the area of study was located in a coastal environment where RMS errors were not uniformly spread across the domain but were rather correlated with the

topographic effects of the coastline. Thus, further error growth studies performed over a more uniform domain may show different results.

For consistency in comparison throughout the experiments, we chose to calculate the NMFE using geopotential heights and wind speed and direction at 500 mb. Although 500mb is less influenced by mesoscale forcing at the surface, this level was found to be representative of model error at all levels. We also calculated the average error throughout the column. Again, the character of the error between the various levels was fairly consistent and thus choosing a single level to represent error growth was representative of the actual error growth throughout the column. Finally, the specific definition of the critical NMFE with regard to the model horizontal grid spacing was the standard deviation about the mean of the chosen model parameter over the given domain.

F. SCALE SEPARATION OF ERROR

To gain a better understanding of the effects of synoptic scale error on the mesoscale, we performed a scale separation of the error unique to each scale of the nested grid. The nonlinear nature of atmospheric processes allows energy exchange among all scales of motion (Anthes 1984) and thus uncertainty or error in any scale will eventually contaminate all scales. The design of the nested grids we have chosen for our study, however, are one-way nested and thus error can only propagate down scale. In other words, error on the 4km domain consists of error inherent to that scale as well as error propagated in from outer

scales while error on the 108 km domain consists only of error unique to that scale. We utilized the following equation to represent the total error for the 4km grid,

$$E_{\text{total}} = E_{108\text{km}} + E_{36\text{km}} + E_{12\text{km}} + E_{4\text{km}}$$

where the total error is the summation of the error unique to each individual scale. This same equation could be applied to the coarser grids as well by simply dropping the error term for the finer grid spacings. Thus, the total error at 12km would be

$$E_{\text{total}} = E_{108\text{km}} + E_{36\text{km}} + E_{12\text{km}}$$

and likewise for other nests.

The first task was to represent each of the larger scale fields (108km, 36km, 12km) for both the "true" atmosphere and the random case atmospheres on the 4km grid. Figure 7 shows the results of this procedure at the twelve hour forecast for a single winter regime case. The 4km domain representation of the larger scale wind fields are each shown on the 4km domain. As expected, the 108km representation shows the long wave pattern while the other three representations show increasing amounts of mesoscale structure. By subtracting the true atmosphere's 4km representation of each scale from the particular case atmosphere's 4km representation, we could systematically calculate the amount of error at the 4km grid scale that was due to other scales.

G. TERMINOLOGY

To avoid confusion when referring to various model forecast runs, the following terminology and notation is used throughout the thesis:

- COAMPS “truth” refers to the original ideal atmosphere created for the purposes of random observational sampling,
- MM5 “control” forecast refers to the best representation of the “true” atmospheric progression through time and is used as the basis for comparison in all experimental forecasts.
- 980206/00Z refers to the winter pattern while the summer pattern is 970825/12Z.
- Analyses performed with COAMPS will be represented as simply “Analysis” while the initial forecast time for the MM5 control forecast (also an analysis) will be represented by F00.
- All other forecast times will be represented in the same manner (i.e.F06, F12, F24, etc.). Thus, 980206/00zF12 will be the winter pattern, 00Z run, 12-hour forecast.
- For each weather pattern, we performed ten random case runs where we selected a seed number for the random number generator which then randomly selected “observations” on the outer domain. Each case is represented by its unique seed number. For example, c148954 is the

case whose seed number was 148954. The same seed numbers were used when sampling the winter and summer cases for consistency.

THIS PAGE INTENTIONALLY LEFT BLANK

III. FINDINGS

The broad scope of this project provided many avenues for exploration into the character of error on the mesoscale and the number of different ways to analyze the data was staggering. It was immediately apparent from the resulting error growth calculations that each of the previously mentioned factors impacted the error growth in different ways, individually as well as in combination. Figures 8[a-d] and 9[a-d] show the complete 500mb wind speed error growth curves for all ten random cases at all domains for both weather patterns, and both boundary conditions. A cursory look at the differences between the various plots shows that differences in weather regime, boundary condition and scale all impact the character of the error growth as well as the skill and predictability of the forecasts. In some cases, these differences affect individual solutions and in other cases, the set of solutions as a whole. The findings for the specific error analyses performed will be presented here with a more in-depth discussion of the results presented in the following chapter.

A. THE EFFECT OF SAMPLE DISTRIBUTION ON ERROR GROWTH

Each random case of selected observations, when used in the initialization of a new model run, produced a distinctly different solution. Thus, within the confines of a particular weather pattern or boundary condition, the

error growth and predictability of each solution was strictly dependent on how well that particular set of observations characterized the structure of dynamically significant atmospheric features.

1. Correlation between Analyses and Forecast Error

The concept that a better analysis will produce a better forecast is one of the reasons for maximizing the amount of information by which a particular mesoscale model is initialized. This thought is generally well accepted in the mesoscale modeling community and thus it also follows that if there is relatively low amounts of error at the analysis, there will be comparatively less error in successive forecasts (Anthes 1986). Our study found, however, that while this may be the case experientially, the error growth characteristics of the various cases show otherwise. Figures 10 - 13 are scatter plot diagrams of 500mb initial and 24 hour forecast wind speed errors for all cases in both weather regimes, using both sets of boundary conditions. Table 2 below lists the summarized correlation coefficients for the same scatter plots, but only for the 108km and 36km domains. The values for the 12km domain are not listed since they did not accurately show the true correlation between the initial and forecast error. The temporal separation between F00 and F24 combined with the small domain size essentially meant that we were correlating two distinctly different parts of the weather pattern. As a result, the correlation coefficients showed a large negative correlation which did not fit with the positive correlation coefficients of the larger

scales. The values for the 4km domain are also not available since the forecasts all initialized from the same first guess fields with no observations present within the innermost domain.

	Winter COAMPS B.C.	Winter NOGAPS B.C.	Summer COAMPS B.C.	Summer NOGAPS B.C.
108km	0.54382	0.03931	0.10863	0.30328
36km	0.65788	0.386276	0.04164	-0.01080

Table 2. Correlation Coefficients between F00 and F24 forecast 500mb wind speed errors (all cases).

Probably the first fact to notice is that there is not a great deal of correlation in general at any scale for either weather regime or boundary condition. This result might be expected due to the random nature of the various solutions and supports the argument for ensemble forecasting which seeks to take advantage of the random nature of various model solutions by perturbing initial conditions in its ensemble members. The result also suggests, however, that a low error at initial forecast time does not guarantee a low error at F24, even though many forecasters use this rule of thumb when analyzing initial forecast fields.

Secondly, these results also show that there is a greater amount of correlation between initial error and forecast error when the the MM5 "control" boundary conditions are used which suggests that the boundary conditions play a significant role in restricting the growth of various solutions away from their

initial dynamic states. Additionally, the results show that there is generally more correlation between initial error and forecast error during the the more synoptically forced winter pattern. This result also supports the impact the boundary conditions have on the forecast error of the mesoscale since the boundary conditions tend to act more upon those types of weather patterns that are synoptically forced.

Though not as useful due to the fact initial fields for all ten cases were the same at the 4km scale, the 4km domain correlation measurements also present some interesting findings. For both weather regimes and boundary conditions, there appeared to be a grouping of solutions vice a natural spread as might be expected (Figure 13). Unlike the random spread seen at the larger scales, this result does not bode well for ensemble forecasting techniques at mesoscale domain sizes. Of course, we must take into account that the representative sample of solutions (10 per weather regime) is fairly small and larger data sets may prove otherwise.

2. Asymptoting Error Values

Following the reasoning that a better analysis produces a better forecast, another reasonable conjecture is that variance in the initial error for the ten case solutions would remain somewhat constant throughout the forecast and would match the variance of the solutions at F24. This however, was not the case. Figures 8[a,b] and 9[a,b] show that particularly at the 108 and 36km domains,

the initial widespread difference in the various solutions eventually disappear as the forecasts progress and that by F24, there is little difference in the error between the various solutions. In addition, the magnitudes of the errors in these cases seem to asymptote to a particular value, suggesting that there may be some constraint on the wavelengths at which the error is allowed to grow for these domain sizes.

B. THE EFFECT OF SAMPLE SIZE ON ERROR GROWTH

1. Increasing Sample Size

As expected for both the winter and summer cases, when the number of sample observations was increased, the RMS errors in geopotential height decreased proportionally. Figure 14 shows the benefit of increasing the number of observations in the analysis of a particular case. For the winter pattern, the largest benefit is obtained when we increase the number of observations to 200 observations from 100 observations, although analysis error continues to decrease when 400 observations are used. Conversely, the benefit gained in the summer pattern is more consistent between 100, 200, and 400 observations. The rate of RMS error decrease was roughly the same at all levels although there were a few instances where a larger increase was found in the lower levels of the atmosphere.

Figures 15[a-d] and 16[a-d] show the impact on NMFE when the respective analyses for 100 and 200 point samples are used to initialize the MM5 model forecasts. The 400 point sample was not used to initialize MM5 due to analysis problems with some variables. The three curves on each plot show the 500 mb error growth for case c148954 with 100 points, the growth curve when 200 points are used, and the standard deviation about the mean wind speed, by which we are measuring forecast skill. The results showed that the increased observations impacted the error growth differently for each type of weather pattern, boundary condition, and domain size.

a) *Impact by weather regime*

Using the increased number of observations seemed to decrease the error for most scales more in the winter than in the summer, regardless of which boundary condition was used. For the summer regime, there was almost no benefit at all at the 108km domain (Figure 16a). This result suggests that the synoptically driven forcing of the winter pattern benefitted more from the added number of points since it was better able to define the synoptic scale features. Since the synoptic features were not as crucial during the summer, the benefit was not as great, particularly at 108km. There is some question about whether the improvement gained by increasing the number of observations in the winter pattern is significant. The answer to this question must take into consideration the specific requirements of the operations requiring the forecast information.

b) *Impact by boundary condition*

For the winter case, the MM5 "control" boundary conditions provided more benefit than when the NOGAPS boundary conditions were used. For the summer pattern, there was little difference between the boundary conditions, neither of which seemed to have a significant impact. A particularly interesting result was that both sets of boundary conditions for both weather patterns seemed to negatively impact the error growth of the 200 sample point case when they were applied at F12. At the larger scales(108 and 36km), applying the boundary conditions seemed to increase error relative to the 100 point sample, while at the smaller scales (12 and 4km), the 200 sample point case actually had greater error than the 100 point case! This was particularly evident for the summer pattern on the 4km domain (Figure 16d). This plot suggests that at least for this case, the initial benefit in the forecast gained by adding more observations is erased when the boundary conditions are applied. Similar experiments with the other cases and different weather patterns may prove otherwise. It should be noted that the influence of the boundary conditions should also decrease as one goes to the inner domains .

c) *Impact by domain size*

Comparing the impact of the increased sample size across the domain sizes showed that for the winter pattern, the decrease in error was about the same while for the summer pattern, there was a greater benefit gained at the

smaller scales. The character of the error at the larger domains remained basically the same between the 100 and 200 sample point cases.

It should be noted that at the 4km domain for both weather patterns, the standard deviation about the mean wind speed of the control is lower than the error associated with the forecasts (see Figures 15d and 16d). Thus in essence, these forecasts have almost no skill. At this scale, the benefit of increasing the number of observations is related to the skill or predictability of the forecasts. For the summer regime (Figure 16d), the 100 sample point case has no initial skill and only gains skill around F12. The 200 sample point case however, has skill from about F04 to about F16 when the error growth curve exceeds the standard deviation curve. The winter regime (Figures 15d) is even less promising as it essentially has no skill at any time in the forecast.

These results point to the fact that increasing the number of sample points at initialization of a mesoscale model does not always guarantee less forecast error at the smallest nest, but does generally reduce error at larger scales.

2. NOGAPS Firstguess Forecast

Another experiment we performed related to sample size was to run the forecast model without any observations. The input into the model would thus only be driven by the NOGAPS first guess fields and the MM5 model physics. The results of this comparison are shown in Figure 17[a,b] for the winter case using the MM5 "control" forecast as the boundary conditions. As expected, the

forecast error associated with a solution containing no observations was much higher than those cases that were initialized with observations, particularly at the 108 and 36km domains (Figure 17a). However, this was not true at the inner nests of 12 and 4km. Figure 17b shows the 500mb RMS wind speed error for the winter regime at the 12km and 4km domains. Note that the firstguess solution shows no real skill at these domain sizes at any time in the forecast whereas it does show relative skill at the 108 and 36km domains. Note also that for the first seven hours of the forecast, the NOGAPS firstguess solution has comparable errors to the solutions that were initialized with observations. By F08 however, the firstguess solution dramatically increases in error and remains high throughout the rest of the forecast cycle. Thus, synoptic scale observations seem to have little benefit in the initial hours of a mesoscale forecast at the smallest nests of the mesoscale model.

C. THE EFFECT OF LATERAL BOUNDARY CONDITIONS ON ERROR GROWTH

One of the more surprising results of the various experiments we performed was the impact that varying boundary conditions had on the character of the error growth. In his early studies of predictability of a limited-area model, Anthes (1986) suggested that by supplying accurate lateral boundary conditions (LBCs) on the outer domain throughout a forecast, the error growth at the mesoscale would be limited. This result was realized when we used the MM5

control forecast as the boundary conditions for the MM5 forecasts. Figure 18 shows the 500mb RMS wind speed error growth (or rather decay) curves for the winter and summer synoptic patterns at the 108km scale when the MM5 control forecast was used as the boundary condition. The downward trend in error is contrary to general predictability theory and the limiting error growth is true irrespective of the weather regime, being observed in both the winter and the summer patterns. Though not shown, a similar result was also found for the 500mb RMS geopotential height errors. The cause of this trend can be explained by the requirement that the forecasts at set intervals (here every 12 hours) meet the conditions of the boundaries provided by the "truth" thus eliminating the errors which may have propagated in from the boundaries at longer wavelengths. This result is supported by the observation that at the outer domain (108 km), both wind speed and geopotential height error growth curves for all ten case runs show a definitive convergence at the forecast times where the boundary conditions were interjected. This was followed by a divergence as the model resumed its characteristic deviation in solutions.

Using the MM5 control as the boundary conditions for the forecasts was of course an indication of the lower bound of the error growth and so in order to provide a more realistic view of the error growth in operational settings, NOGAPS was used as the boundary conditions for the MM5 forecasts. Figure 19 shows the resulting 500mb RMS wind speed error growth when the NOGAPS boundary conditions were used for the winter pattern. As shown, the character of the error

is significantly different than the forecasts which used the MM5 control boundary conditions. The upward trend in error growth is more representative of predictability theory and the realistic errors that can be introduced by inaccurate LBCs. Figure 20 shows the average RMS wind speed error growth (or decay) of the ten random solutions for the winter pattern. One might think of this plot as the ensemble average of the winter pattern forecast error. This plot shows how significant lateral boundary conditions are to the character of the error growth (or decay). Though the initial error is very similar, the error growth curves diverge at around F06, and by F24 the average of the solutions between the two sets of boundary conditions show almost a 4 m/s spread in wind speed error.

D. THE EFFECT OF MODEL SPIN UP ON ERROR GROWTH

We observed that in the forecast runs for each case, the model required a certain amount of time to spin up the mesoscale structure not present at F00. This was particularly evident at the 4km domain as seen in Figures 8d and 9d, where no mesoscale structure was present at F00. By about F06, there was a considerable spread in the solutions provided by each random case, essentially defining the maximum variance in the error for the forecast cycle. The requirement that the model "spin up" the mesoscale structure in the forecast by initializing directly from a synoptic scale model analysis or forecast is often termed a "cold start" at operational numerical forecasting centers (Hodur 1997). Monterossa (1999) documented the impact of cold starts on a mesoscale

forecast showing that in some cases, forecasts were actually better when a “cold start” was performed. The observable error growth using a previous 6 hour forecast, which is known as a “warm start,” was not performed during this study although comparing the results might prove interesting.

Additionally, almost every error growth curve at all domains for both weather regimes and boundary conditions showed an initial downward trend in error, which is also attributable to the effects of the model spin up. Recalling the theoretical NMFE growth curve in Figure1, this initial downward trend reaches an error minimum before the forecast error begins to grow. This is the point at which the model’s initial state becomes consistent with the physical equations that govern the model’s behavior. Another interesting study for future research would involve manipulating the initial conditions in such a way as to achieve the lowest error minimum for the longest period of time.

E. WEATHER REGIME DEPENDENCIES

1. Kinetic Energy

As expected, there also appeared to be a weather regime dependence in the error growth characterized by smaller error values for the summer case than for the winter case. The reason for this can be assumed to be the smaller amount of kinetic energy associated with the summer regime. The benefit gained from increasing the number of observations was also less distinct in the summer

regime than in the winter regime for the same reason. It should be noted, however, that the relative size of mesoscale error for both weather patterns when compared to the mean values of those patterns were similar. In other words, the summer pattern was not any more predictable than the winter pattern just because the magnitude of its errors were less.

2. Unique Mesoscale structure

We noted that for all the case runs, the type of mesoscale structure present seemed to impact the character of the error growth at certain times in the forecast runs. For example, in the winter case at the 4km domain, there was a sharp increase in 500mb RMS wind speed error at F18 followed by a sharp decrease in error. As mentioned earlier in the description of the winter weather pattern, the passage of the cyclone's cold front occurs around this same time. This trait is also reflected in the 500mb wind speed errors bias (Figure 21), which shifted significantly from positive pre-cold front to negative post-cold front (recall that bias estimates were performed by subtracting the random case from the "control" case). For the summer regime, the character of the error throughout the forecast cycle was fairly constant due to the less well defined mesoscale structure of this pattern (see Figures 9[a-d]). Furthermore, there was no jump in error for the summer case primarily because the sea/land breeze feature that was present is thermally forced by the well known surface boundary and is spatially fixed in the domain throughout the forecast. The winter frontal structure

however, is forced on all sides throughout the column and moves in space as the forecast develops. Thus, the winter pattern showed a more perceptible jump in error.

F. DOMAIN SIZE DEPENDENCIES

There was also a difference in the way that errors grew between scale sizes. In general, there was less error at the larger domain sizes while error magnitudes increased with decreasing scale sizes, reaching 10m/s for some solutions at the winter pattern's 4km domain (Figure 8d). Again, this was more evident with the winter pattern than in the summer pattern. This result combined with the larger errors at the smaller scales suggests that mesoscale structure is more important at these scales.

Note in Figures 8d and 9d that each of the random case solutions start with the same error value at F00 at the 4km domain. This is due to the fact that no observations were located within this domain size at initialization and thus each case was initialized with the same NOGAPS first guess fields. After initialization, the error growth curves depart due to the impact of the observations at the larger scales.

Comparing the random case solution's error growth curves with the standard deviation about the mean of the control forecast shows that model skill decreases with scale. While all the model solutions show skill throughout the entire forecast at the 108 and 36km domains, some of the solutions begin to lose

skill at 12km in the winter pattern. At the 4km domain, there is little to no skill at all, regardless of weather pattern or boundary condition.

G. SYNOPTIC SCALE INFLUENCE ON THE MESOSCALE

One of our hypotheses stated that variation in the observational sampling pattern at the synoptic scale leads to variation in analyses that directly impact error growth and predictability in mesoscale forecasts. Some of the more interesting results we found throughout the course of this work dealt with how synoptic scale error impacts mesoscale error.

1. Synoptic and Mesoscale Correlation

Contrary to our hypothesis and general consensus among forecasters (Gunderson 1999), there was not a great amount of correlation between the errors on the synoptic scale and those on the mesoscale. Figure 22 shows the correlation scatter plots of 500mb wind speed errors between the 108km and 4km domains for both weather regimes and boundary conditions. Table 3 below summarizes the correlation coefficients between the synoptic scale (108km) and mesoscale (4km) 500mb wind speed errors. All random cases and all forecast times are included in these calculations.

10 cases x 24 fcst times = 240 pts	Winter	Summer
COAMPS B.C.	0.05694	0.407778
NOGAPS B.C.	0.47736	-0.00923

Table 3. Correlation Coefficients between synoptic scale (108km) and mesoscale (4km) 500mb wind speed errors (all cases, all forecast times)

It is evident from these results that there is not much correlation between the synoptic scale and mesoscale errors regardless of weather regime or boundary condition. Even the winter pattern using NOGAPS as boundary conditions which has the greatest amount of correlation shows a rather bi-modal distribution on its scatter plot diagram. These results must be somewhat tempered since the RMS errors we calculated were calculated across the entire domain for each domain size. Thus, the low correlation values between the 108km and 4km scales are expected.

2. Scale Separation of Error

The scale specific 500mb wind speed error for case c148954 on 980206/00zF12 is shown in Table 4. These values were obtained by first projecting the three larger scale fields from both the random case run and the MM5 "control" onto the 4km grid scale (Figure 7). We then created the difference fields by subtracting the scale specific fields of the case from the

control fields. RMS and bias errors were then calculated from the difference fields.

	RMS (m/s)	BIAS (m/s)
108km	1.95 (46%)	-1.41
36km	1.02 (23%)	-0.35
12km	0.86 (20%)	-0.05
4km	0.45 (11%)	0.02
Total	4.28	-1.79

Table 4. Scale separation of 500mb wind speed error for 980206/00zF12 (case c148954)

As can be seen by the results listed in Table 4 above, the majority of the total error at the smaller scales is due to the characteristic error of the synoptic scale. The summation of the errors at each scale also shows, however, that our initial assumption about the independence of the errors at each scale was not completely correct. The calculated RMS error on the 4km domain which should be a sum of all the representative scale errors was 2.5 m/s while the summed value above, calculated by separating out the representative scales and then summing them is 4.28 m/s. This suggests that that the error at the smaller scales is not exactly additive and we have not accounted for all of the scale interactions actually present. This fact however, does not change the fact that the largest amount of error at the 4km scale is still dominated by 108km scale error present on the 4km domain.

THIS PAGE INTENTIONALLY LEFT BLANK

IV. DISCUSSION

Further examination led us to develop some possible reasoning behind the results we achieved from our experiments. Though limited to two case studies, the analysis of these results have shed considerable light on the character of numerical model error on the mesoscale and the limits of predictability on these scales. The discussion in this section will thus explain the results from the previous section in more detail and will tie key concepts together.

A. CHARACTERISTIC WAVELENGTHS

On the outer (108km) domain, the model error has a characteristic wavelength which is based on the domain size, location, and the distance between the observations. Numerical models can resolve features that have wavelengths of $2\Delta x$ or greater, where Δx is the observational spacing. Thus, a typical observational spacing of 200km for instance, will allow the model to resolve wavelengths on the order of 400km (Nuss 1998). Domain size and location is also important when considering a specific weather system as in this study. For example, in the winter regime, the 108km domain was situated in such a way as to be able to capture the entire long wave trough and its associated short wave pattern. Thus, error associated with timing and location of

that trough was fairly accurate when compared to a domain location that may have only captured a portion of the trough.

Many of the findings of our study seemed to indicate that there were characteristic wavelengths of error that were allowed to grow while other wavelengths were unresolvable. The effect of the various domain sizes as well as the number of observations on the error growth both point to this conclusion. The value to which the error asymptoted at F24 for the outer two domains can be thought of as the error associated with the minimum resolvable wavelength at those domain sizes. We can expect this value to change with different combinations of domain size, location, and observational spacing. For example, increasing the number of observations in our study reduced the spacing between the observations (Figure 4), effectively reducing the size of the wavelengths that could be resolved. As a result, the magnitude of the error was reduced.

B. LATERAL BOUNDARY CONDITIONS

Related to the characteristic wavelength of the error due to domain size and location is the understanding that the different lateral boundary conditions imposed on the model in effect limited the wavelengths of the allowable solutions at the largest domain. The error growth at this domain then consists only of the error associated with the scales that could freely grow within the domain. For this reason, when the MM5 "control" forecast was used as the boundary

condition, the error for all cases actually decreased with forecast time, because the conditions at the boundary had to be met. Of course, this also occurred when NOGAPS was used as the boundary condition but since the NOGAPS conditions didn't maintain as strict a control over the true mesoscale structure of the system as the "control" conditions, certain wavelengths that were fixed under the "control" boundary conditions were allowed to grow under the NOGAPS boundary conditions. This resulted in the conventional error growth that we observed in Figures 8 and 9.

The significant influence of the lateral boundary conditions on the outer domain and therefore the character of the error at all domains is further supported by the results of the scale separation experiment we performed. These results showed that the error at all domains is dominated by the error at the largest domain, which is primarily influenced by the boundary conditions.

Recalling the result of the reversal of the error at F12 when 200 observation points were used adds further insight into the impact of the boundary conditions. Increasing the number of observations from 100 to 200 points caused the dynamic structure of the field to be better defined, making it become, in essence, more sensitive to the impact of the boundary conditions. This, in turn, created a larger error when compared to the less sensitive 100 point case.

The sensitivity of a particular regime to the boundary conditions is also confirmed when we compare the impact of the boundary conditions on the different weather regimes. The winter pattern, which was a synoptically forced

system, was particularly sensitive to the boundary conditions while the summer regime was not. The summer pattern on the other hand was dominated primarily by local forcing and had a less well-defined mesoscale structure.

It is clear from the various ways in which we examined the effect of the boundary conditions on error growth, that lateral boundary conditions play an important role in the character of error at all scales. Especially for the case of a synoptically forced system such as the winter pattern in our study, it is more important to have accurate boundary conditions at the outer domain than to have lower initial error when trying to achieve the best mesoscale forecast.

C. SYNOPTIC SCALE INFLUENCES

One of the difficulties of understanding error at any scale is being able to get at the unique error associated with that scale while still maintaining a proper perspective of the influences other scales have on the total error. Though only performed for a single case, the findings from the scale separation experiment showed that total error in a mesoscale forecast is dominated by error at the largest scales. This may explain why common mesoscale forecasting experience has shown that even though errors are large at the mesoscale, mesoscale forecast fields look reasonable and are useful tools for the forecaster. Although the correlation measurements between the synoptic and the mesoscale error were not as definitive as we might have hoped, we must consider that we did not correlate the exact representation of the synoptic scale error on the 4km

domain with the error unique to the 4km scale. Rather, we correlated the error across the entire 108km domain with that across the significantly smaller 4km domain. When this is considered, the small correlation coefficients were a reasonable result. We should not expect that there would be a great deal of correlation between error across so large a domain with error on such a small domain. The understanding the forecaster must have however, is that synoptic scale error does impact the error at the mesoscale, but that the correlation of such error is only significant at the domain size of interest. Thus, even if a model seems to be handling the synoptic scale pattern well, if the synoptic scale error is large in the location of the mesoscale nest, there will be a great deal of error associated with the mesoscale forecast.

Our findings with the scale separation experiment also showed that error at each scale is not truly separable. The error at a specific scale is more likely to be the integral of error contributed by all the wavelengths represented. Since our assumption was based on a finite differencing approach to the calculation of the total error based only on the scales included in the nested grid, our results did not completely match up with our expectations. Furthermore, even though the smaller nested domains are linked to the larger domains, they are still in essence separate forecasts. Thus, the larger scale fields we projected onto the 4km grid did not completely correspond at every grid point.

D. OBSERVATIONAL SAMPLE SIZE AND DISTRIBUTION

The random distribution of observations in this study provided unique insight into the error variance associated with different model solutions. The fact that our findings suggest very little correlation between analysis error and 24 hour forecast error was particularly enlightening.

It was clear from the results of the scale separation experiment that the spread in the various cases at the smaller domains as seen in Figures 8d and 9d was due to the small differences at synoptic scales exciting particular mesoscale frequencies. Thus, the spread is in essence the measure of the sensitivity of the small scale error to synoptic scale differences. For our study, the winter case was more sensitive most likely because of its higher kinetic energy, more well-defined mesoscale structure, and the fact that it was a synoptically forced system.

Increasing the number of observations from 100 to 200 points at initialization showed that more points does not always equal a better forecast, particularly at smaller scales. The added observations must define realistic and dynamically significant mesoscale structure in order to provide any benefit.

E. WEATHER REGIME DEPENDENCIES

It was clear that there were some weather regime dependencies on mesoscale error growth and predictability. However, the weather regimes did not play as great a role in influencing the error growth as the boundary conditions

did. In general, the more mesoscale structure and kinetic energy a system has, the more likely it will be to have greater magnitude errors and the more likely it is to be influenced significantly by the accuracy of the boundary conditions. Weakly forced systems, such as the summer pattern in this study, are not greatly influenced by error at the boundaries. Initial error in the summer pattern was high and error remained saturated throughout the forecast cycle, particularly at the 12km and 4km scales. This suggests that we do have a great amount of skill at these scales, even at initial times in the forecast.

Though we did not address specific mesoscale features directly influenced by topography, we may assume that the magnitude of the error associated with the summer pattern was less than that of the winter pattern in part because most of the mesoscale structure was forced by the surface. This fact requires that in order to ensure that mesoscale structure will be correctly forced, the model's representation of the topography must also be accurate. Current mesoscale model topographies smooth out many significant features in addition to misrepresenting elevations (Monterrosa 1999), making the calculation of error at the smallest scales even more complex. Performing a study of the error associated only with the representation of the topography would be a worthwhile future endeavor.

THIS PAGE INTENTIONALLY LEFT BLANK

V. CONCLUSIONS

The results of this thesis have shown that although there have been some marked improvements in mesoscale forecasting, there are still some questions with regards to how accurate we can be at the smallest domain sizes. We showed that error growth is affected by many different variables, some of which we can control and others which we cannot, but all of which we must understand in order to provide accurate forecasts. Specifically, we showed how error growth on the mesoscale is dependent upon:

- Lateral Boundary Conditions
- Weather regime
- Sample size and distribution
- Synoptic scale error
- Domain size

For these specific model solutions, we also showed the relationship between:

- Analysis error and forecast error.
- Synoptic scale error and mesoscale error.
- Unique error at different scales through scale separation.

A. MESOSCALE CERTAINTIES AND UNCERTANTIES

Many of our initial expectations and hypotheses were confirmed by the results of the various experiments while other results were more surprising. Some results actually varied from previous work in this field. For instance, unlike Anthes' (1986) results, which showed that 72-hour simulations in limited-area models are not sensitive to random uncertainties in initial wind, temperature, and moisture fields, our results have shown that even in a 24 hour simulation, error growth does occur at the 4km scale.

The following statements reflect the summary of our findings and help to clarify those ideas which we hope will add to the understanding of mesoscale error growth and predictability.

1. **Lateral boundary conditions** – LBC's play a critical role in defining how error grows, particularly for weather patterns that are synoptically forced such as the winter regime in this study. The stronger the synoptic scale forcing, the more important the boundary conditions become in interjecting error or correcting error in the forecast.
2. **Weather patterns** - For weather patterns that are weakly forced such as the summer regime in this study, error growth remains small throughout the first 24 hours. Initial error is large for these systems at all scales and becomes quickly saturated throughout the forecast cycle.

3. **Forecast skill** - For these cases, there was little to no forecast skill at the 4km domain when comparing error to the standard deviation about the mean of the control field.
4. **Synoptic and mesoscale correlation** - There is very little correlation between synoptic scale error and mesoscale error, hence, a good synoptic scale forecast does not guarantee a good mesoscale forecast. According to the scale separation of error, however, synoptic scale error dominates the error at the mesoscale. Thus, a poor synoptic scale forecast will also result in a poor mesoscale forecast, particularly if the error is located at the domain of interest.
5. **Analysis and Forecast error correlation** - While correct sampling of the atmosphere through sample distribution is critical to ensuring good analyses, there is very little correlation between initial error and forecast error. Thus, a good analysis does not guarantee a good 24 hour forecast, particularly for weakly forced weather regimes.
6. **Sample size** - Error is generally reduced when more observations are used at initialization, particularly at large domain sizes for weather regimes that are synoptically forced. Also, some observations are better than no observations when calculating error growth. Increasing the number of observations for a nested grid, can in some cases increase error at the smallest nest.

B. FURTHER RESEARCH

The unique approach of this study and the relative ease of its implementation opened up a vast number of opportunities for further research. The advantage of using numerical experiments in a controlled "ideal" atmosphere cannot be overlooked. The consistency we were able to produce with our results and the certainty we gained by comparing the model experiments to an ideal atmosphere added to the validity of this research approach. The following suggestions represent possibilities for further research and study in the subject of mesoscale model error and predictability.

1. Vary Weather Regimes and Geographic Locations

Natural atmospheric variability as well as the growth rate of small errors varies with geographic locations and synoptic pattern (Anthes 1986). While this study provided a good representation of the typical weather regimes found in the winter and summer off the west coast of the U.S., performing this study for other weather patterns in other geographic locations would lend more credibility to our results. This is especially important since most of the error across the smaller domains in the nested model were linked to the topographic features common to the West Coast of the U.S.

2. Calculate Error Growth Using other Model Parameters

While the error growth and predictability patterns we found were consistent for the two model parameters we studied (wind speed and geopotential heights), this may not be the case for all variables. Further results could easily be obtained for temperature and moisture parameters in the forecast model, which would add more depth to the results we have shown.

3. Better Experimental Design

Some constraints were placed on this study due to choices that were made early on and better experimental design would lead to more robust results. The most useful of these changes would be to represent the control and experimental forecasts at the full 40 levels within the MM5 model. This change would result in more accurate error growth calculations. In addition, we could have calculated the true model error within the study and then subtracted it out from the total error.

Another design change would include adding a second model initialization method. All of the results in this study were performed with a model initialized from a "cold" start. If a "warm" start initialization was also performed, we could compare the resulting error growth with the "cold" start results and draw some conclusions on which method produced better forecasts.

Thirdly, while the controlled environment of this study afforded great flexibility in design, the use of real time observations to calculate error would help to support some of the results we found.

4. Error Growth Compared to Synoptic Forecast Over Time

While we did perform a forecast experiment by using only the synoptic scale NOGAPS fields to initialize the mesoscale forecast, it would certainly be interesting to calculate error growth statistics for a completely synoptic scale forecast. This may answer the question: "Can a synoptic scale forecast actually be a better forecast than a mesoscale forecast?"

5. Use of Spectral Analysis to Perform Scale Separation

The scale separation experiment provided some interesting results which could easily be repeated for different weather regimes and forecast times. However, since our results showed that we were not able to capture the error specific to all wavelengths, a spectral analysis of the error might be a good approach in performing scale separation in the future.

6. Topography

Topography played a major role in the character of the error throughout this study, yet the model topography within the model was much smoother than

reality. If the forecast error specifically due to topographic errors was able to be removed, a more accurate representation of error growth could be given.

THIS PAGE INTENTIONALLY LEFT BLANK

APPENDIX A. FIGURES

The following pages of figures are grouped together in this appendix in order to facilitate the reading of this work.

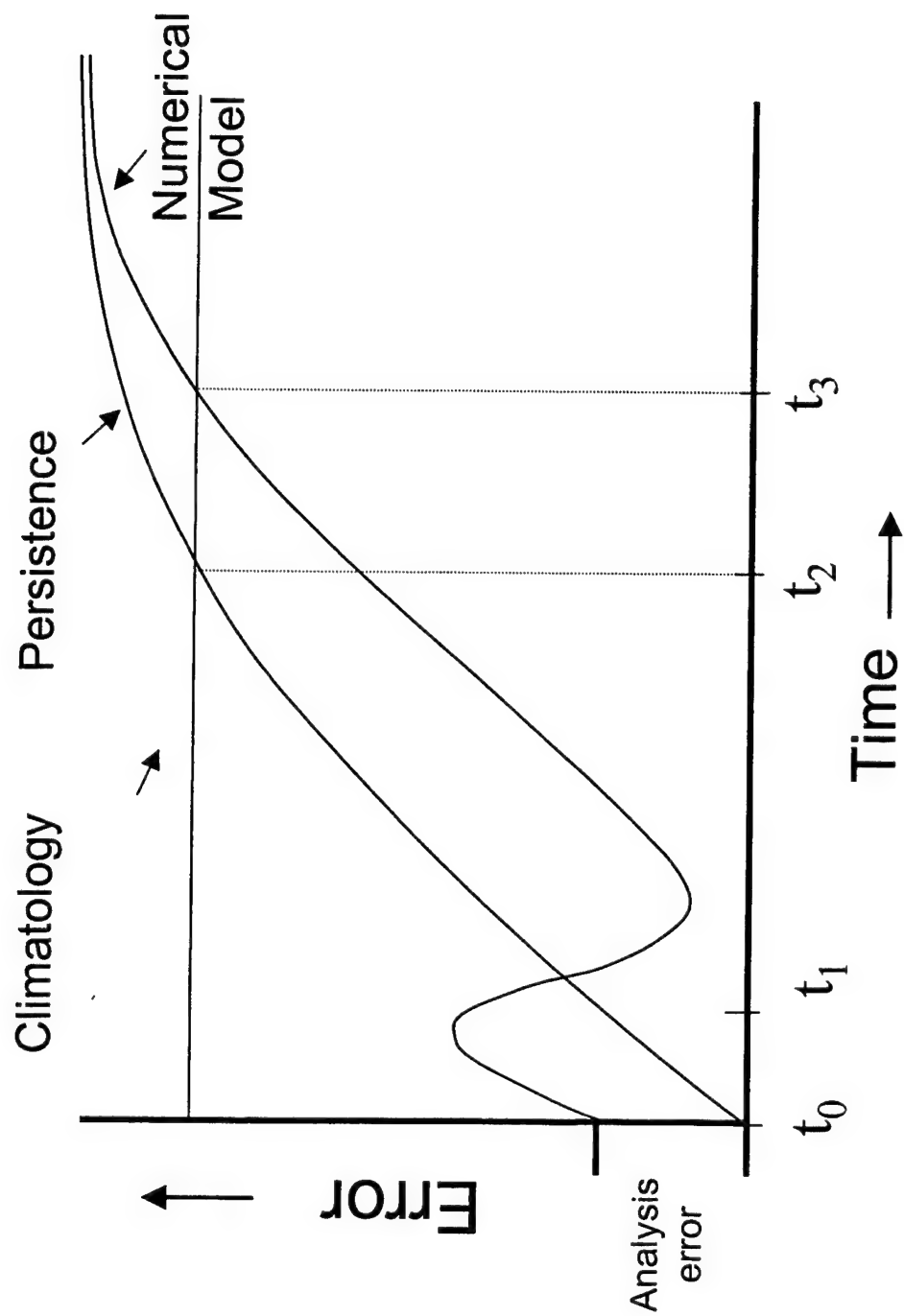


Figure 1. Theoretical NMFE growth curves

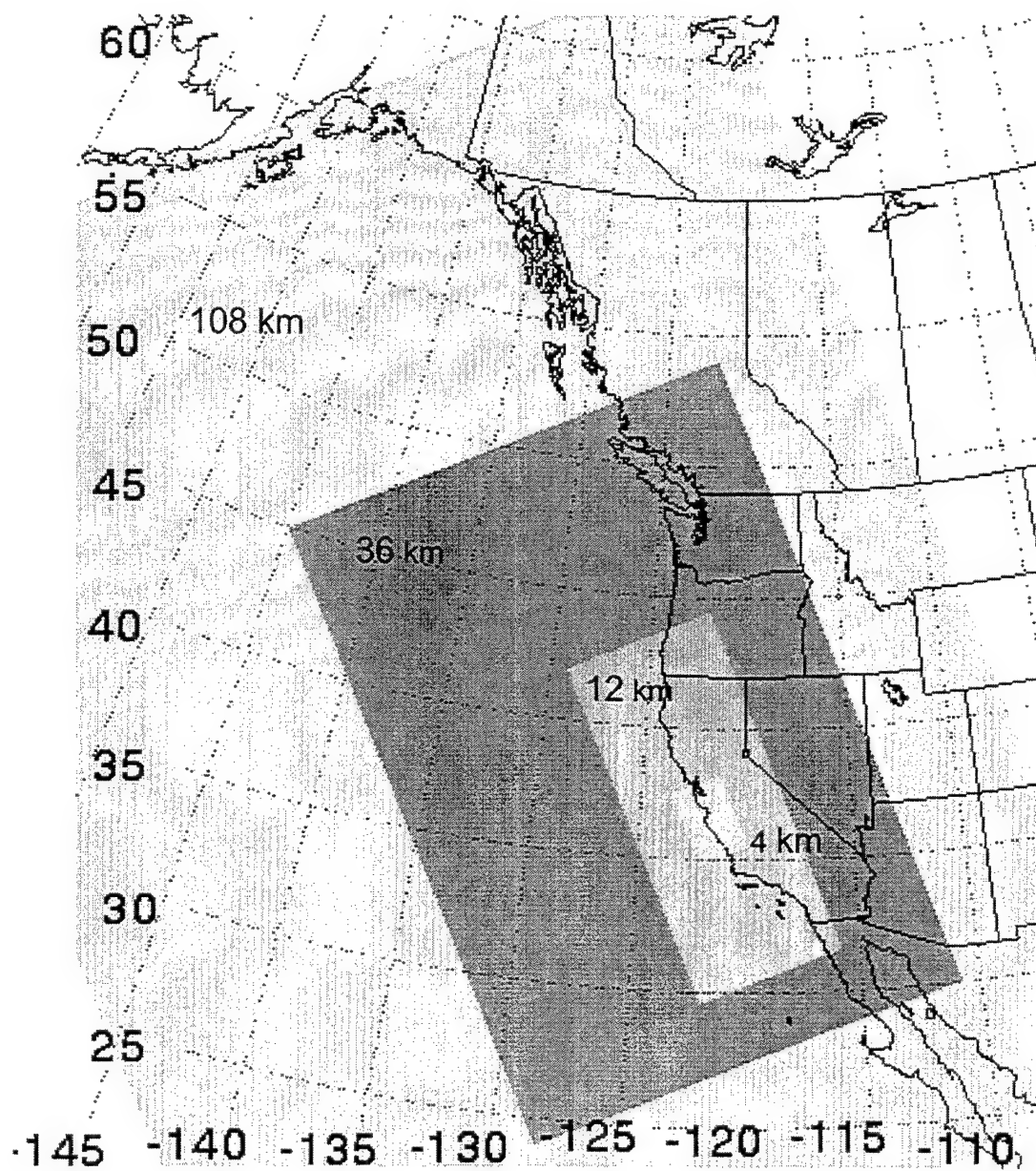
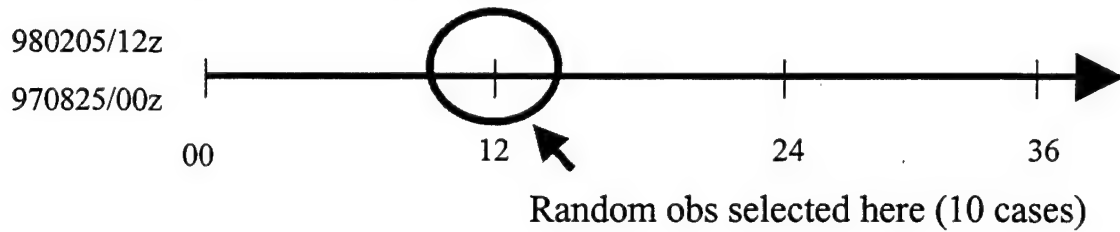


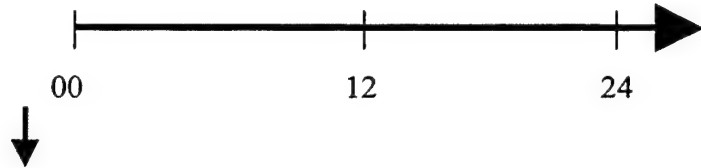
Figure 2. Domain sizes for the experiment's nested grid.

Ideal Atmosphere Schematic

Step1. Original COAMPS truth at 40 levels

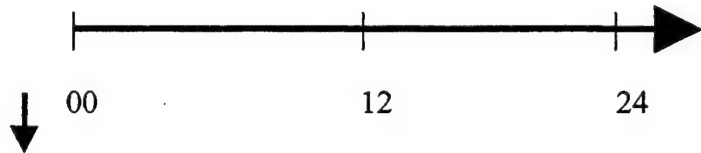


Step 2. MM5 “control” at 12 levels (interpolated down from above)



Step 3. Experiments using MM5 at 12 levels (10 cases)

(NOGAPS 1st guess at 12 levels + random obs from COAMPS truth)



Step 4. Error Growth calculations

Error = “control” - experiment

RMS and bias

- geopotential height
- wind speed
- at 500 mblevel

Figure 3. Schematic diagram describing the design of the ideal atmosphere for the study.

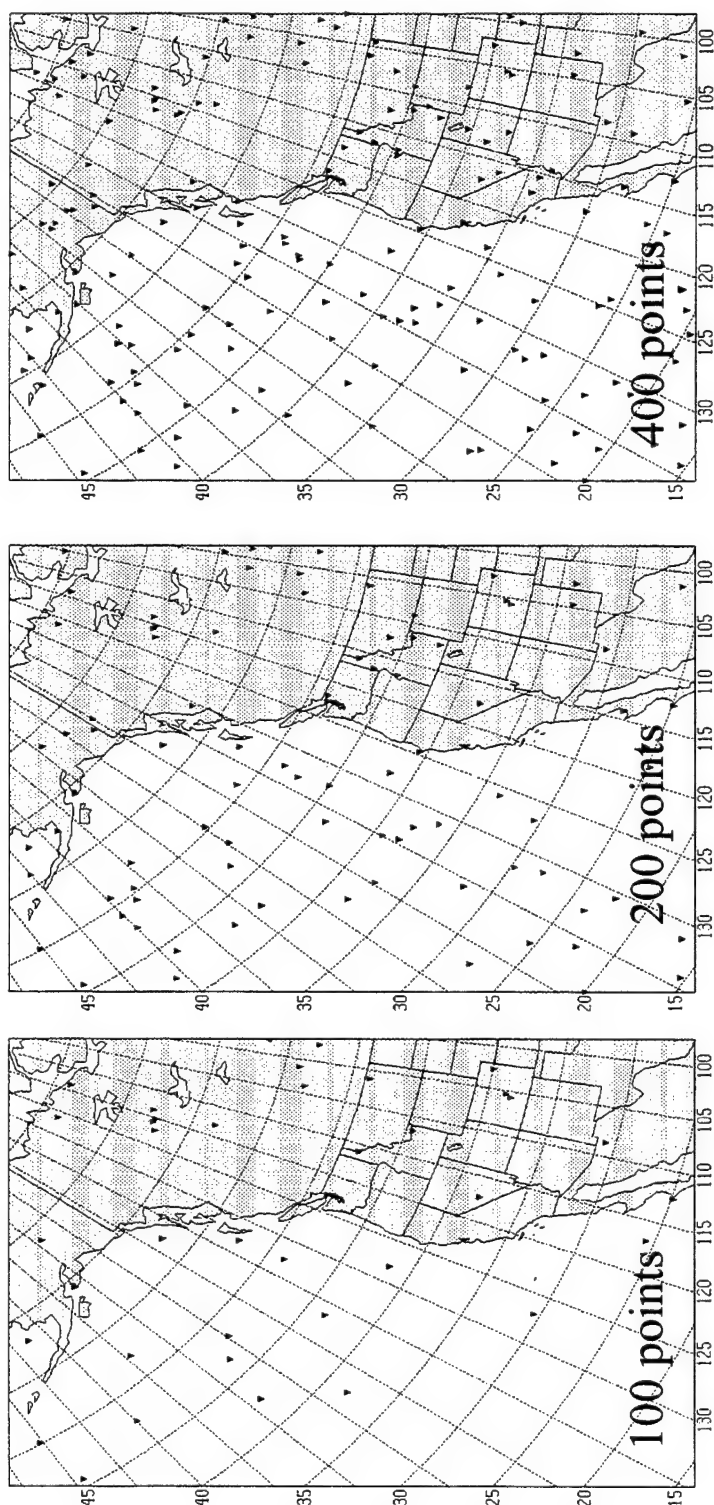


Figure 4. Random distribution of 100,200, and 400 observations for case c148954.

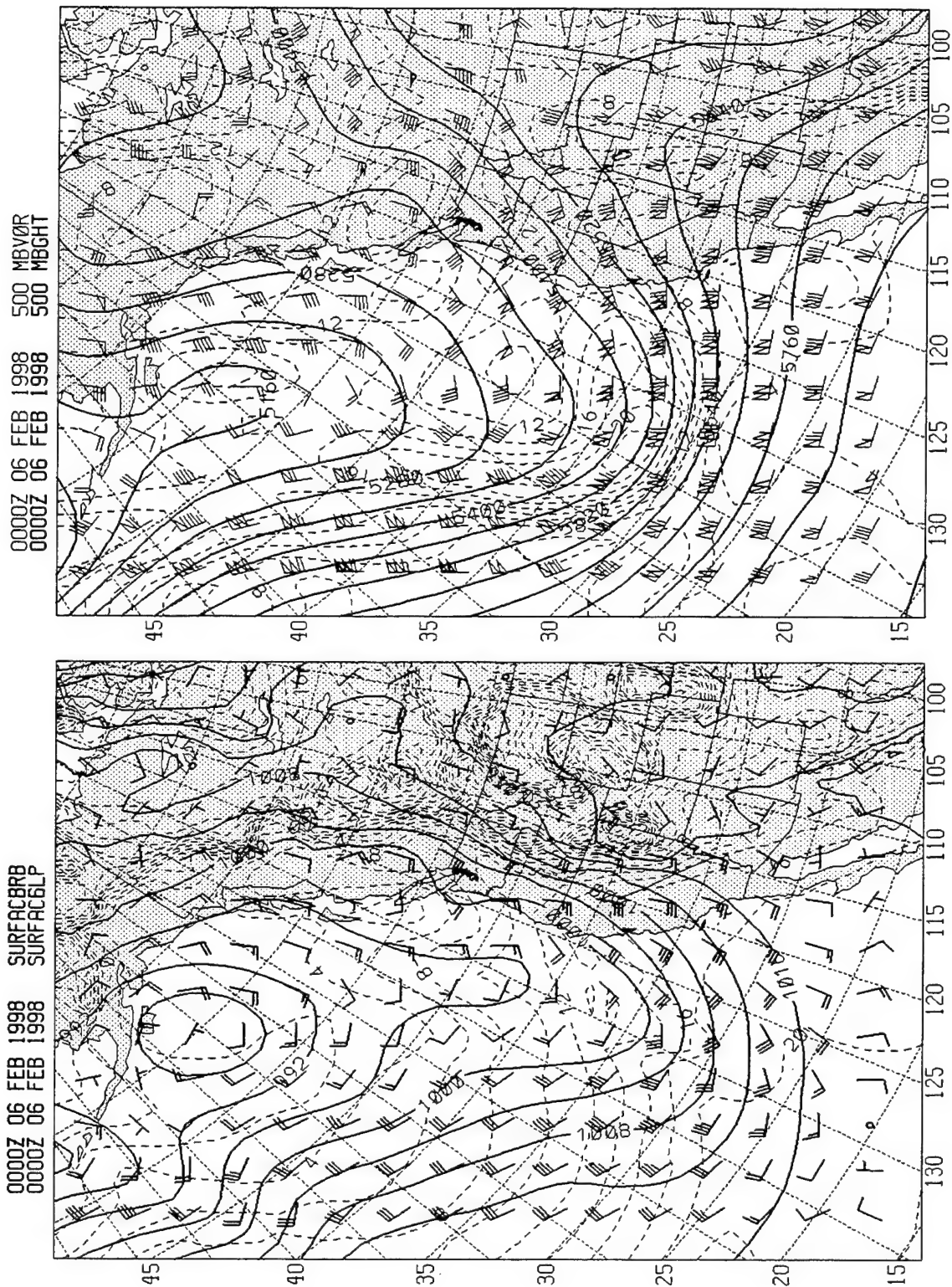


Figure 5a. MM5 control F00 forecast for winter pattern. Fields are 500mb geopotential hts,vorticity, and winds (top) and surface pressure,temperature, and winds(bottom).

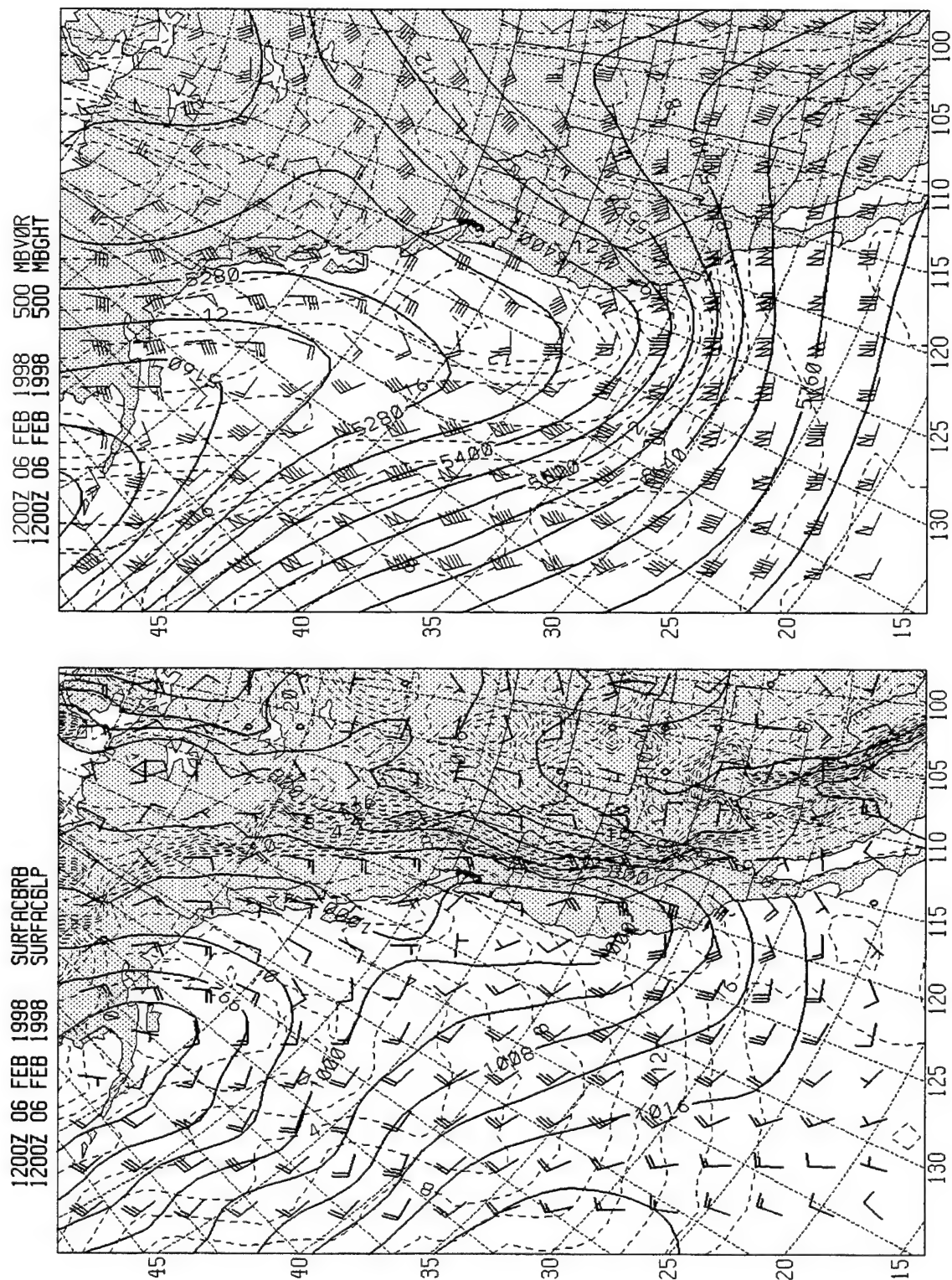


Figure 5b. MM5 control F12 forecast for winter pattern. Fields are 500mb geopotential hts,vorticity, and winds (top) and surface pressure,temperature, and winds(bottom).

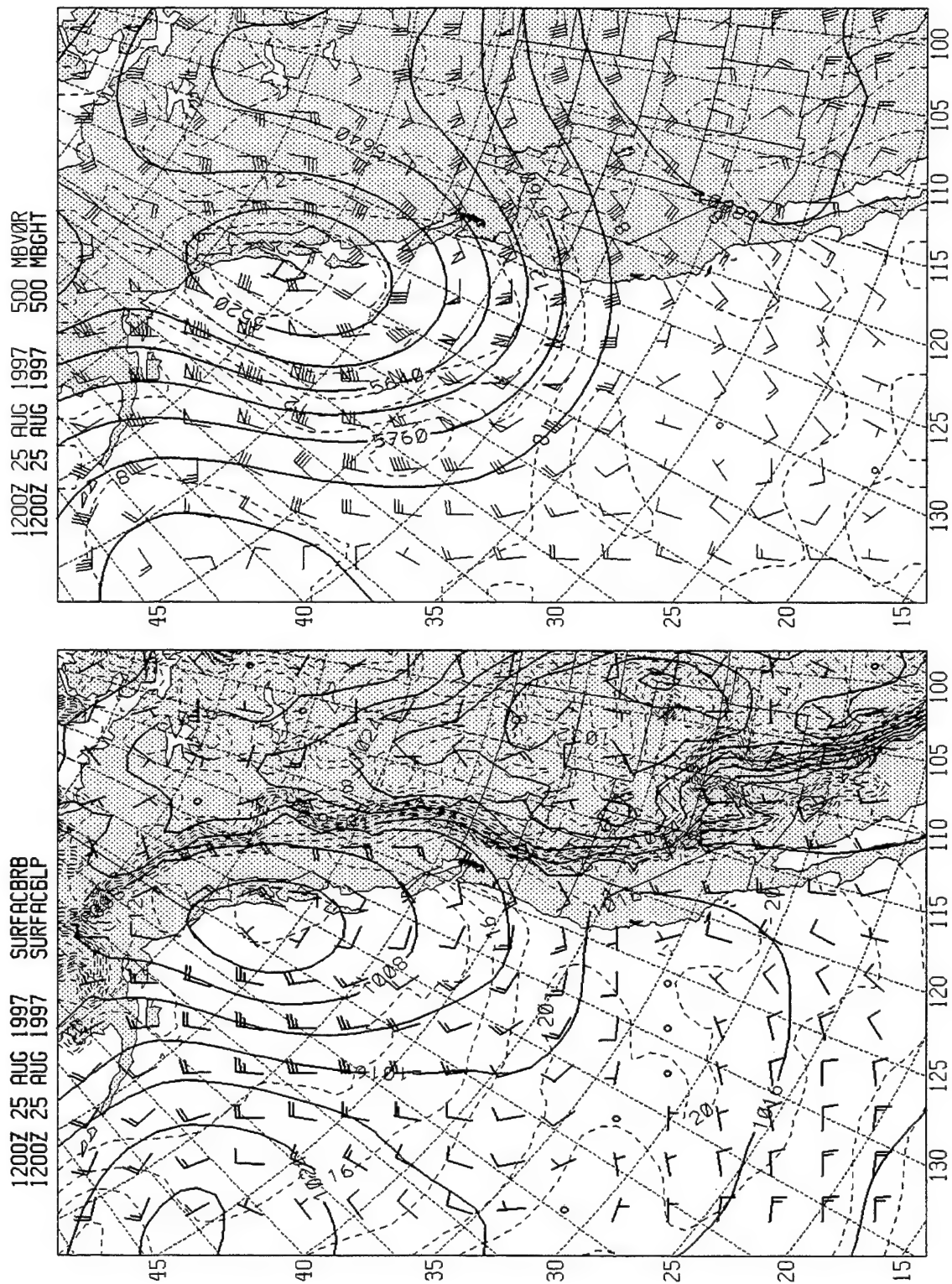


Figure 6a. MM5 control F00 forecast for summer pattern. Fields are 500mb geopotential hts,vorticity, and winds (top) and surface pressure,temperature, and winds(bottom).

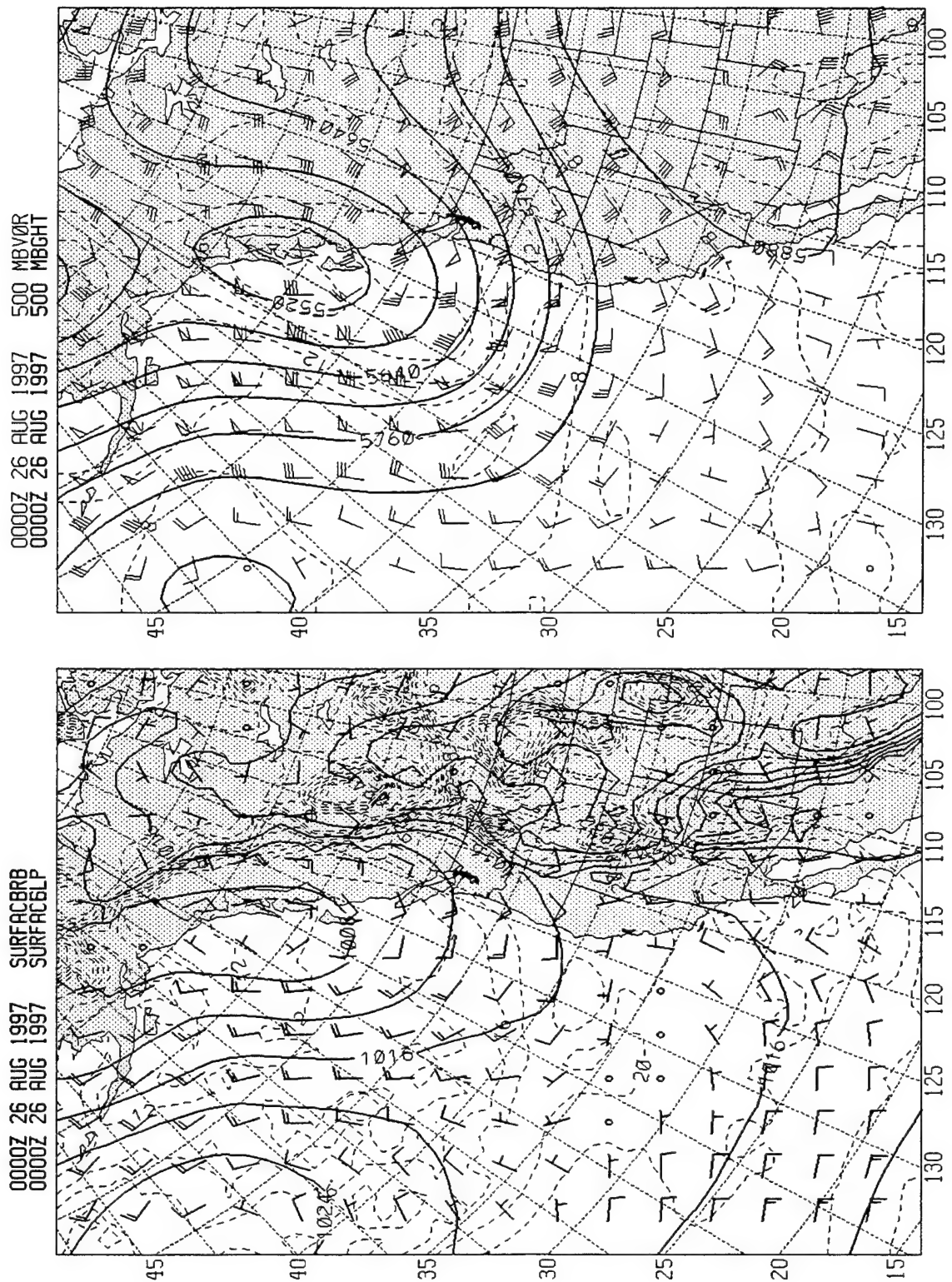


Figure 6b. MM5 control F12 forecast for summer pattern. Fields are 500mb geopotential hts,vorticity, and winds (top) and surface pressure,temperature, and winds(bottom).

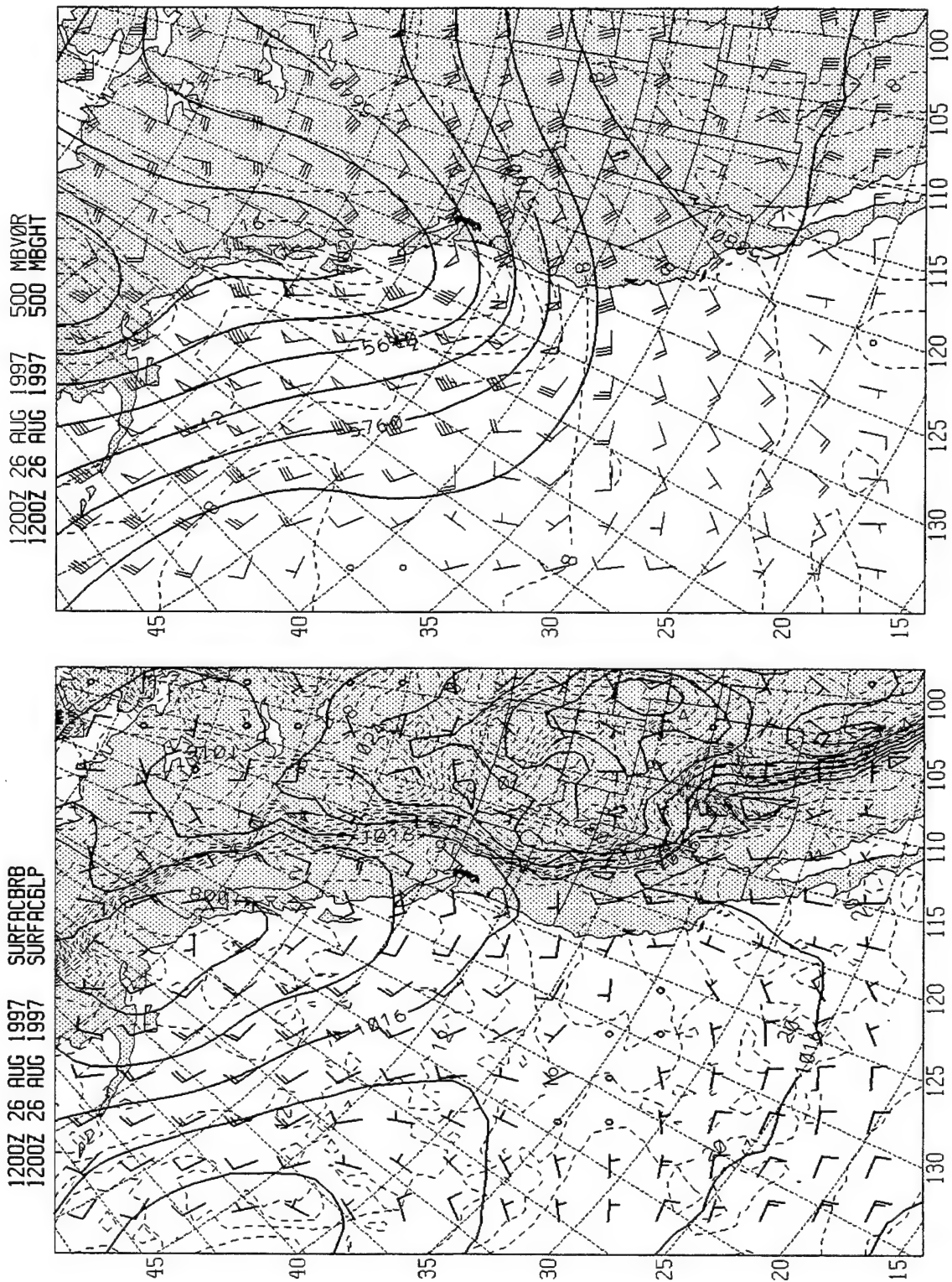


Figure 6c. MM5 control F24 forecast for summer pattern. Fields are 500mb geopotential hts,vorticity, and winds (top) and surface pressure,temperature, and winds(bottom).

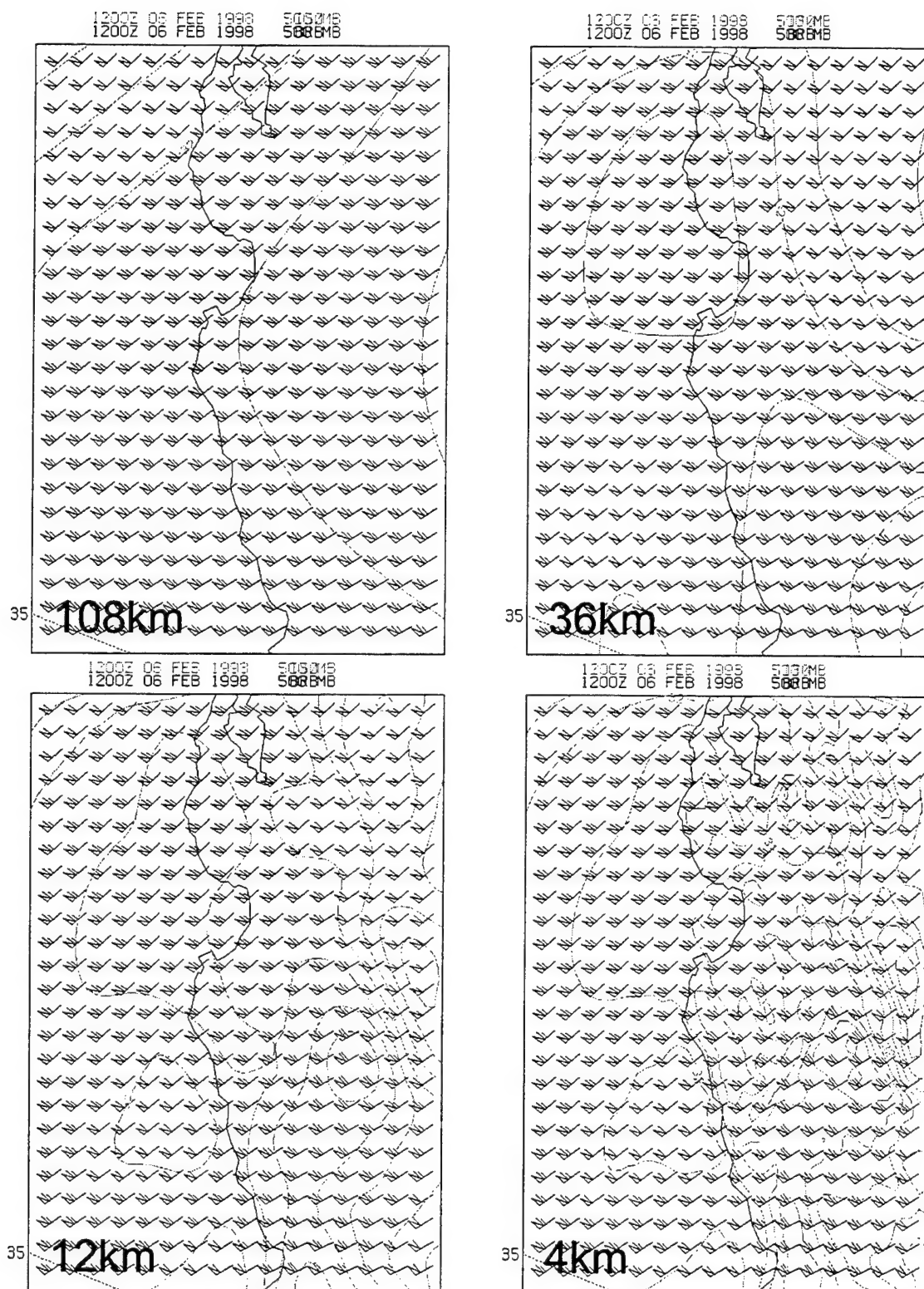


Figure 7. 108, 36, 12, and 4km scale projections on the 4km domain grid for the winter pattern (MM5 control). Fields are wind barbs and isotachs at 500mb.

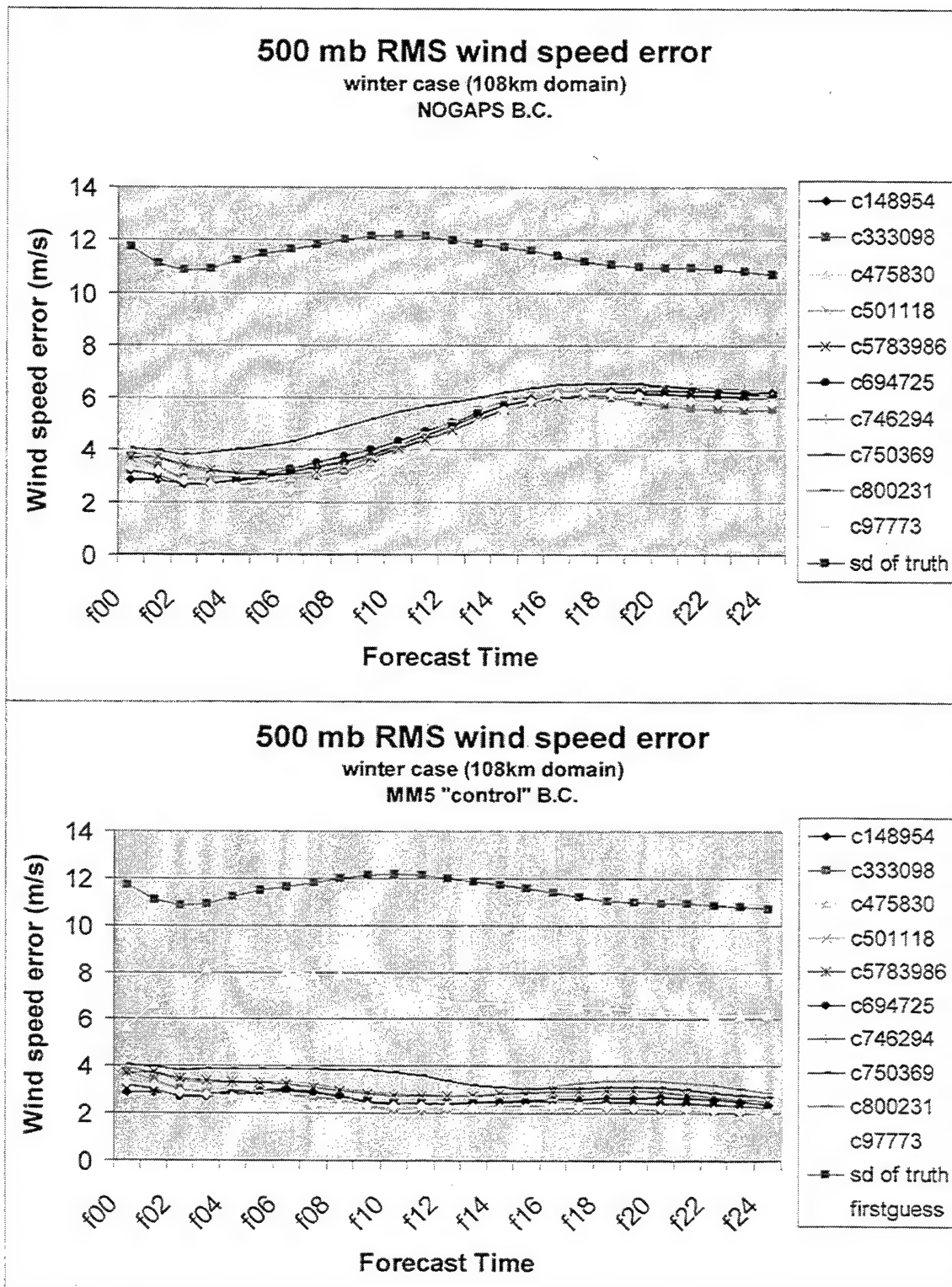


Figure 8a. 500mb wind speed error growth curves on 108 km domain for ten random case solutions when compared to the MM5 control forecast. Boundary conditions are NOGAPS (top) and MM5 control (bottom).

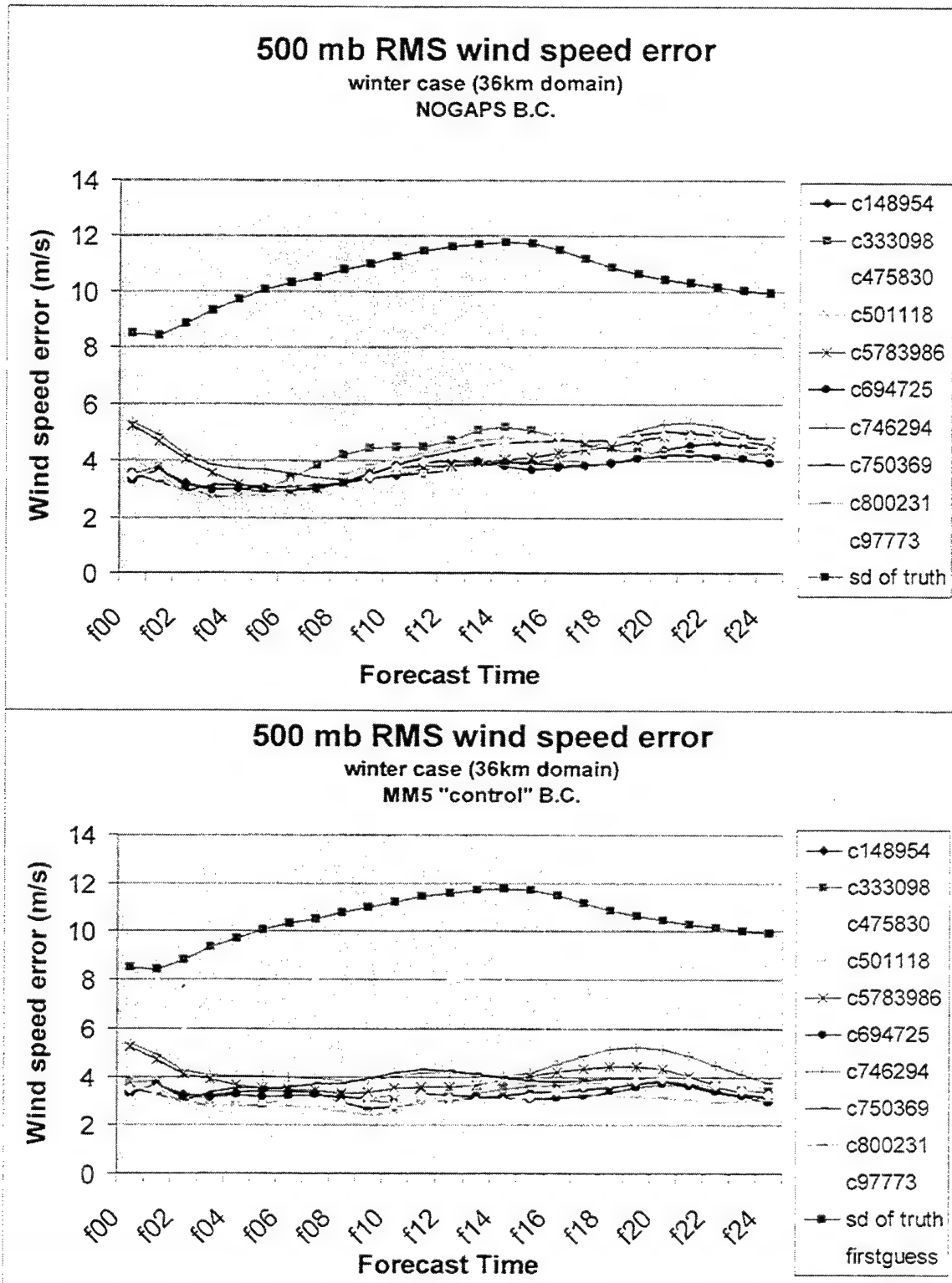


Figure 8b. 500mb wind speed error growth curves on 36 km domain for ten random case solutions when compared to the MM5 control forecast. Boundary conditions are NOGAPS (top) and MM5 control (bottom).

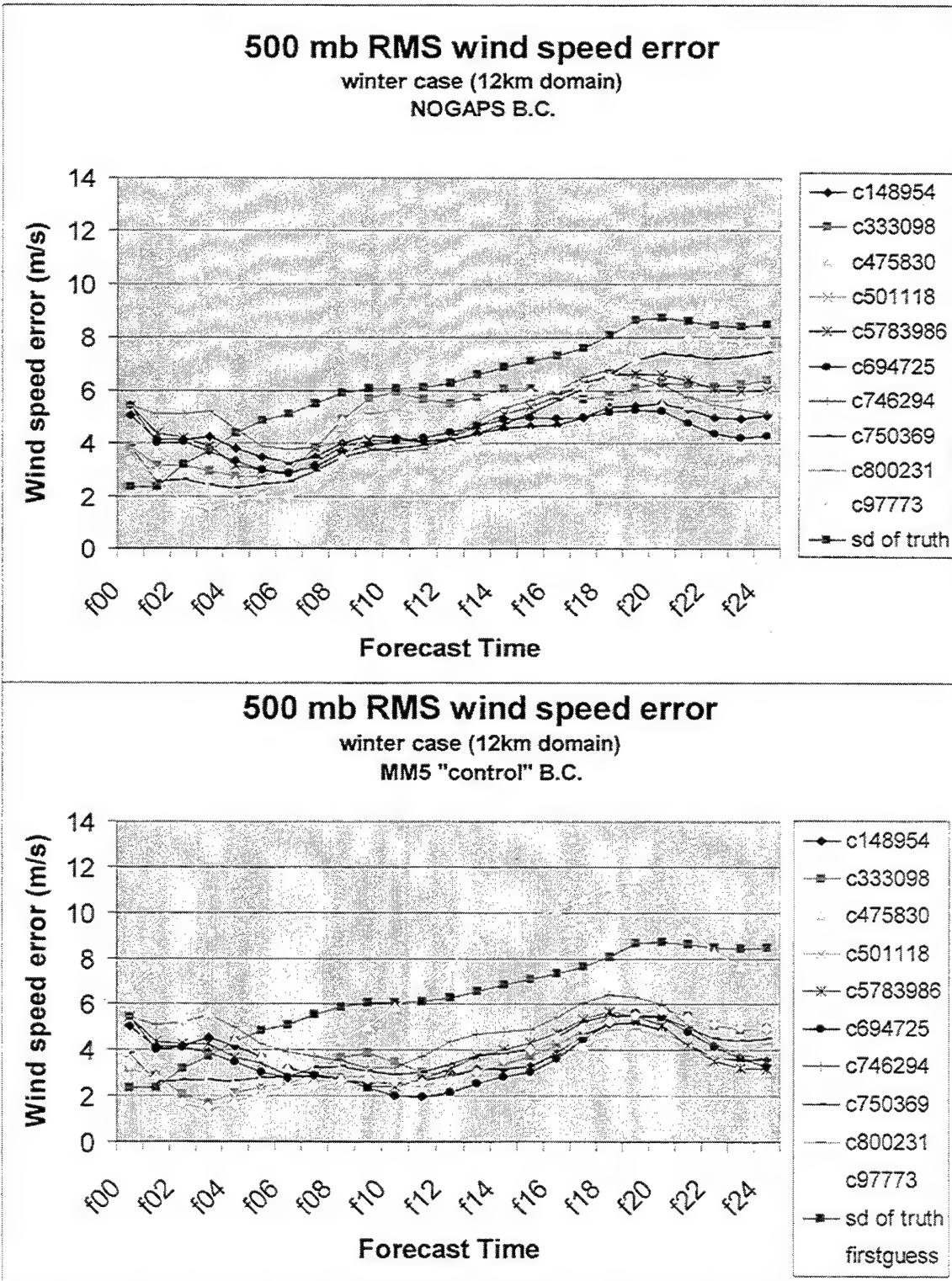


Figure 8c. 500mb wind speed error growth curves on 12 km domain for ten random case solutions when compared to the MM5 control forecast. Boundary conditions are NOGAPS (top) and MM5 control (bottom).

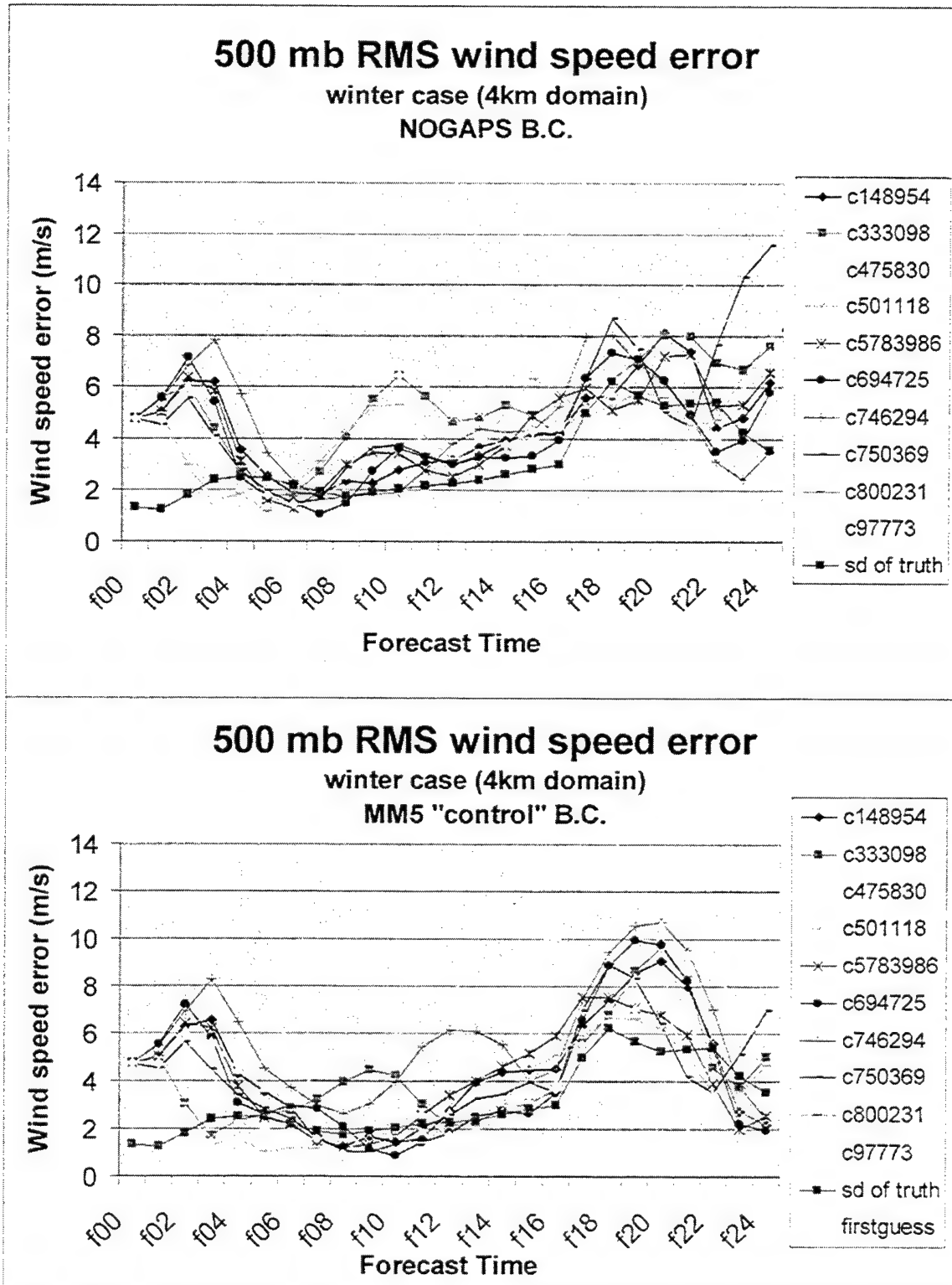


Figure 8d. 500mb wind speed error growth curves on 4 km domain for ten random case solutions when compared to the MM5 control forecast. Boundary conditions are NOGAPS (top) and MM5 control (bottom).

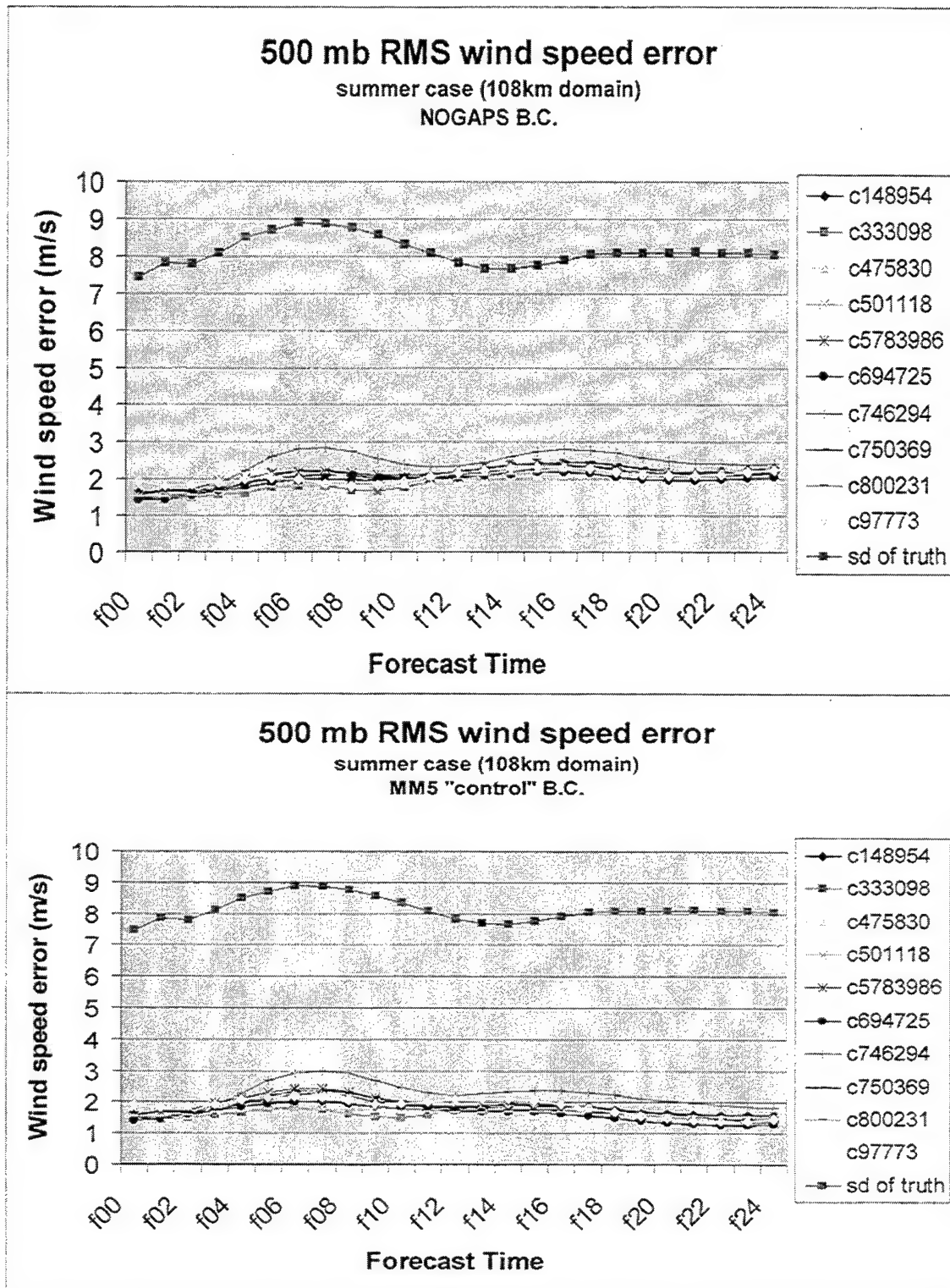


Figure 9a. 500mb wind speed error growth curves on 108 km domain for ten random case solutions when compared to the MM5 control forecast. Boundary conditions are NOGAPS (top) and MM5 control (bottom).

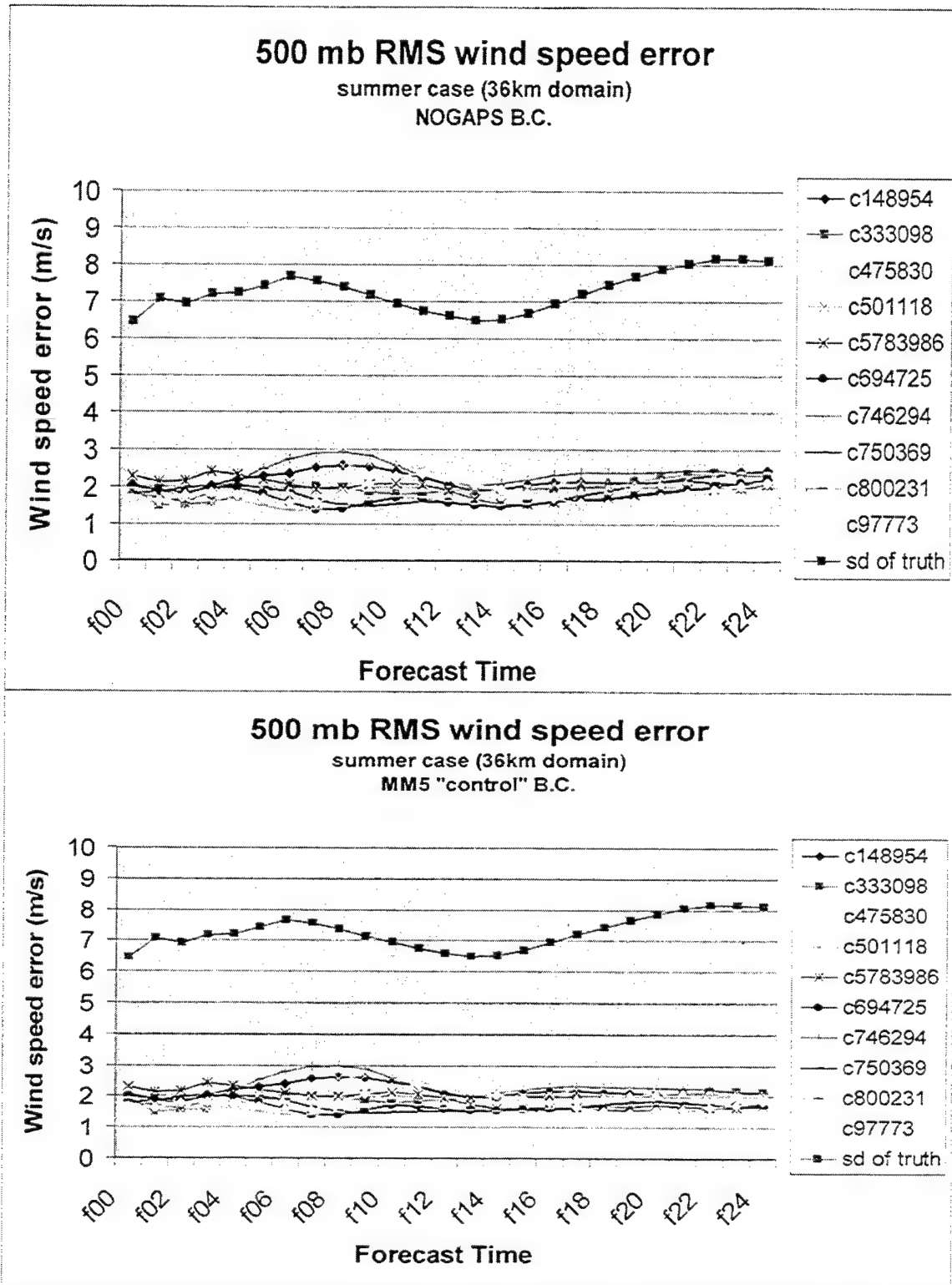


Figure 9b. 500mb wind speed error growth curves on 36 km domain for ten random case solutions when compared to the MM5 control forecast. Boundary conditions are NOGAPS (top) and MM5 control (bottom).

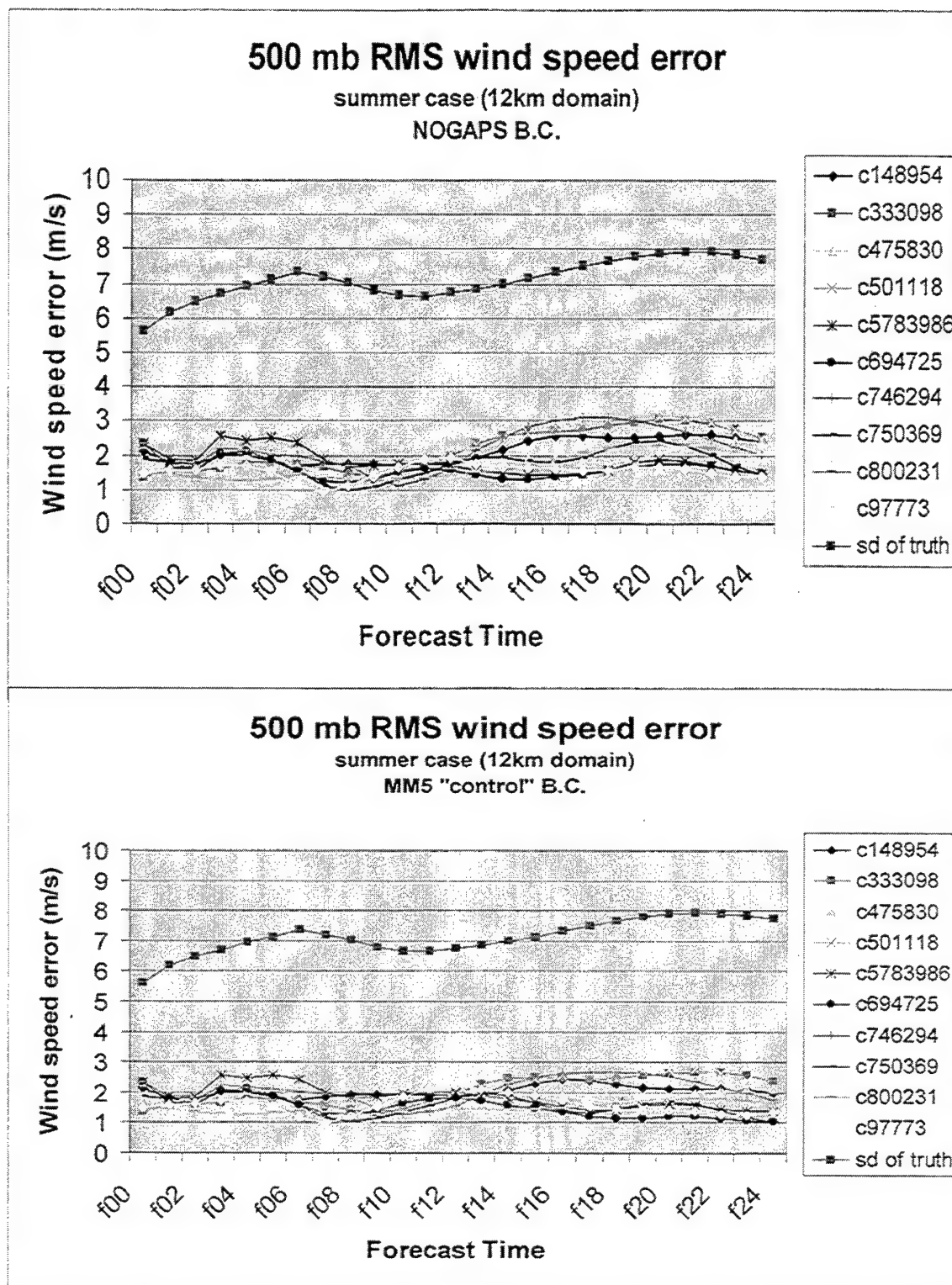


Figure 9c. 500mb wind speed error growth curves on 12 km domain for ten random case solutions when compared to the MM5 control forecast. Boundary conditions are NOGAPS (top) and MM5 control (bottom).

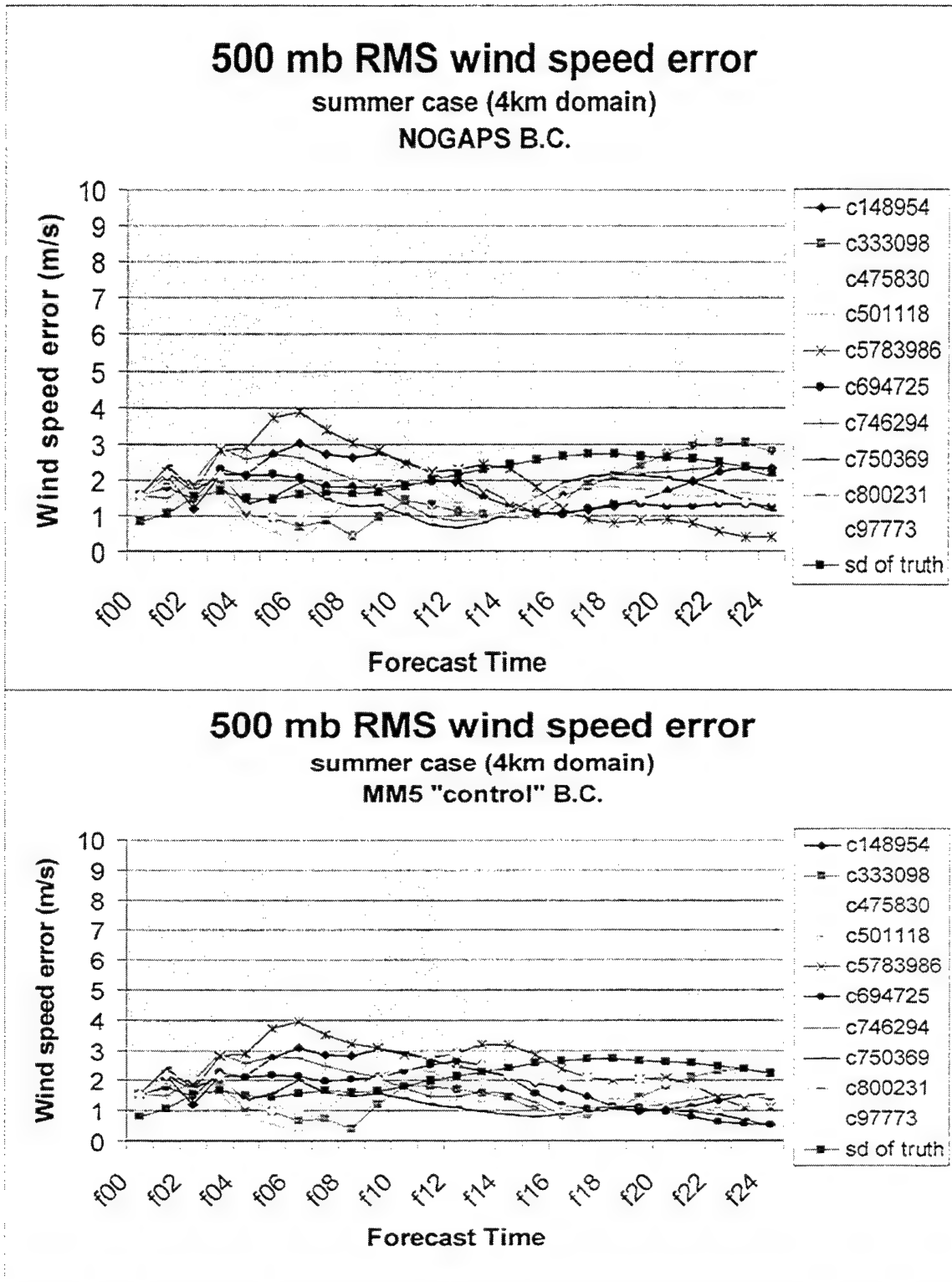


Figure 9d. 500mb wind speed error growth curves on 4 km domain for ten random case solutions when compared to the MM5 control forecast. Boundary conditions are NOGAPS (top) and MM5 control (bottom).

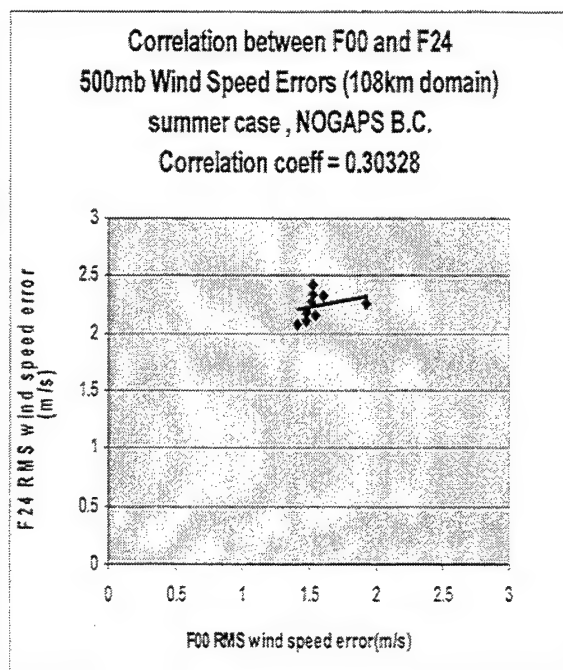
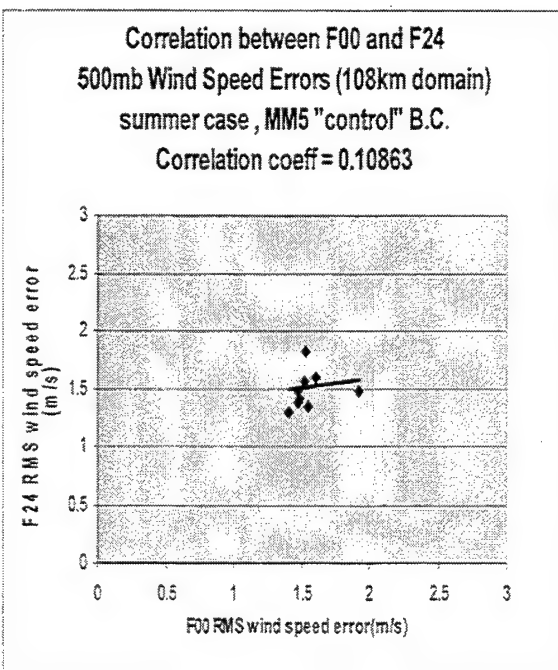
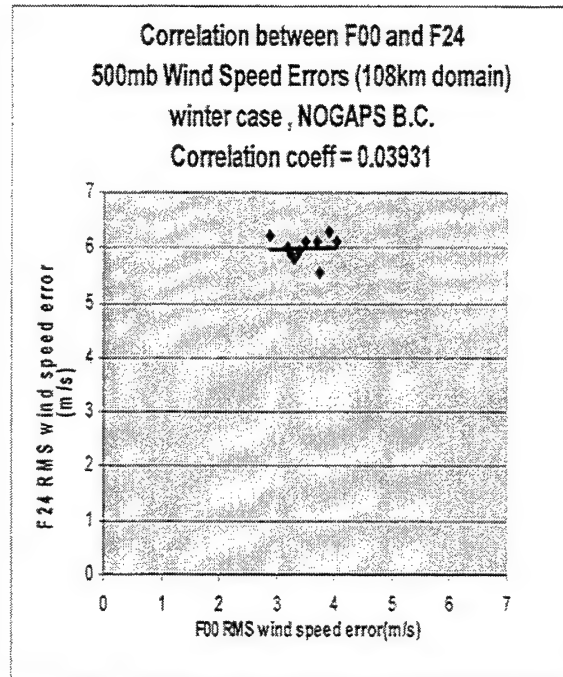
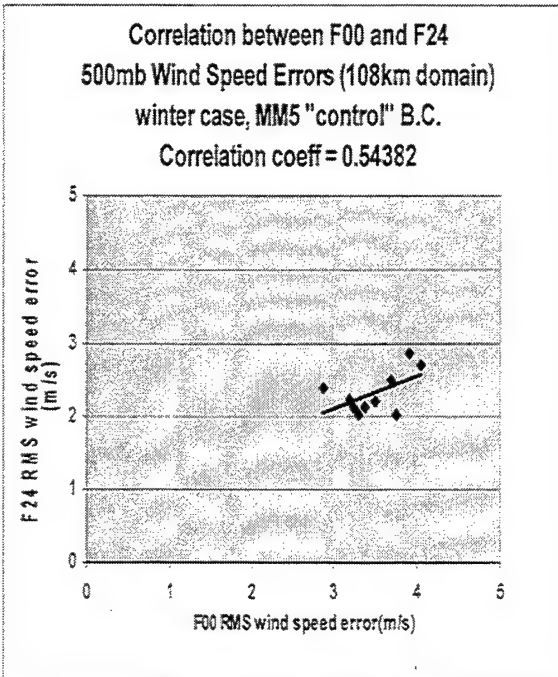


Figure 10. Correlation diagrams of 500mb wind speed errors between F00 and F24 for the winter (top) and summer (bottom) patterns (108km domain) using MM5 control (left) and NOGAPS (right) boundary conditions.

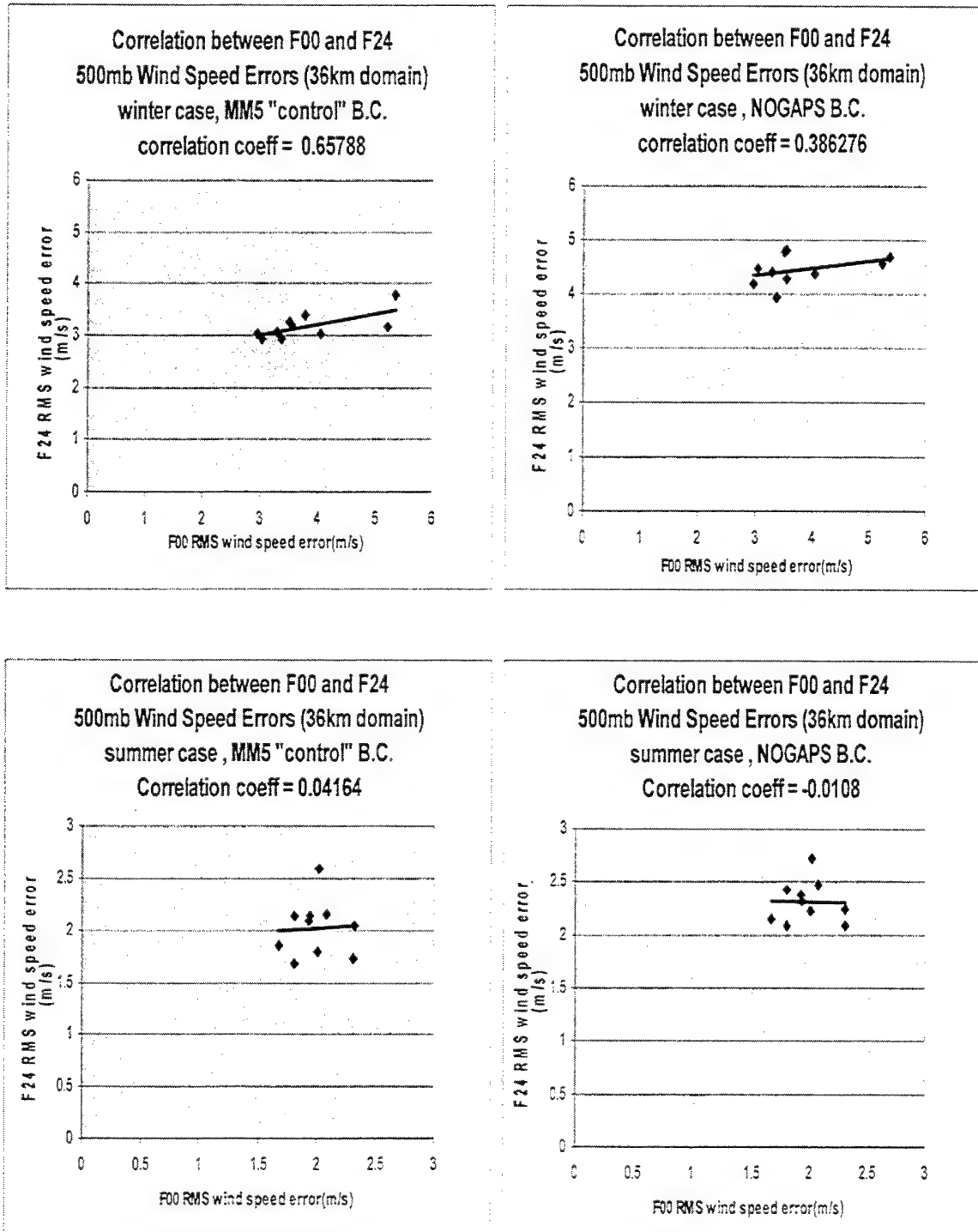


Figure 11. Correlation diagrams of 500mb wind speed errors between F00 and F24 for the winter (top) and summer (bottom) patterns (36 km domain) using MM5 control (left) and NOGAPS (right) boundary conditions.

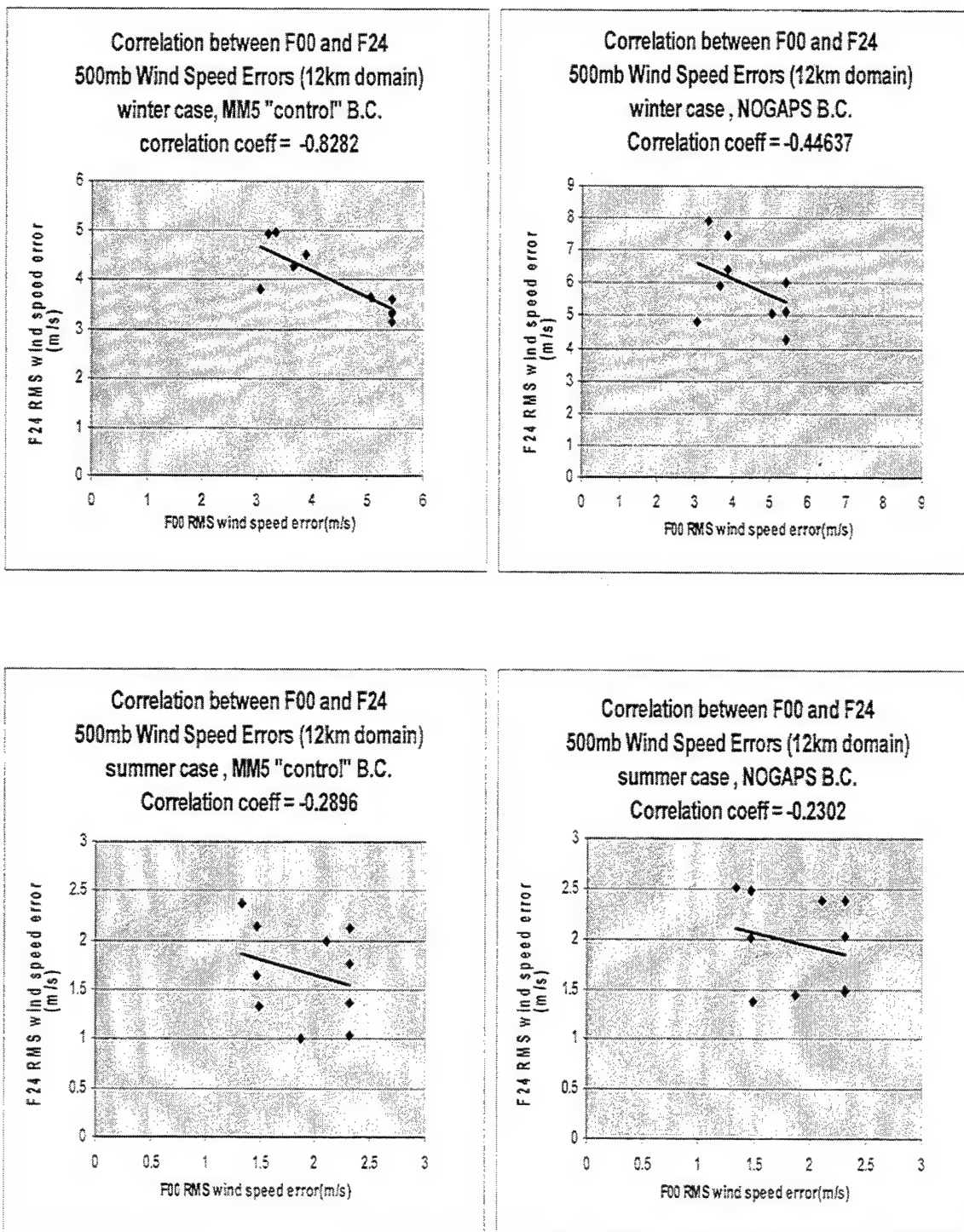


Figure 12. Correlation diagrams of 500mb wind speed errors between F00 and F24 for the winter (top) and summer (bottom) patterns (12km domain) using MM5 control (left) and NOGAPS (right) boundary conditions.

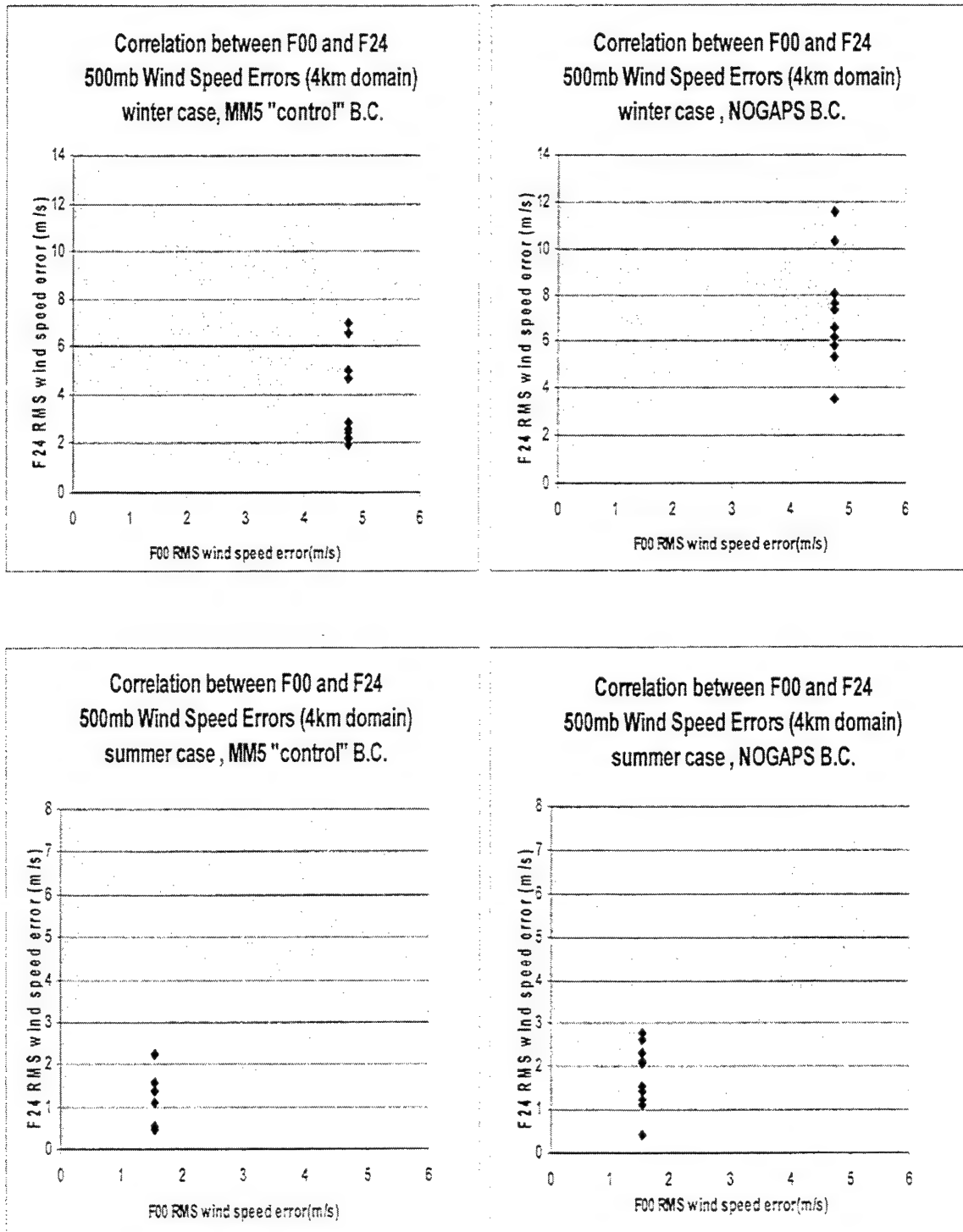


Figure 13. Correlation diagrams of 500mb wind speed errors between F00 and F24 for the winter (top) and summer (bottom) patterns (4 km domain) using MM5 control (left) and NOGAPS (right) boundary conditions.

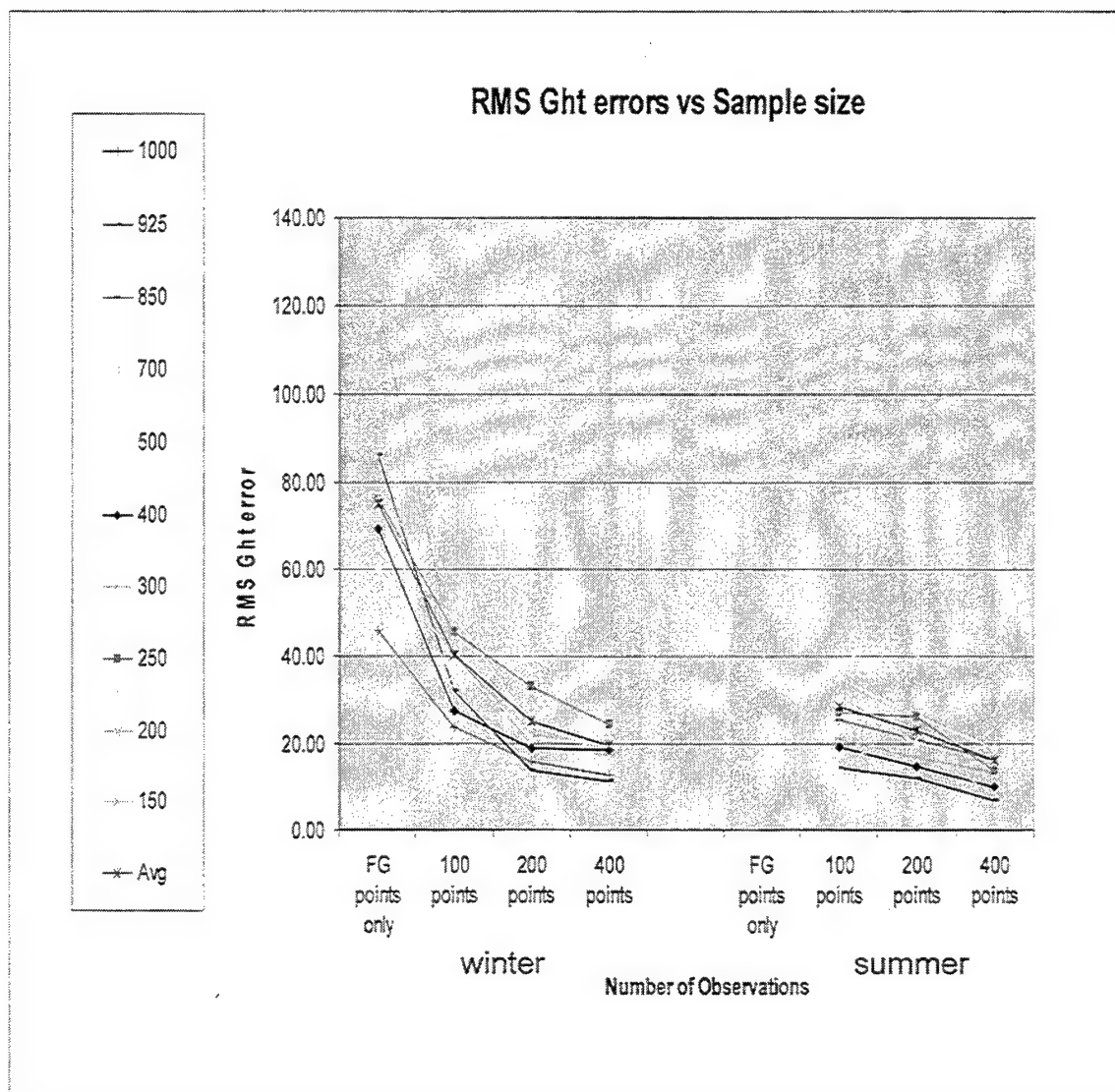


Figure 14. RMS geopotential height error at analysis for winter (left) and summer (right) patterns.

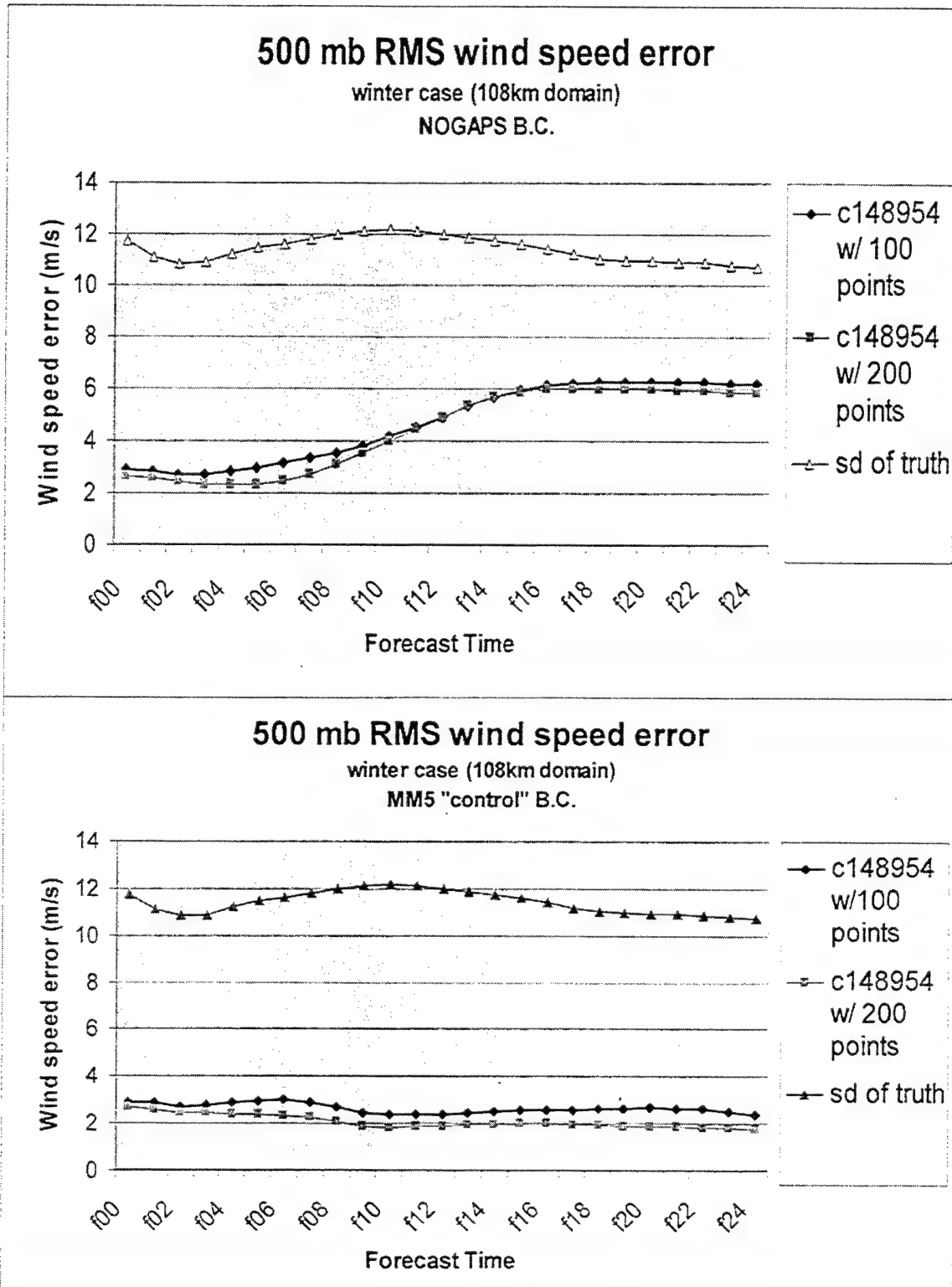


Figure 15a. 500mb wind speed error growth curves on 108 km domain for case c148954 with 100 and 200 point initializations in the winter pattern. Boundary conditions are NOGAPS (top) and MM5 control (bottom).

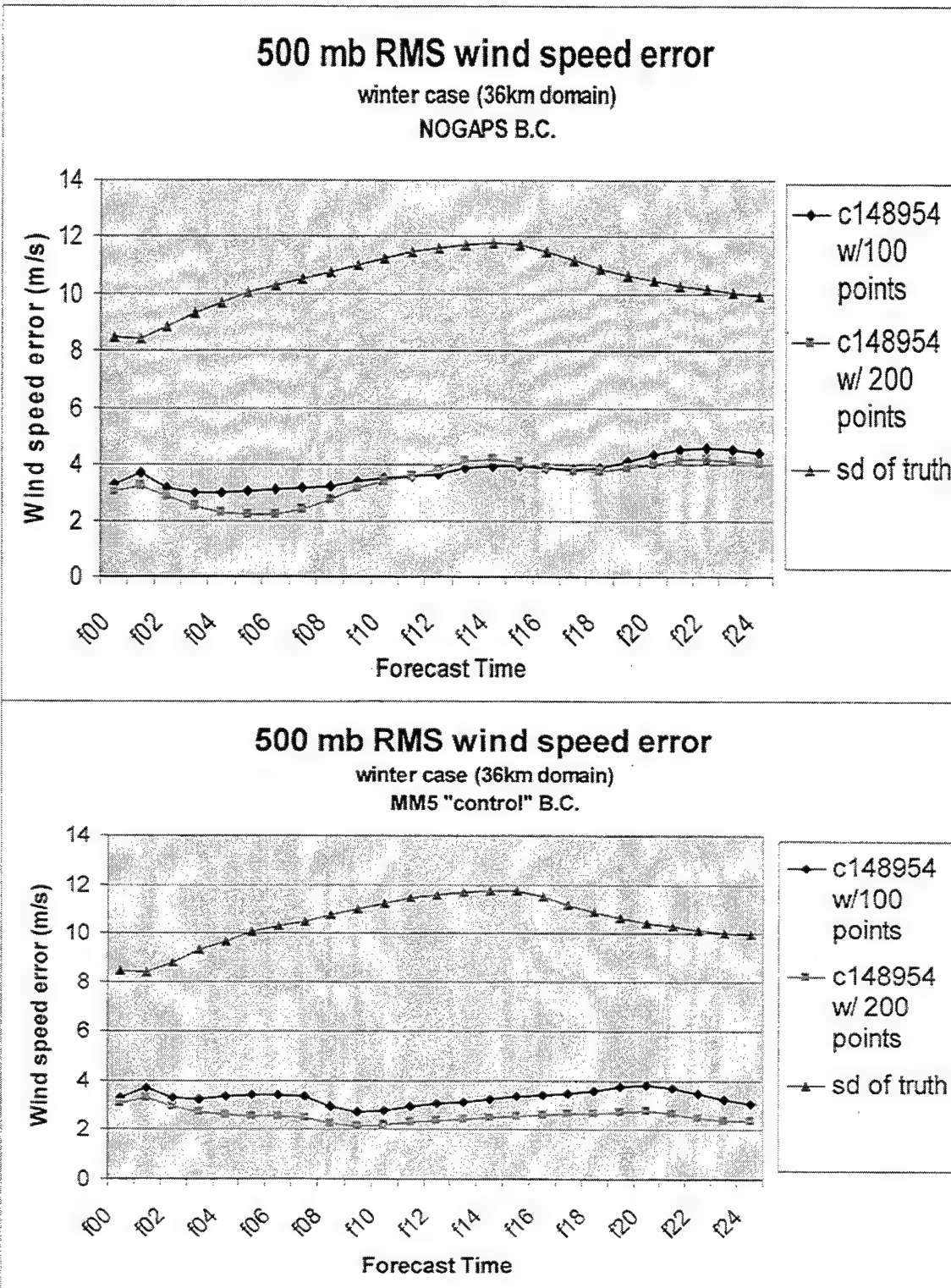


Figure 15b. 500mb wind speed error growth curves on 36 km domain for case c148954 with 100 and 200 point initializations. Boundary conditions are NOGAPS (top) and MM5 control (bottom).

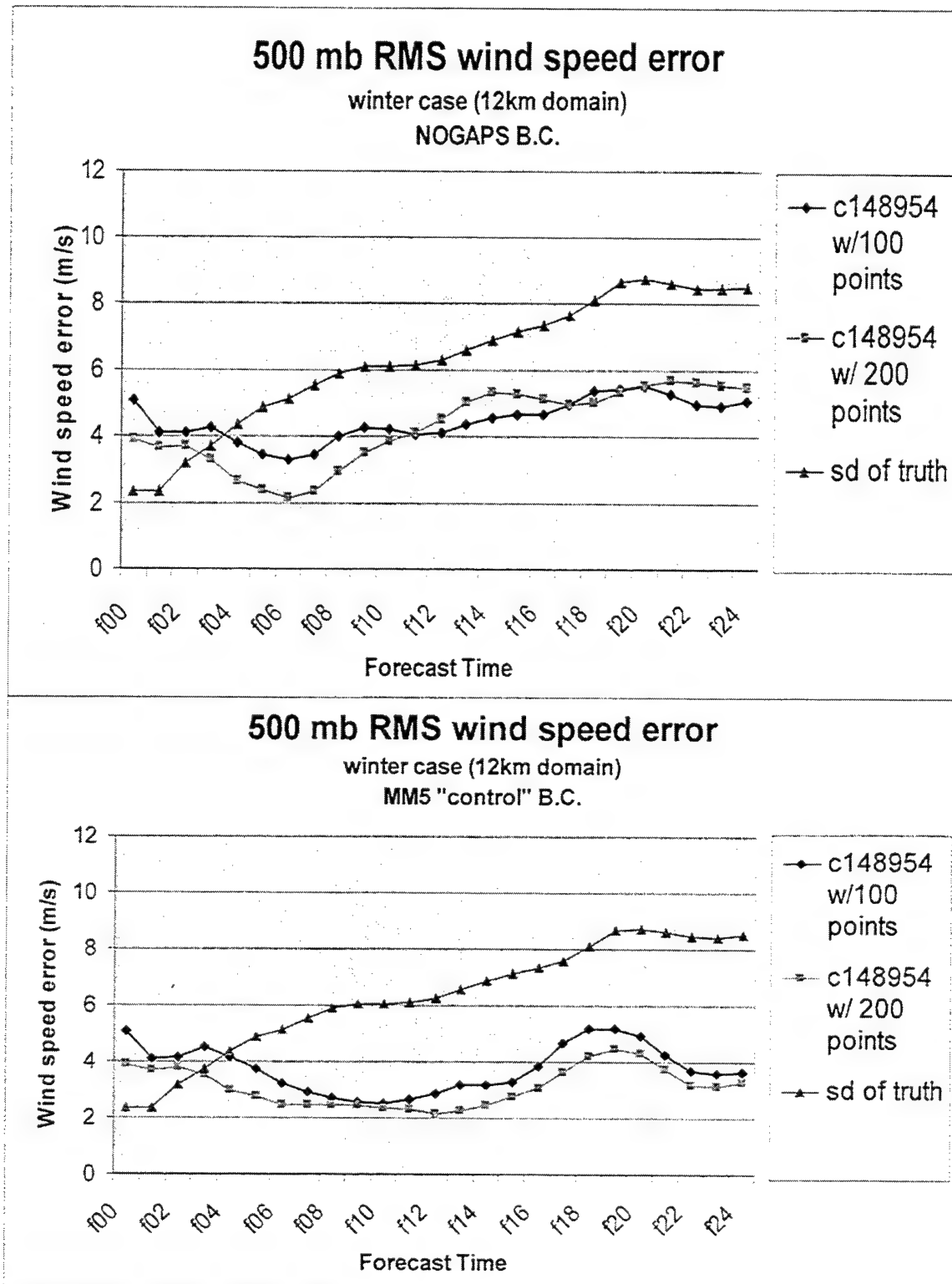
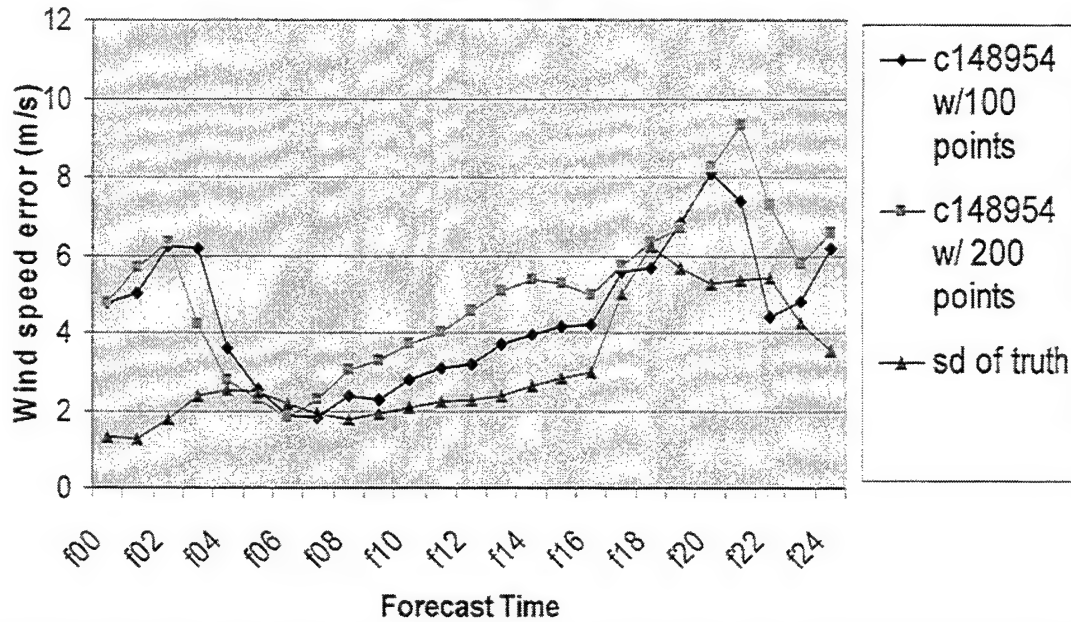


Figure 15c. 500mb wind speed error growth curves on 12 km domain for case c148954 with 100 and 200 point initializations. Boundary conditions are NOGAPS (top) and MM5 control (bottom).

500 mb RMS wind speed error

winter case (4km domain)

NOGAPS B.C.



500 mb RMS wind speed error

winter case (4km domain)

MM5 "control" B.C.

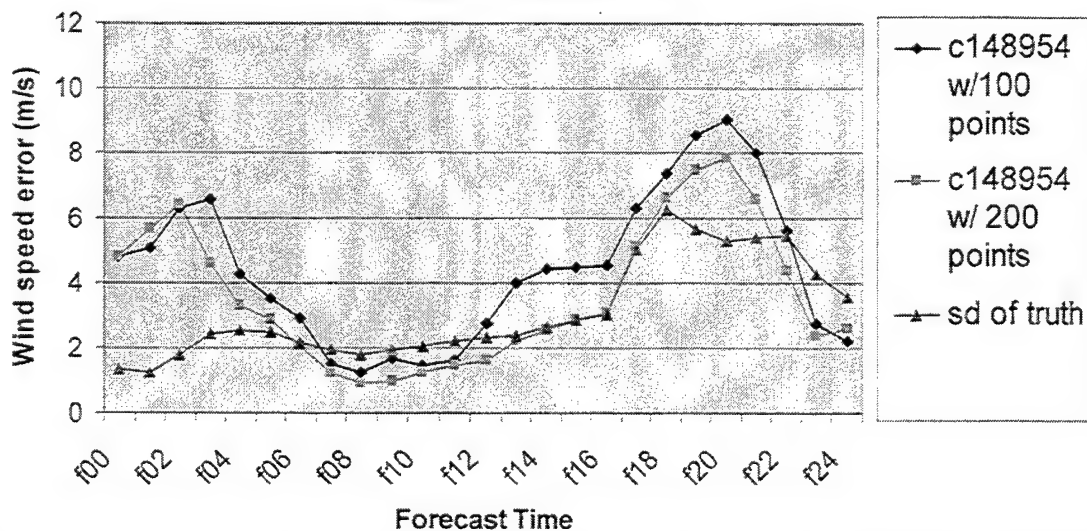


Figure 15d. 500mb wind speed error growth curves on 4 km domain for case c148954 with 100 and 200 point initializations. Boundary conditions are NOGAPS (top) and MM5 control (bottom).

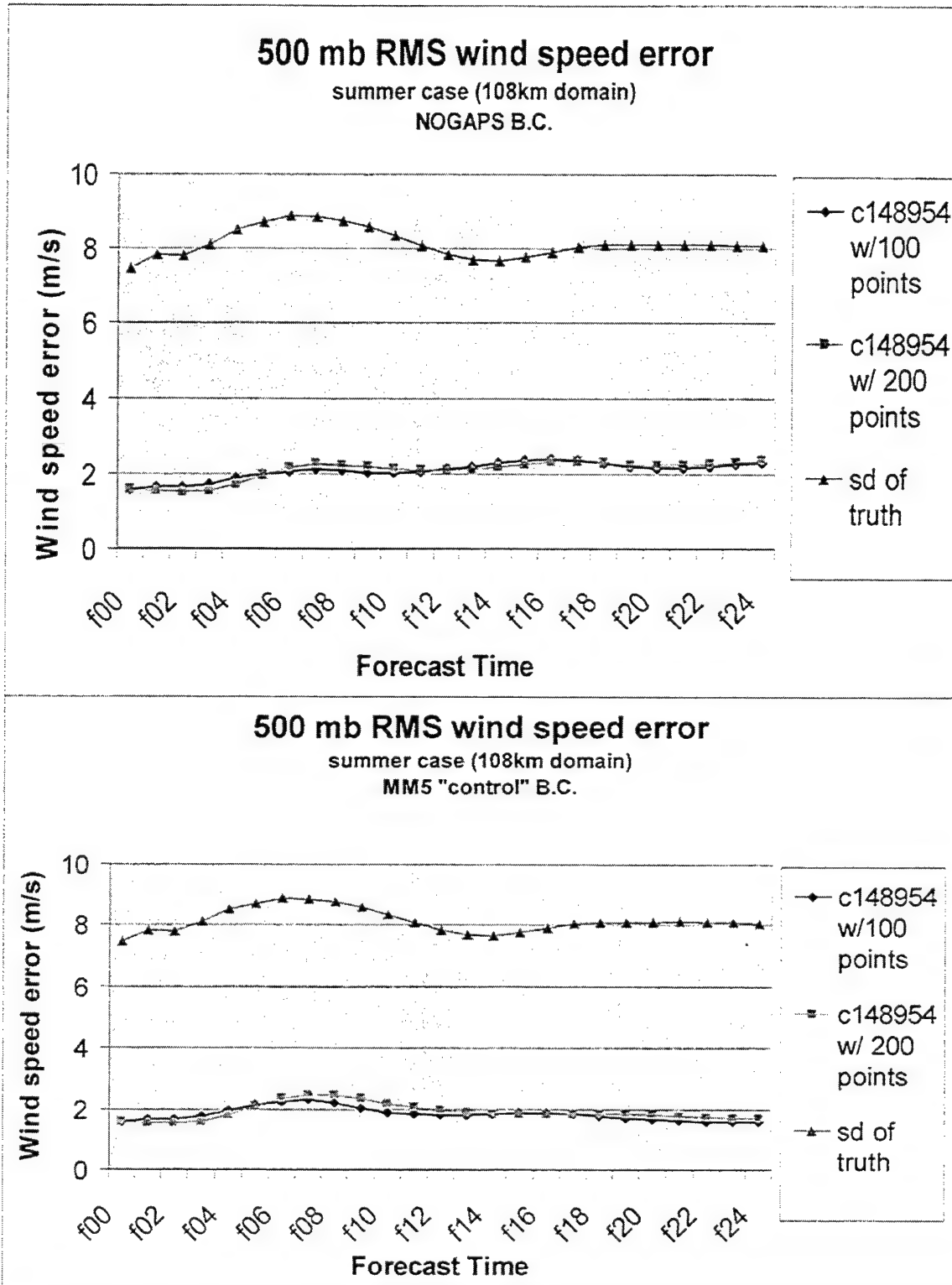


Figure 16a. 500mb wind speed error growth curves on 108 km domain for case c148954 with 100 and 200 point initializations for summer case. Boundary conditions are NOGAPS (top) and MM5 control (bottom).

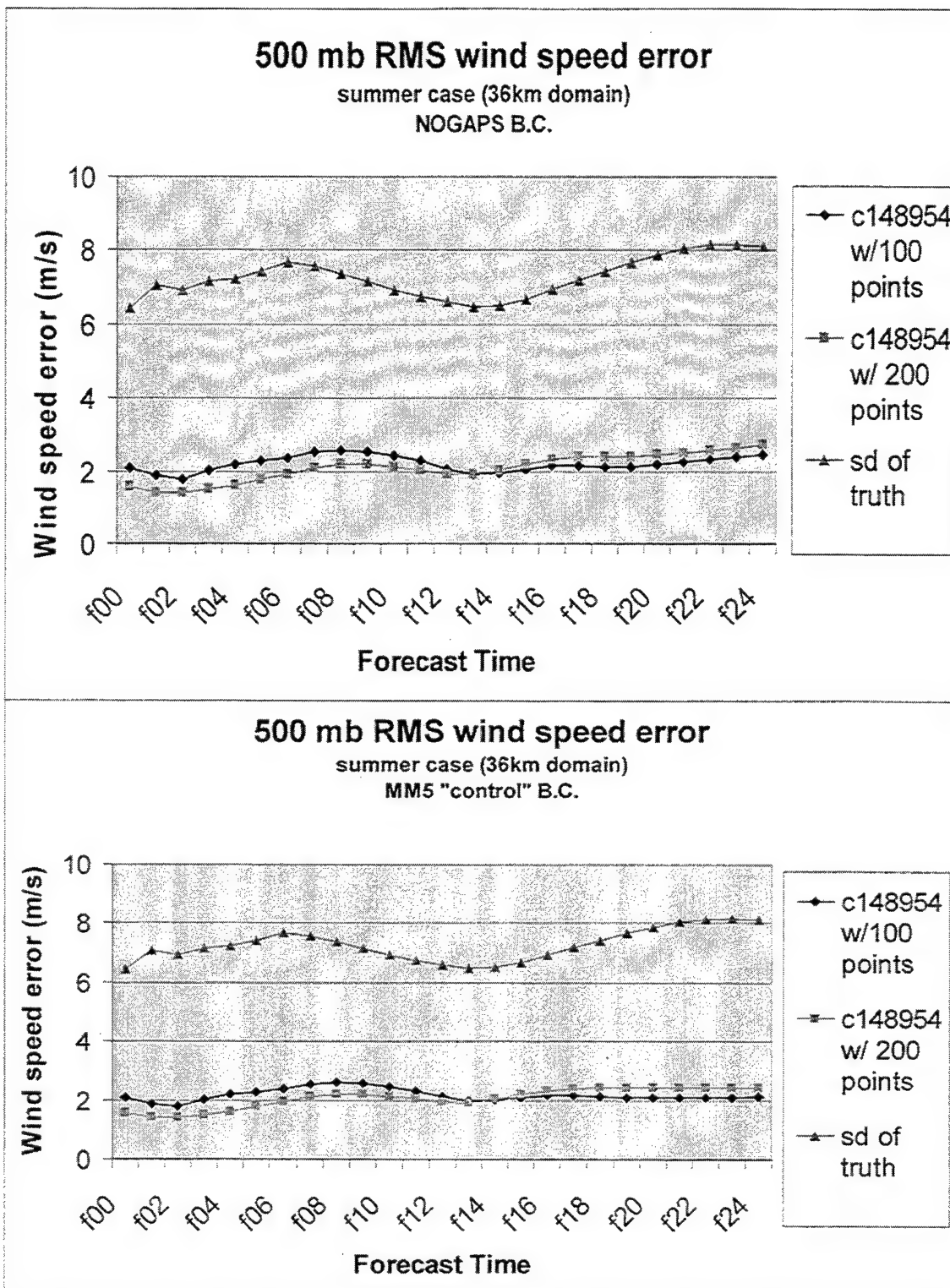


Figure 16b. 500mb wind speed error growth curves on 36 km domain for case c148954 with 100 and 200 point initializations for summer case. Boundary conditions are NOGAPS (top) and MM5 control (bottom).

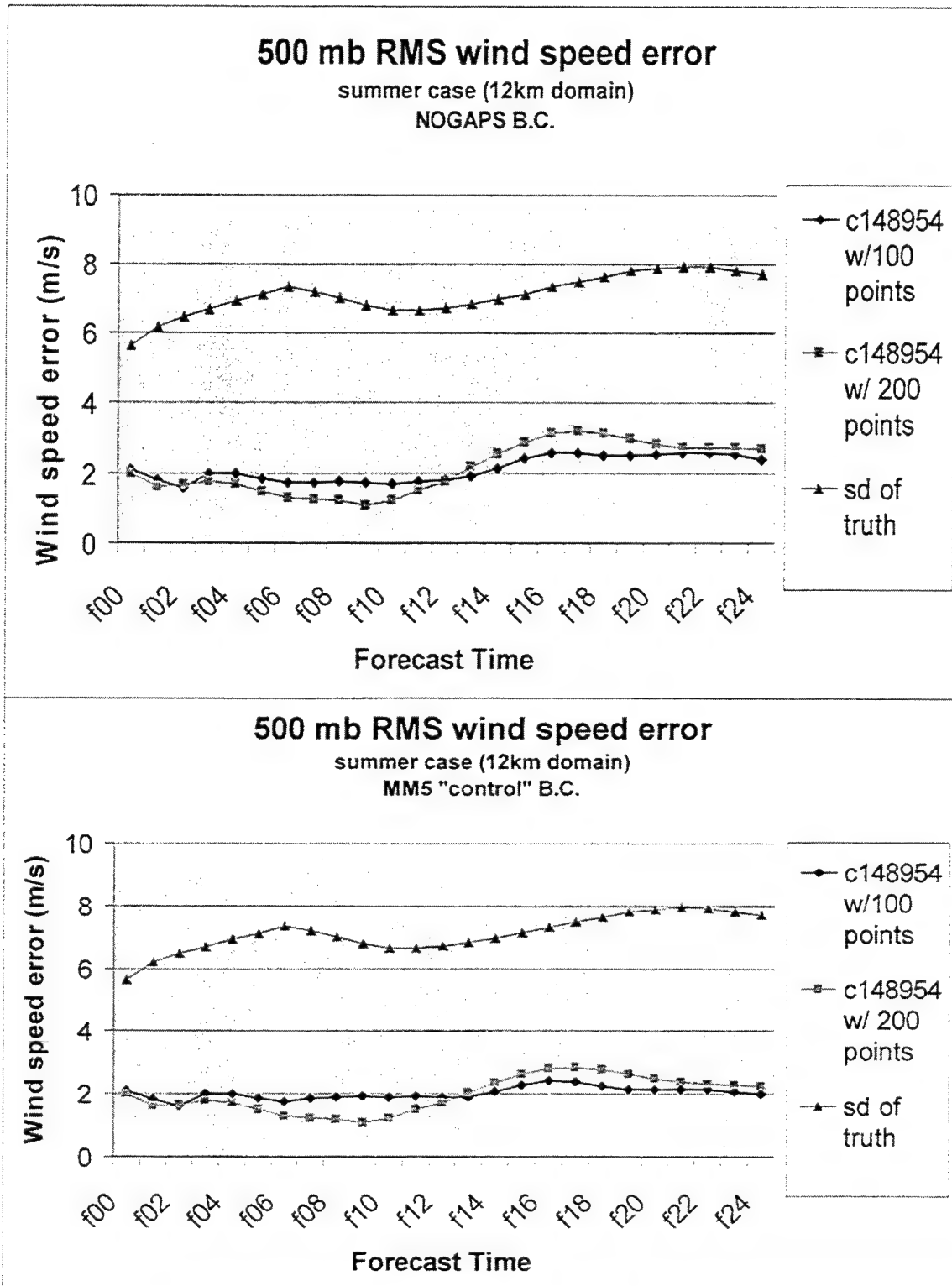


Figure 16c. 500mb wind speed error growth curves on 12 km domain for case c148954 with 100 and 200 point initializations for summer case. Boundary conditions are NOGAPS (top) and MM5 control (bottom).

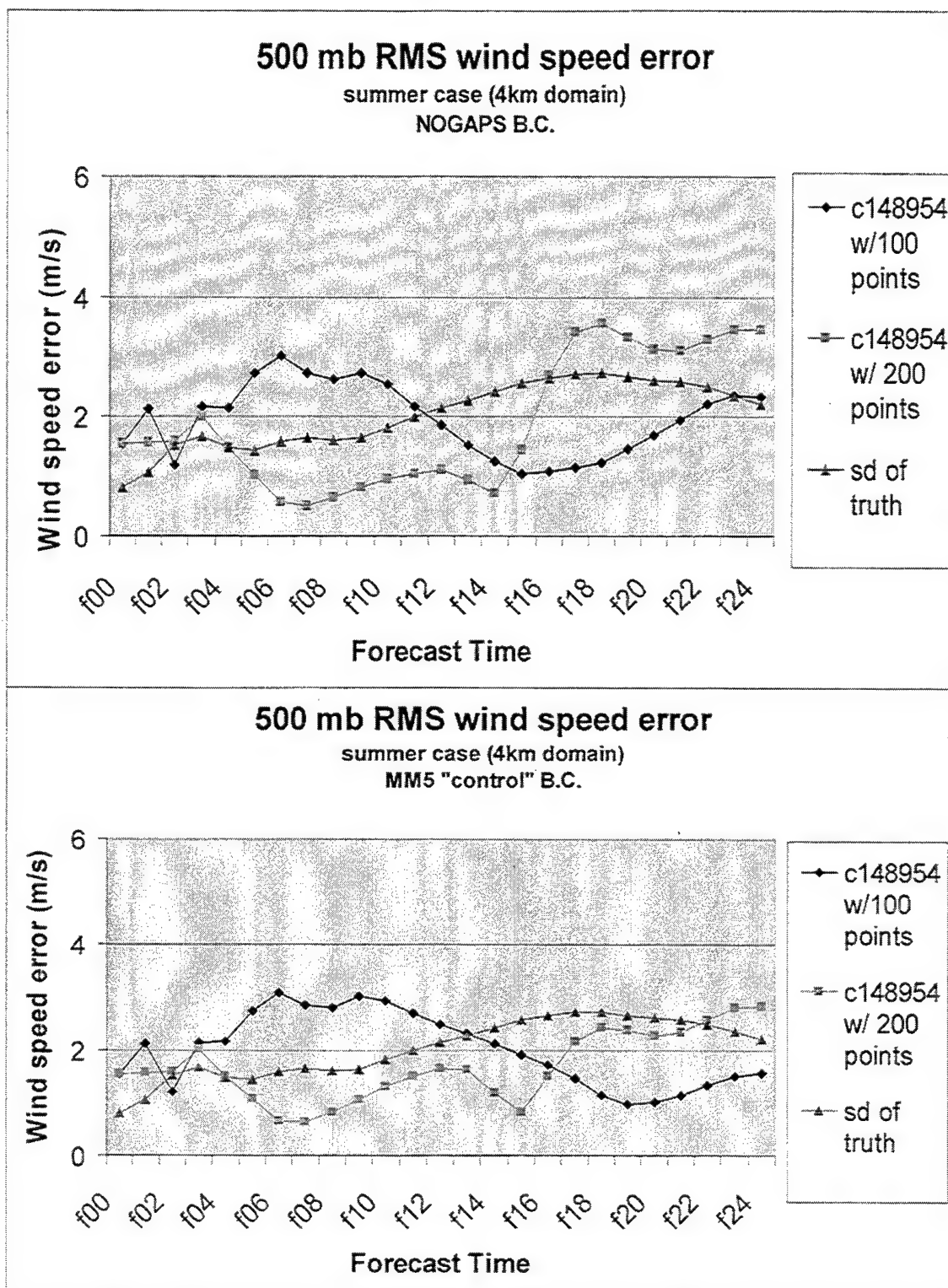


Figure 16d. 500mb wind speed error growth curves on 4 km domain for case c148954 with 100 and 200 point initializations for summer case. Boundary conditions are NOGAPS (top) and MM5 control (bottom).

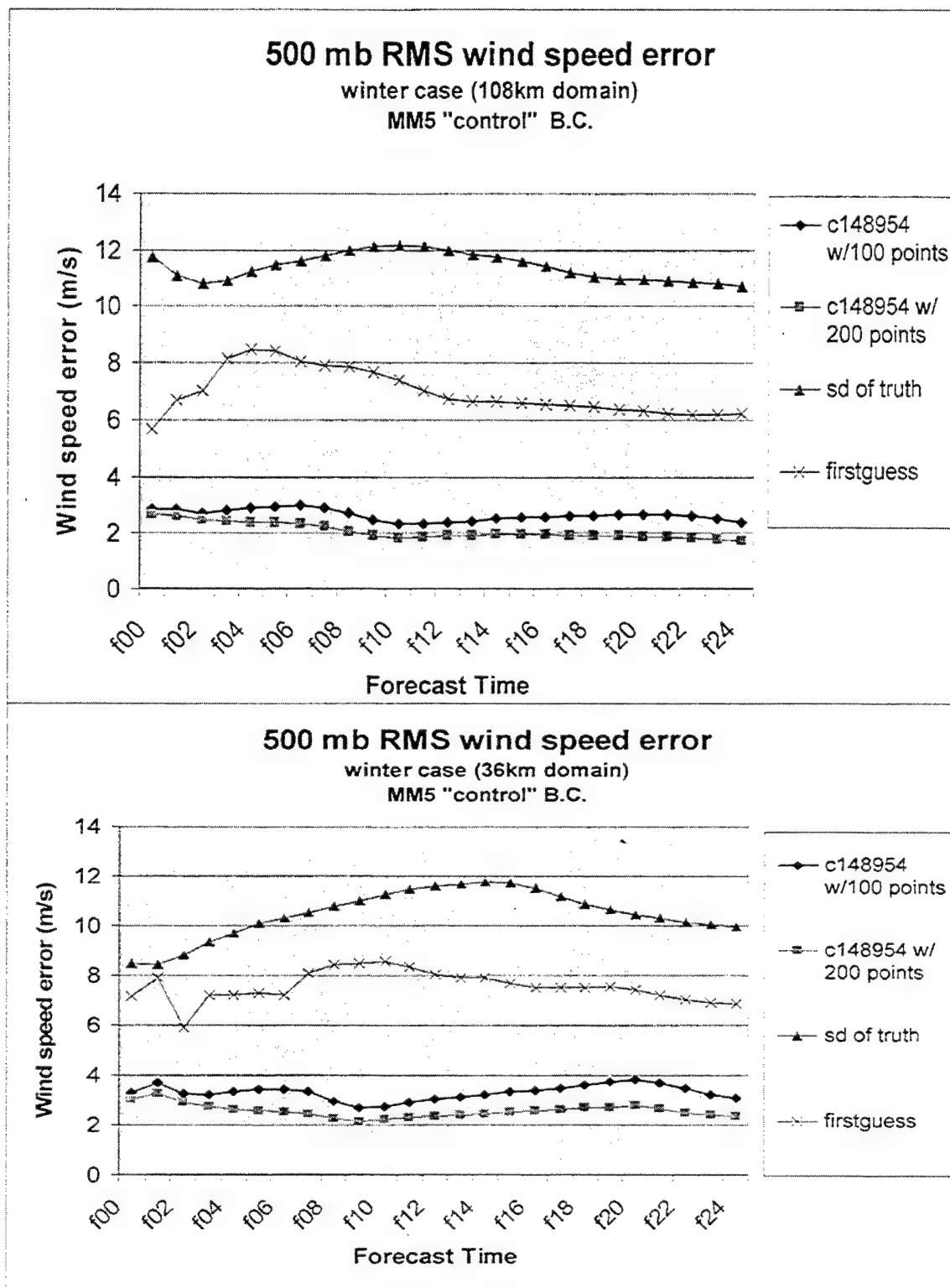


Figure 17a. 500mb wind speed error growth curves on 108 km (top) and 36 km (bottom) domains for case c148954 with 100 point, 200 point, and firstguess only initializations. Plots are for the winter case with MM5 "control" boundary conditions.

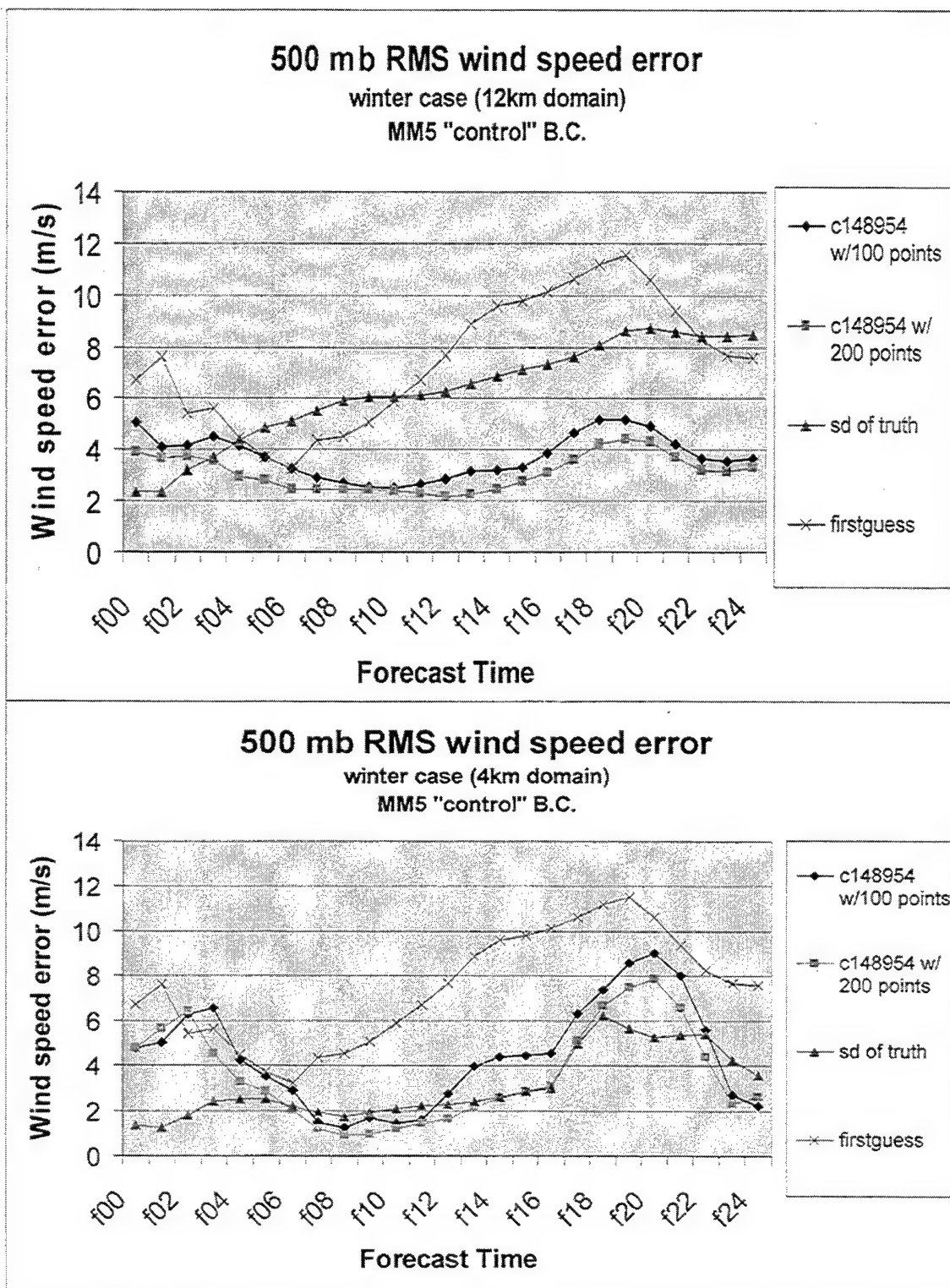


Figure 17b. 500mb wind speed error growth curves on 12 km (top) and 4 km (bottom) domains for case c148954 with 100 point, 200 point, and firstguess only initializations. Plots are for the winter case with MM5 "control" boundary conditions.

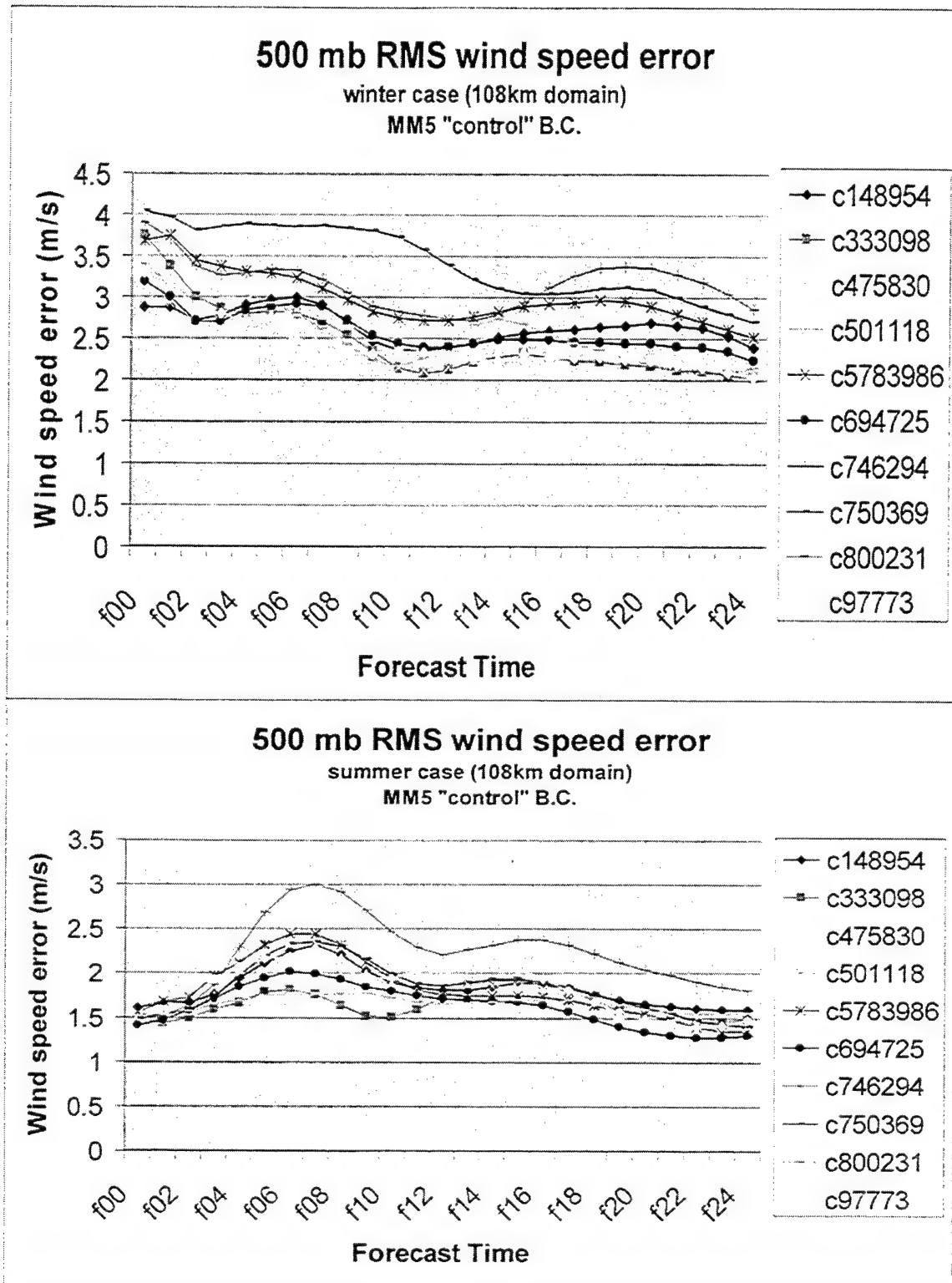


Figure 18. 500mb RMS wind speed error growth curves on 108 km domain for ten random case solutions in the winter (top) and summer (bottom) patterns using MM5 "control" boundary conditions.

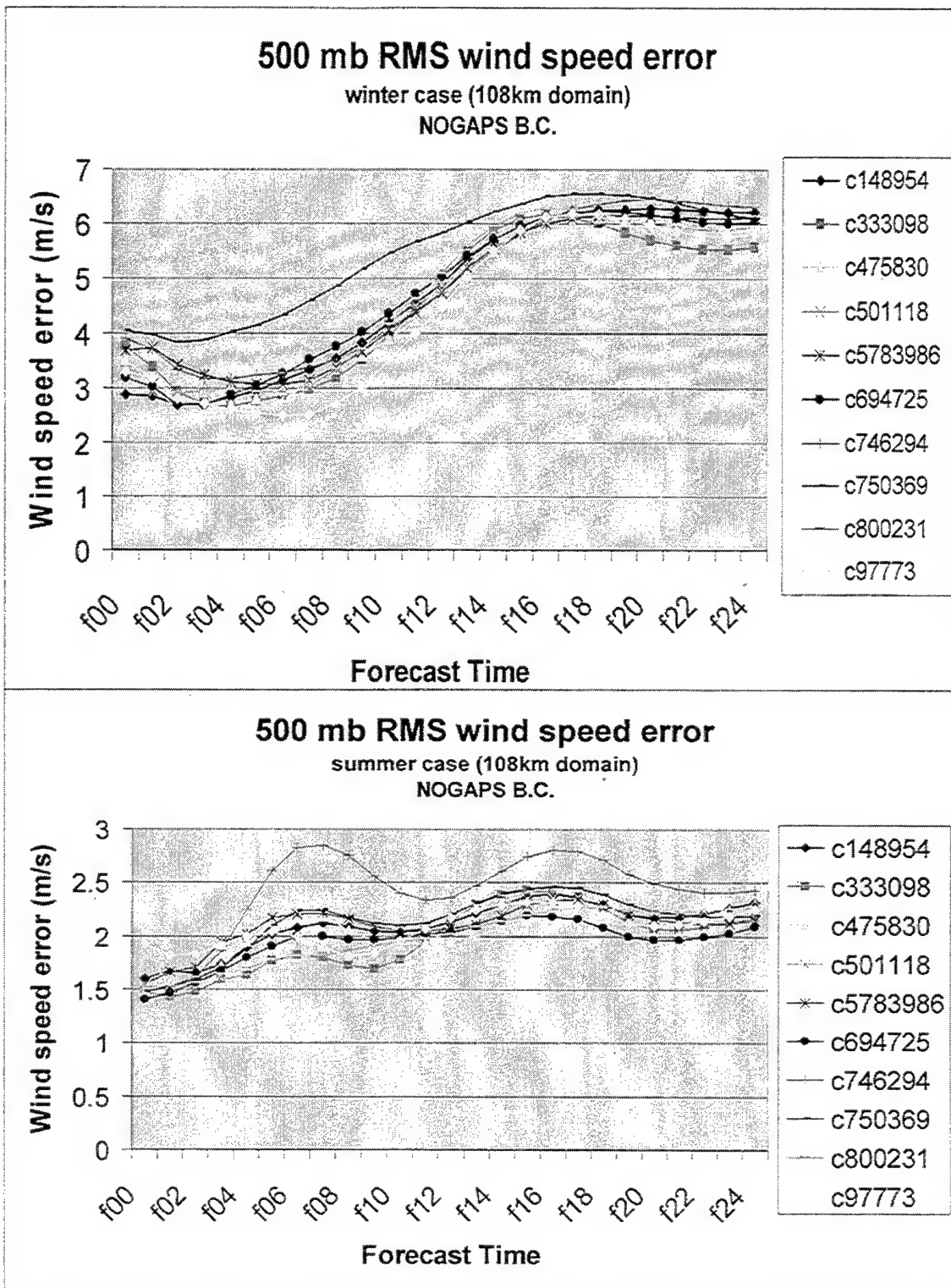


Figure 19. 500mb RMS wind speed error growth curves on 108 km domain for ten random case solutions in the winter (top) and summer (bottom) patterns using NOGAPS boundary conditions.

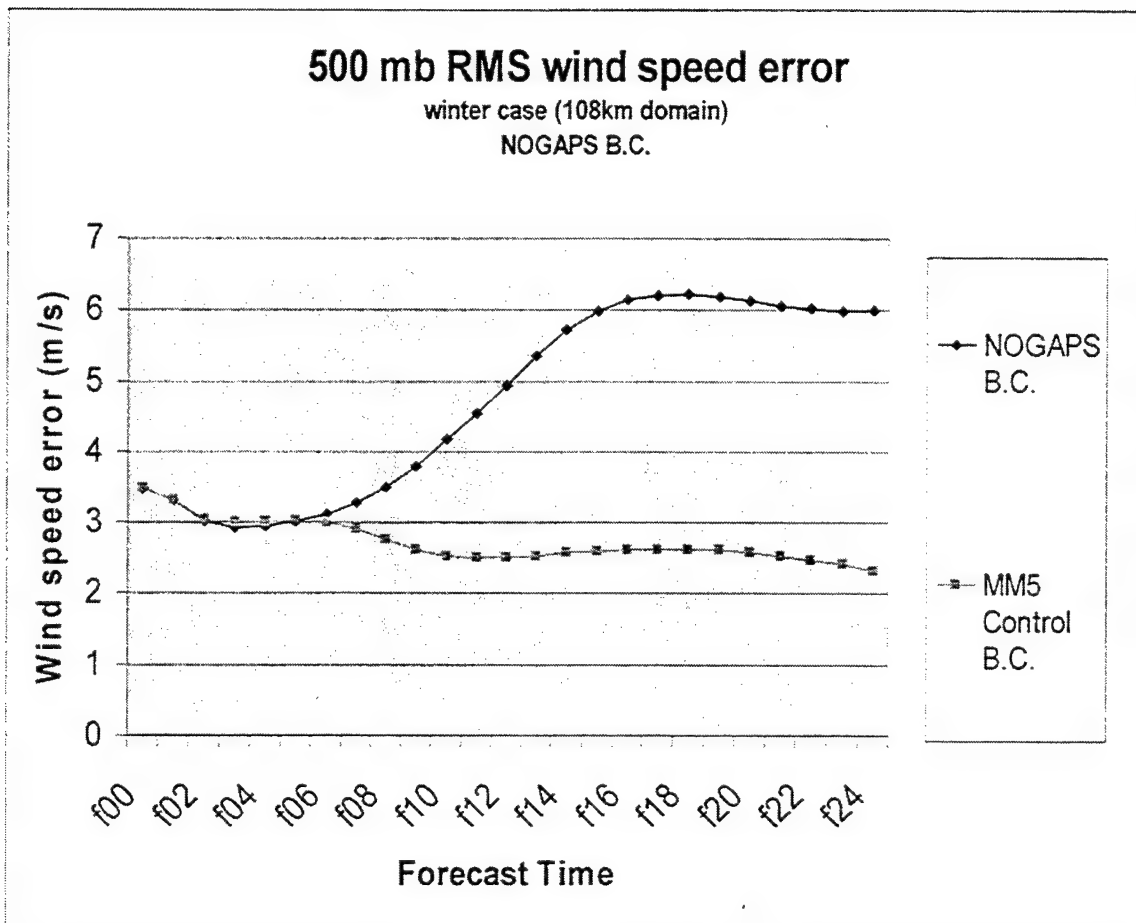


Figure 20. "Ensemble" average of 500mb RMS wind speed error growth curves on 108 km domain for all ten random case solutions in the winter pattern using both MM5 "control" and NOGAPS boundary conditions.

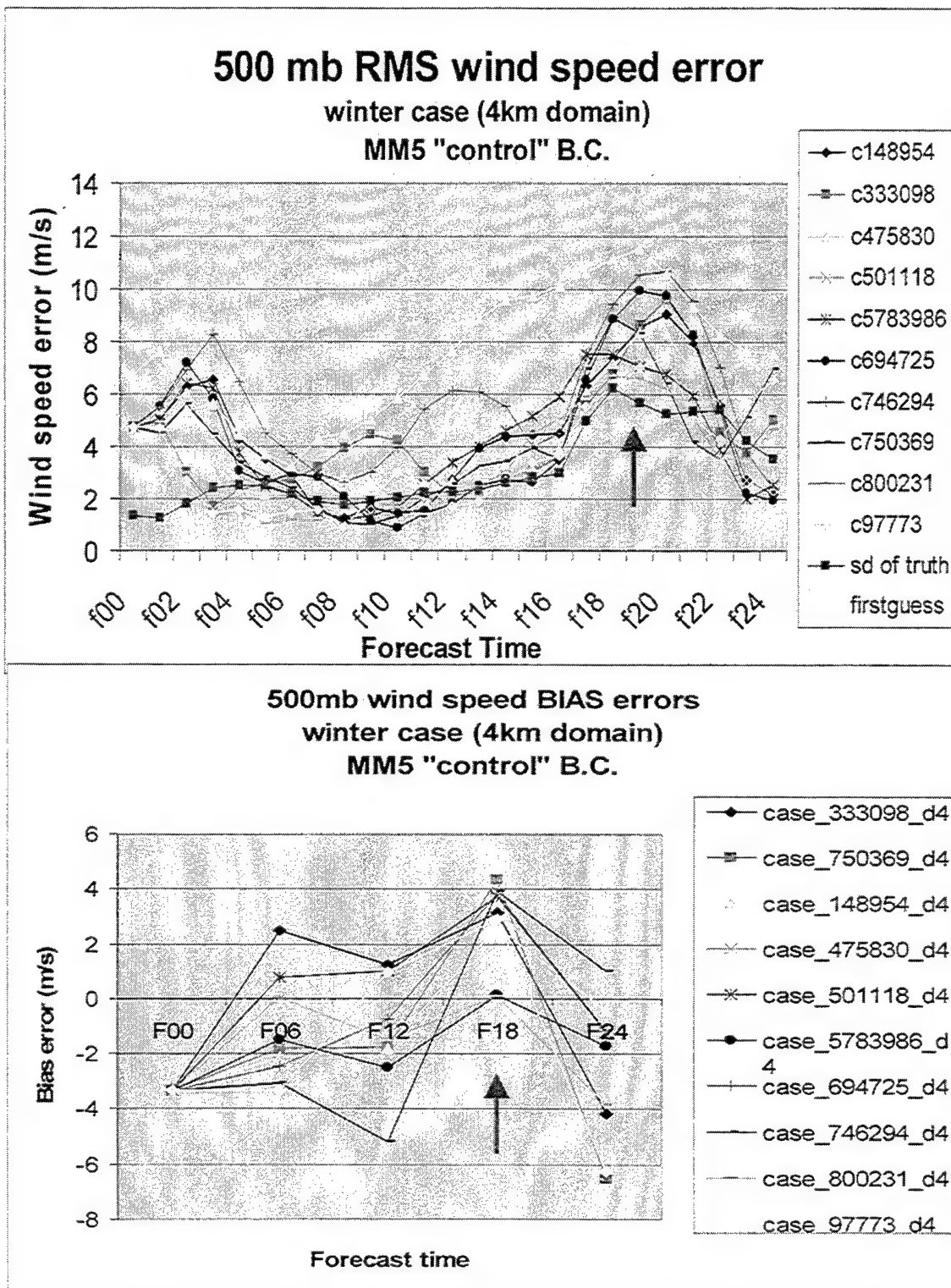


Figure 21. 500mb RMS (top) and Bias (bottom) wind speed error growth curves on 4 km domain for all ten random case solutions in the winter pattern using MM5 "control" boundary conditions.

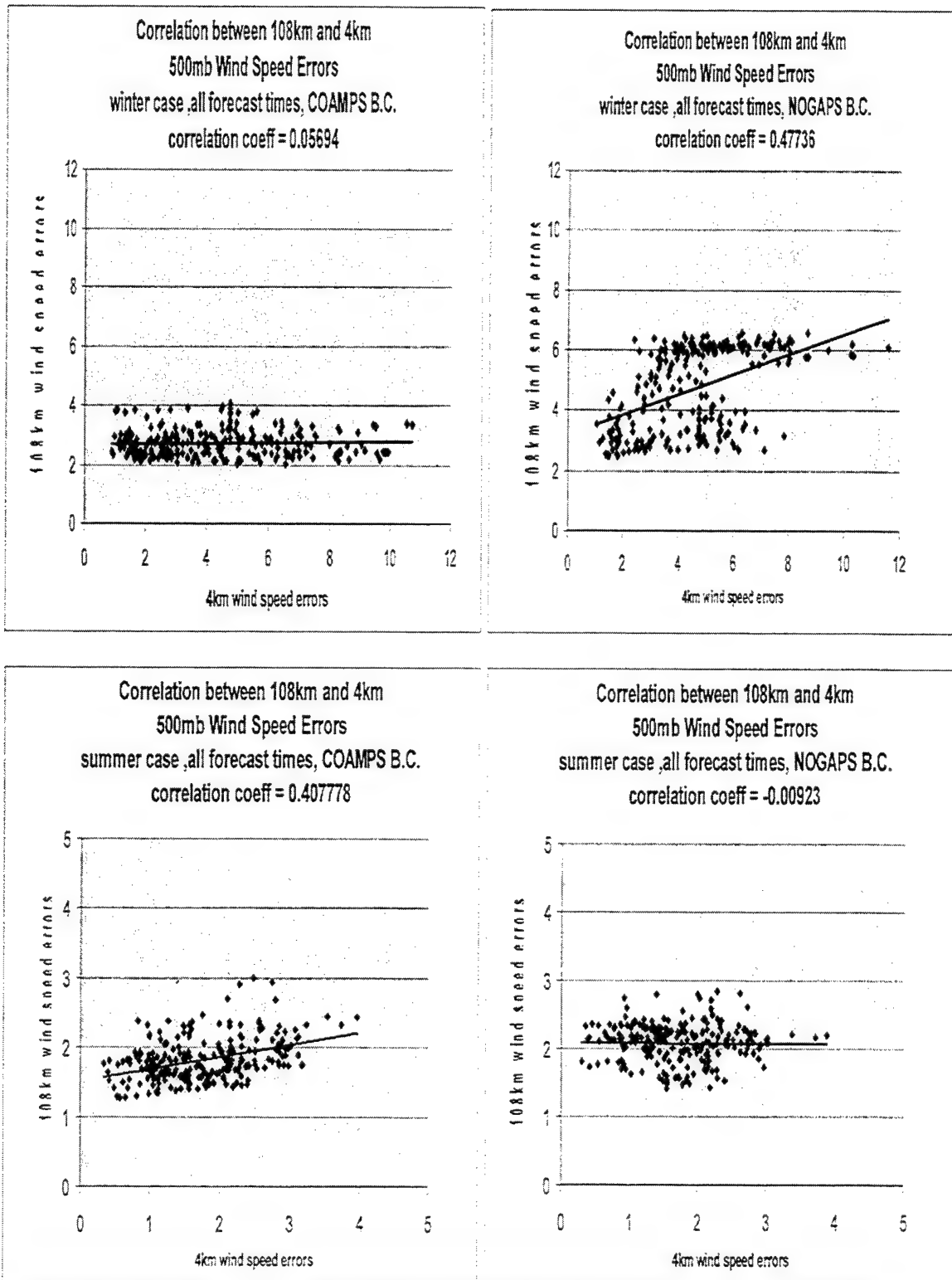


Figure 22. Correlation between 108km and 4km 500mb wind speed errors for the winter (top) and summer (bottom) patterns using MM5 "control" (left) and NOGAPS (right) boundary conditions

LIST OF REFERENCES

- Anthes, R.A. 1984: Predictability of mesoscale meteorological phenomena. In *Predictability of Fluid Motions* (La Jolla Institute - 1983). G. Holloway and B.J. West (Eds.), American Institute of Physics, New York, 247-270
- Anthes, R.A. 1986: The General Question of Predictability. *Mesoscale Meteorology and Forecasting*, P.S. Ray (Ed.), Amer.Meteor. Soc., 636-655.
- Anthes, R.A. and D.P. Baumhefner, 1984: A diagram depicting forecast skill and predictability. *Bull. Amer. Meteor. Soc.*, 65, 701-703.
- Baumhefner, D.P., 1984: The relationship between present large-scale forecast skill and new estimates of predictability error growth. In *Predictability of Fluid Motions* (La Jolla Institute-1983). G. Holloway and B.J. West (Eds.), American Institute of Physics, New York, 169-180.
- Doyle, J. 1997: The influence of mesoscale orography on coastal jet and rainband. *Mon. Wea. Rev.*, 125, 1465-1488
- Gunderson, C., 1999. Early returns on the San Diego local mesoscale modeling initiative. NPMOC San Diego, CA, 11 pp. [Available from Commanding Officer, NPMOC San Diego, PO BOX 357076, San Diego, CA 92135-7076, Tel. (619) 545-6027.]
- Hodur, R.M., 1997: The Naval Research Laboratory's Coupled Ocean/Atmosphere Mesoscale Prediction System (COAMPS). *Mon. Wea. Rev.*, 125, 1414-1430.
- Lorenz, E.N., 1982: Atmospheric predictability experiments with a large numerical model. *Tellus*, 36A, 505-513.
- Lorenz, E.N., 1993: *The Essence of Chaos*. University of Washington Press, Seattle, 227pp.
- Monterrosa, A.E., 1999: Comparison of TAMS/RT surface wind, temperature, and pressure fields with surface observations and model analyses in the SOCAL area. M.S. thesis, Dept. of Meteorology, The Naval Postgraduate School, 72 pp. (submitted to NTIS). [Available from Dept. of Meteorology, Naval Postgraduate School, 589 Dyer Road, Room 254, Monterey, CA 93943-5114, Tel. (831) 656-2516.]
- Nuss, W.A., and D.W. Titley, 1994: Use of multiquadric interpolation for meteorological objective analysis. *Mon. Wea. Rev.*, 122, 1611-1631.

- Shukla, J., 1984: Predictability of a large atmospheric model. In *Predictability of Fluid Motions* (La Jolla Institute - 1983). G. Holloway and B.J. West (Eds.), American Institute of Physics, New York, 449-456.
- Tennekes, H., 1978: Turbulent flow in two and three dimensions. *Bull. Amer. Soc.*, 59, 22-28.
- Thompson, W.T., T. Haack, J.D. Doyle, S.D. Burk, 1997: A nonhydrostatic mesoscale simulation of the 10-11 June 1994 coastally trapped wind reversal. *Mon. Wea. Rev.*, 125, 3211-3230.
- Warner, T.T., 1992: Modeling of surface effects on the mesoscale. In *Mesoscale Modeling of the Atmosphere*, R.A. Pielke and R.P. Pearce (Eds.), American Meteorological Society, 21-27.

INITIAL DISTRIBUTION LIST

1. Defense Technical Information Center.....2
8725 John J. Kingman Road, Suite 0944
Ft. Belvoir, VA 22060-6218

2. Dudley Knox Library.....2
Naval Postgraduate School
411 Dyer Road
Monterey, CA 93943-5101

3. Meteorology Department.....1
Code MR/Wx
Naval Postgraduate School
589 Dyer Road, Rm 254
Monterey, CA 93943-5114

4. Dr. Wendell A. Nuss.....2
Code MR/Nu
Naval Postgraduate School
589 Dyer Road, Rm 254
Monterey, CA 93943-5114

5. Dr. Douglas K. Miller1
Code MR/DM
Naval Postgraduate School
589 Dyer Road, Rm 254
Monterey, CA 93943-5114

6. Scott Sandgathe1
Office of Naval Research
800 N. Quincy St.
Arlington, VA 22217-5660

7. Dr. Rich Hodur1
Naval Research Laboratory
7 Grace Hopper Ave.
Monterey, CA 93943

8. Mr. John Cook, Code 75421
Naval Research Laboratory
7 Grace Hopper Ave.
Monterey, CA 93943

9. Commanding Officer 1
Fleet Numerical Meteorology and Oceanography Center
7 Grace Hopper Ave. Stop A
Monterey, CA 93943
10. Commander 1
Naval Meteorology and Oceanography Command
1020 Bach Boulevard
Stennis Space Center, Mississippi 39529-5005
11. LCDR Michael A. Kuypers 2
4701 Newman Ave.
Cypress, California 90630